論文 / 著書情報
Article / Book Information

題目(和文)	
Title(English)	System capacity enhancement using advanced interference mitigation receivers in cellular networks
著者(和文)	佐野洋介
Author(English)	Yousuke Sano
出典(和文)	学位:博士(工学), 学位授与機関:東京工業大学, 報告番号:甲第10884号, 授与年月日:2018年3月26日, 学位の種別:課程博士, 審査員:府川 和彦,植松 友彦,中山 実,山田 功,髙田 潤一
Citation(English)	Degree:Doctor (Engineering), Conferring organization: Tokyo Institute of Technology, Report number:甲第10884号, Conferred date:2018/3/26, Degree Type:Course doctor, Examiner:,,,,
学位種別(和文)	博士論文
Type(English)	Doctoral Thesis

System capacity enhancement using advanced interference mitigation receivers in cellular networks

Yousuke Sano

Department of Information and Communications Engineering

School of Engineering

Tokyo Institute of Technology

Contents

Chapter 1. Introduction

1.1. Background

In recent years, the increase in the number of mobile phone users, especially smart phone users, and the diversification of mobile services, e.g. video streaming service, have significantly changed the situation for mobile communication in the world. For example, an amount of mobile data traffic has grown 4,000-fold from 2005 to 2015 [1]. Due to further increase of smart phone users and expected familiarization of IoT (Internet of Things) / M2M (Machine-to-Machine) devices/services in future, it is predicted that the amount of the mobile data traffic continuously increases 1.47-fold per year from 2016 to 2021 [2]. Therefore, countermeasure to deal with this traffic explosion, i.e. system capacity enhancement of mobile communication system, is urgently needed.

Recently, the Third Generation Partnership Project (3GPP) standardized the radio interface specifications for the fourth-generation mobile communication system, called Long-Term Evolution (LTE) [3, 4]. The first release of LTE was finalized in 2008 as LTE Release 8 (simply LTE hereafter) [5]. One key feature for LTE is multi-antenna techniques, i.e., multiple-input multiple-output (MIMO) techniques. It was theoretically proven that the capacity of the MIMO channel increases linearly with the number of transmit and received antennas by data stream multiplexing in the spatial domain [6, 7]. In LTE downlink, therefore, multiplexing of maximally 4 data streams was supported to improve a peak data rate [8]. Furthermore, orthogonal frequency division multiplexing (OFDM) based radio access was adopted in LTE downlink [5], while code division multiplexing (CDM) based radio access was utilized in the third-generation mobile communication system [9]. This is because OFDM has inherent immunity to multipath interference (MPI) through a low symbol rate by utilizing a cyclic prefix (CP) [10], and OFDM has naturally a high affinity to different transmission bandwidth arrangements. In order to improve system capacity, standards development for LTE is continued toward establishing an enhanced

LTE radio interface, which is called LTE-Advanced. The first release of LTE-Advanced was finalized in 2010 as LTE Release 10 (simply LTE-Advanced hereafter) [11], which has backward compatibility with LTE for smooth migration from LTE based service. One of the key technologies of LTE-Advanced is utilization of wider spectrum compared with LTE. In LTE-Advanced, up to 100 MHz can be utilized as a system bandwidth, while up to 20 MHz can be used in LTE. This technique is called carrier aggregation since the multiple carriers, up to 5 carriers, of LTE are aggregated to achieve wider spectrum.

To date, various commercial services based on LTE and LTE-Advanced have been launched in many countries. In Japan, NTT DOCOMO launched a commercial LTE service in December 2010 under the new service brand of "Xi" (crossy) [12]. To develop LTE further, the commercial service of LTE-Advanced started in March 2015 under the service brand "PREMIUM 4G" [13]. In order to address mobile traffic explosion in future, development of LTE-Advanced is further required.

Generally, the following three approaches can be considered to improve system capacity of mobile communication system (see Fig. 1-1):

i) Utilization of wider spectrum
ii) Dense cell deployment (e.g. small cell deployment)
iii) Archiving higher spectrum efficiency

For the first approach, i.e., utilization of wider spectrum, further enhancement of carrier aggregation was specified in LTE Release 13, and up to 640 MHz, i.e., the aggregation of 32 LTE carriers can be utilized as a system bandwidth [14]. Since spectrum allocation for a mobile network operator is regulated by governments in most countries, the system bandwidth of LTE-Advanced will be further extended taking the frequency situation of each country into account. For the second approach, there has been intensive investigation of technologies to deal with the dense cell deployment, e.g., [15, 16]. Especially in 3GPP, dense deployment of "small cell", which has lower transmission power compared with existing cell (macro cell), was investigated and specified in LTE Release 12 [17]. Small cell environments have different characteristics from the conventional macro cell environments: fewer users per cell, significantly good signal reception quality due to receiving signals directly from nearby base stations, and ability to accommodate users with low mobility only. Those characteristics can improve system capacity of the mobile communication system, however, spectrum efficiency of users especially at the cell-edge area would be degraded without appropriate management/mitigation of strong inter-cell interference from adjacent cells due to dense cell deployment. To do this, for example, inter-cell interference coordination (ICIC) [18, 19], coordinated multi-point transmission (CoMP) [20, 21] and interference mitigation at mobile terminal side have been investigated. For improving the spectrum efficiency, i.e., for the third approach, there are various candidate technologies in

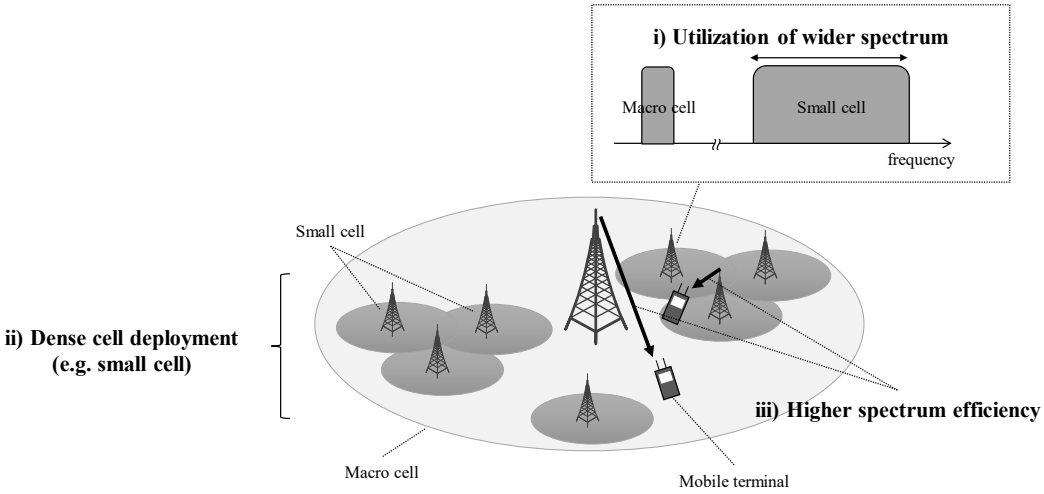

Figure 1-1. Approaches for improving system capacity

addition to above inter-cell interference management/mitigation technologies. For example, enhancement of MIMO technologies, channel coding schemes and multiple access schemes, such as multi-user MIMO [22], Polar coding [23] and non-orthogonal multiple access (NOMA) [24], are promising candidates.

1.2. Overview and Objectives

As previously stated, archiving higher spectrum efficiency is the important issue for improving system capacity of mobile communication system. Especially, handling of an inter-cell interference is significantly important to enable dense cell deployment without any performance degradation at the cell-edge area. 3GPP has been studying a variety of technologies in recent years to mitigate the inter-cell interference at mobile terminal. In particular with LTE-Advanced downlink, advanced radio signal processing for receivers has been investigated. In LTE Release 11, the interference rejection combining (IRC) receiver, which can suppress the inter-cell interference based on minimum mean square error (MMSE) criteria [25], was investigated and specified [26, 27]. In LTE Release 12, the network assisted interference cancellation and suppression (NAICS) receiver, which is a further enhancement of the interference mitigation technology based on successive interference cancellation (SIC) receiver [28] and maximum likelihood detector (MLD) such as complexity reduced MLD with QR decomposition and M-algorithm (QRM-MLD) [29], was investigated and specified [30, 27]. Those receives are expected to improve system capacity especially in the cell-edge area. In addition, further capacity gain can be expected by utilizing the IRC and NAICS receivers together with other techniques, e.g. ICIC and CoMP. For example, in CoMP transmission, an interference alignment technique [31] can

align the two interference signals so that the receiver can treat these sources of interference as one source. As a result, the IRC receiver expends only one degree of freedom to suppress two sources of interference. To investigate such a combination of the IRC receiver and ICIC/CoMP transmission techniques, a system level simulation needs to be developed rather than a link level simulation for the IRC receiver. This is because the system capacity, which includes the effect of the user pairing algorithm and the tradeoff relationship between the cell-edge and cell center user throughput, should be investigated.

Generally, in order to reduce the computational complexity of the system level simulation employing the multi-cell environment where multiple sets of mobile terminals (UEs: user equipment hereafter) are distributed, the demodulation process at the receiver is not implemented. For this purpose, the block error rate (BLER) is estimated directly from the received signal qualities. This kind of the BLER estimation scheme is usually called link performance modeling (or link abstraction, etc). It is highly depending on simulation assumptions how much computational complexity can be reduced by employing link performance modeling, but in general the computational complexity is incredibly high if such link performance modeling is not employed and the demodulation process at the receiver is explicitly implemented in the system level simulation. This is because the large number of UEs (and base stations) is generally distributed in the system level simulation. If totally 1000 UEs are distributed in the cells, for example, all of the demodulation process, e.g., channel estimation, channel equalization/signal decomposition and channel decoding for all 1000 links need to be explicitly calculated to obtain just one sample in time domain, and generally several hundreds to thousands of the samples are required to converge system performance. Hence, in order to reduce the computational complexity, the link performance modeling is usually needs to be implemented. When no channel coding scheme is employed, the bit error rate (BER) of the modulated symbols in the respective subcarriers is independent. Therefore, the resultant BLER is simply estimated from the BER of all modulated symbols. However, some channel coding schemes are employed in actual systems, e.g., turbo coding is specified in LTE/LTE-Advanced. In this case, the BLER depends on the variation in the channel qualities during one coded block, which is derived from the frequency-selective fading channel. In [32]-[34], several link performance modeling methods were proposed to estimate the BLER including the channel coding gain. In these models, the BLER is defined as a function of the signal-to-interference-plus-noise power ratio (SINR) for the respective modulated symbols, i.e., the respective subcarriers in OFDM-based radio access. Therefore, for the link performance modeling of the IRC receiver, the SINR including the capability of inter-cell interference suppression needs to be appropriately modeled. Hence, the first objective of this dissertation is to investigate the link performance modeling of the IRC receiver for evaluating its system capacity. Note that the link performance modeling scheme for the NAICS receiver was

developed and system capacity analysis was summarized in [30].

On the other hand, as described above, the OFDM based radio access was adopted as a multiple access scheme in LTE/LTE-Advanced. This type of orthogonal multiple access scheme is a reasonable choice for achieving good system capacity in packet-domain services such as LTE/LTE-Advanced with simple single-user detection. When considering advanced (non-linear) multi-user interference canceller, however, there is room for achieving higher performance using NOMA [24]. In 3GPP, as a further enhancement of the NAICS receiver, NOMA were investigated and specified in LTE Release 13 and 14 [35, 27]. There are multiple candidate receivers as a multi-user interference canceller for NOMA. In [36, 37], it has been shown by the link level simulation that the BLER performances of those receivers are almost the same. On the other hand, each receiver has different advantage and disadvantage from the system level perspective, e.g. user scheduling flexibility and signaling overhead, as reported in [38]. To investigate those system level aspects, system capability of NOMA employing the candidate receiver should be investigated by the system level simulation. Therefore, the second objective of this dissertation is to investigate the most efficient interference canceller for NOMA form the view point of the system capacity.

1.3. Structure of the Dissertation

This dissertation is organized as follows. Chapter 2 gives a detail of the IRC receiver. Both link and system level analysis are provided. Firstly, the signal transmission model and link level analysis of the IRC receiver are described in detail. After that, system level analysis of the IRC receiver is provided. For the system level analysis, the link performance modeling is developed for the IRC receiver. Chapter 3 gives a system level analysis of NOMA employing various multi-user interference cancellers. To do this, the link performance modeling of the interference canceller is developed. Finally, Chapter 4 provides the dissertation summary.

References

[1] Cisco Visual Networking Index: Global Mobile Data Traffic Forecast Update, 2015–2020 (https://www.cisco.com/c/dam/m/en_in/innovation/enterprise/assets/mobile-white-paper-c11-520862.pdf)

[2] Cisco Visual Networking Index: Forecast and Methodology, 2016–2021 (https://www.cisco.com/c/en/us/solutions/collateral/service-provider/visual-networking-index-vni/complete-white-paper-c11-481360.html)

[3] M. Tanno et al., “Evolved UTRA — Physical Layer Overview,” i*n Proc. IEEE SPAWC 2007*,

June 2007.

[4] E. Dahlman, S. Parkvall, and J. Sköld, 4G –LTE/LTE-Advanced for Mobile Broadband, Academic Press, 2011.

[5] 3GPP, TS36.201 (V8.1.0), “LTE physical layer - general description,” Nov. 2007.

[6] P. Rostaing, O. Berder, G. Burel and L. Collin, "Minimum BER diagonal precoder for MIMO digital transmissions," *IEEE Trans. Signal processing*, vol. 50, pp. 1051-1064, May 2002.

[7] L. Collin, O. Berder, P. Rostaing and G. Burel, “Optimal minimum distance-based precoder for MIMO spatial multiplexing systems,” *IEEE Trans. Signal Processing*, vol. 52, pp. 617-627, Mar. 2004.

[8] 3GPP, TS36.211 (V14.5.0), “Evolved Universal Terrestrial Radio Access (E-UTRA); Physical channels and modulation,” Jan. 2018.

[9] 3GPP, TS25.201 (V 3.4.0), “Physical layer - general description,” Jun. 2002.

[10] W. Henkel, G. Taubock and P. Odling, "The cyclic prefix of OFDM/DMT - an analysis, " *in Proc. IEEE International Zurich Seminar on Broadband Communications*, pp. 221–223, Feb. 2002.

[11] 3GPP, TS36.201 (V10.0.0), “LTE physical layer - general description,” Dec. 2010.

[12] http://www.nttdocomo.com/pr/2010/001494.html

[13] https://www.nttdocomo.co.jp/info/news_release/2015/03/23_02.html

[14] 3GPP, TS36.300(V13.10.0), “Evolved Universal Terrestrial Radio Access (E-UTRA) and Evolved Universal Terrestrial Radio Access Network (E-UTRAN); Overall description; Stage 2,” Jan. 2018.

[15] T. Nakamura, et. al., “Trends in small cell enhancements in LTE advanced,” *IEEE comm, mag.*, vol.51, issue 2, Feb. 2013.

[16] 3GPP, TR36.932 (V12.1.0), “Scenarios and requirements for small cell enhancements for E-UTRA and E-UTRAN,” Mar. 2013.

[17] 3GPP, TS36.300(V12.10.0), “Evolved Universal Terrestrial Radio Access (E-UTRA) and Evolved Universal Terrestrial Radio Access Network (E-UTRAN); Overall description; Stage 2,” Jul. 2016.

[18] K. Giridhar, S. Charai, J. J. Shynk, and R. P. Gooch “ Joint demodulation of cochannel signals using mlse and mapsd algorithms,” *in Proc. of IEEE ICASSP*, pp. 17-21, Feb.1995.

[19] 3GPP, TR 36.814(V9.0.0), “Further Advancements for E-UTRA Physical Layer Aspects,” Mar. 2010.

[20] S. Das, H. Viswanathan, and G. Rittenhouse, “Dynamic Load Balancing Through Coordinated Scheduling in Packet Data Systems,” *IEEE Infocom*, San Francisco, Apr. 2003.

[21] 3GPP TR36.819(V11.2.0), “Coordinated multi-point operation for LTE physical layer aspects,” Sept. 2013.

[22] F. R. Farrokhi, G. J. Foschini, A. Lozano and R. A. Valenzuela, “Link optimal blast processing with multiple-access interference,” *in Proc. IEEE VTC Fall*, vol. 1, pp. 87–91, Sept. 2000.

[23] E. Arikan, “Channel polarization: A method for constructing capacity achieving codes for symmetry binary-input memoryless channels,” *IEEE Trans. Inform. Theory*, vol. 55, pp. 3051 – 3073, Jun. 2009.

[24] K. Higuchi and Y. Kishiyama, “Non-orthogonal access with random beamforming and intra-beam SIC for cellular MIMO downlink,” *IEICE RCS2012-89*, vol. pp. 85-90, July 2012.

[25] J. Winters, “Optimum combining in digital mobile radio with cochannel interference,” *IEEE J. Sel. Areas Commun.*, vol. SAC-2, no. 4, pp. 528–539, Apr. 1984.

[26] 3GPP, TR36.829 (V11.1.0), “Enhanced performance requirement for LTE User Equipment (UE),” Jan. 2013.

[27] 3GPP, TS36.101 (V15.0.0), “Evolved Universal Terrestrial Radio Access (E-UTRA); User Equipment (UE) radio transmission and reception,” Sept. 2017.

[28] P. W. Wolniansky, G. J. Foschini, et. al. "V BLAST: An Architecture for Realizing Very High Data Rates Over the Rich-Scattering Wireless Channel," *in Proc. ISSSE*, pp.295-300, Sept. 1998.

[29] H. Kawai, K. Higuchi, et. al., "Performance of QRM-MLD Employing Two-Dimensional Multi-Slot and Sub-Carrier-Averaging Channel Estimation Filter Using Orthogonal Pilot Channel for OFCDM MIMO Multiplexing in Multipath Fading Channel," *in Proc. Wireless 2004*, pp. 208-214, Jul. 2004.

[30] 3GPP, TR36.866 (V12.0.1), “Study on Network-Assisted Interference Cancellation and Suppression (NAIC) for LTE,” Mar. 2014.

[31] V. R. Cadambe and S. A. Jafar, “Interference alignment and degrees of freedom of the K-user interference channel,” *IEEE Trans. Inf. Theory*, vol. 54, no. 8, pp. 3425-3441, Aug. 2008.

[32] K. Brueninghaus, D. Astély, T. Sälzer, S. Visuri, A. Alexiou, S. Karger, and G.-A. Seraji, “Link performance models for system level simulations of broadband radio access systems,” *in Proc. IEEE PIMRC2005*, pp. 2306–2311, Sept. 2005.

[33] V. Pauli, I. Viering, C. Buchner, E. Saad, G. Liebl, A. Klein, "Efficient link-to-system level modeling for accurate simulations of MIMO-OFDM systems," *in Proc. IEEE ICC2009*, pp. 1-6, June 2009.

[34] 3GPP, TR25.892 (V6.0.0), “Feasibility study for orthogonal frequency division multiplexing (OFDM) for UTRAN enhancement,” June 2004.

[35] 3GPP, TR36.859(V13.0.0), “Study on Downlink Multiuser Superposition Transmission (MUST) for LTE,” Jan. 2016.

[36] C. Yan, A. Harada, A. Benjebbour, Y. Lan, A. Li, and H. Jiang, “Receiver design for downlink

non-orthogonal multiple access (NOMA)," *in Proc. VTC-Spring 2015*, May 2015.

[37] O. Nakamura, J. Goto, Y. Hamaguchi, S. Ibi, and S. Sampei, "Performance Comparison of Superposition Coding Schemes for Downlink Non-Orthogonal Multiple Access," *IEICE Technical Report,* RCS2015-43, May 2015.

[38] O. Nakamura, J. Goto, and Y. Hamaguchi, "Frequency Selection Diversity Effect for Downlink Non-Orthogonal Multiple Access with Maximum Likelihood Detection," *IEICE Technical Report*, RCS2014-284, Jan. 2015.

Chapter 2. Interference Rejection Combining Receiver

2.1. Introduction

To improve the cell edge user throughput especially in dense cell deployment, reception processing should suppress the inter-cell interference signals in addition to detecting the desired signal as shown in Fig. 2-1 since the cell edge user throughput is severely deteriorated by inter-cell interference. The IRC receiver, which can suppress the inter-cell interference with the aid of multiple receiver antenna branches, is considered to be a promising approach. To suppress the interference signals with a feasible level of complexity, linear filtering based on the MMSE criterion is investigated for the IRC receiver in [1]. This filtering can be extended to iterative signal detection such as a turbo equalizer using soft interference cancellation [2, 3], which can possibly improve the detection performance. Regarding such signal processing based on an iterative manner, the enhancement of the detection performance in the first stage can possibly bring about improvement in the final attainable performance in the last stage. Therefore, this dissertation focuses on linear filtering based on the MMSE criteria, as a signal processing technique for the first stage. Hereafter, this type of receiver is simply referred to as the "IRC receiver."

This chapter provides two analyses for the IRC receiver. Firstly, Sect. 2.2 shows the detailed signal processing and the link level performance of the IRC receiver. Especially, RS structure in the serving and interfering cell(s) have an impact on the link performance of the IRC receiver. Therefore, we deeply analyze the reason and that impact. Furthermore, Sect. 2.3 shows the system level analysis of the IRC receiver. As described in chapter 1, the link performance modeling of the IRC receiver, which is required to conduct system capacity analysis of the IRC receiver, is developed. Finally, the conclusion of this chapter is described in the Sect. 2.4.

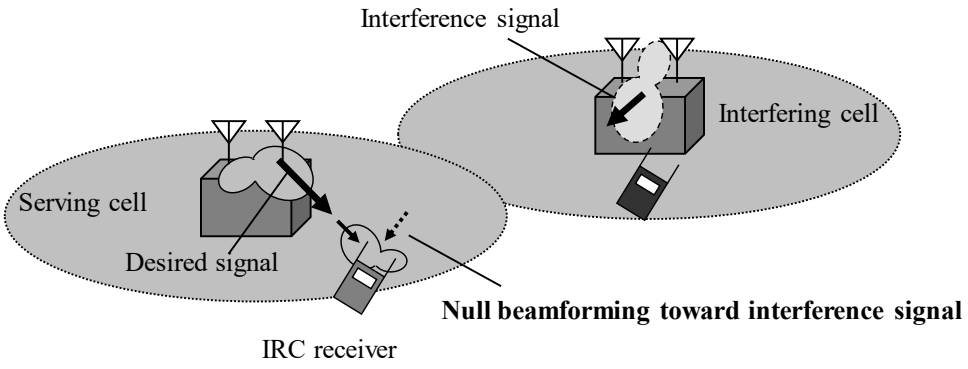

Figure 2-1. IRC receiver concept

2.2. Link Level Analysis

In order to suppress the inter-cell interferences, the IRC receiver requires knowledge of the such interference signals, i.e., the covariance matrix including the interference signals, in addition to knowledge of the desired signal, i.e., the channel matrix of the serving cell. Therefore, to achieve a gain from the IRC receiver, highly accurate estimation schemes of these matrices are important. In practical applications such as LTE/LTE-Advanced, the channel matrix of the serving cell can be estimated using downlink reference signals (RSs). For covariance matrix estimation, the RS based scheme proposed in [4] is effective as an accurate estimation as described in [4] and [5]. This scheme separates the serving cell part and the interference and noise part from the covariance matrix. The former part, i.e., the covariance matrix of the serving cell, can be obtained using the channel amplitudes and phases of the serving cell, which are estimated using the RS of the serving cell. In contrast, the latter part, i.e., the covariance matrix including only the interference and noise, can be estimated by subtracting the replica symbols of the serving cell based on the estimated channel matrix and the known RS sequence from the received RSs. In particular, the estimation accuracy of the latter is more sensitive to the suppression of the interference signals than the former.

In LTE/LTE-Advanced, various transmission modes are supported. To achieve this, multiple RSs, e.g., the cell-specific RS (CRS) and demodulation RS (DMRS) [6], are defined. In this section, we focus on the transmission modes using the CRS. The properties of the CRS are different from those of the data signals, especially when precoding transmission is assumed for the data signals, since the CRS is transmitted without precoding. This difference between the CRS and the data signals poses two problems to the IRC receiver. First, it results in different levels of accuracy for the covariance matrix estimation. More precisely, although the estimated covariance

matrix including the interference and noise is accurate when the data signals from the interfering cell interfere with the CRS of the serving cell, it is inaccurate when the CRS from the interfering cell collides with the CRS of the serving cell as illustrated in Fig. 2-2. This is because the covariance matrix including the interference and noise should include the properties of the data signals from the interfering cell in order for the IRC receiver to suppress the interference of the data signals. Second, assuming the case where the CRS from the interfering cell collides with the desired data signals of the serving cell as illustrated in Fig. 2-2, the effect of suppressing interference signals for the IRC receiver is expected to degrade compared to the case where the data signals interfere among cells. This is because the IRC receiver suppresses the interference data signals from the interfering cells. Therefore, we investigate these two factors that degrade the performance of the IRC receiver.

As the CRS based transmission modes in LTE/LTE-Advanced, closed-loop and open-loop MIMO multiplexing including transmit diversity, i.e., single-stream transmission, are mainly supported. For the closed-loop MIMO system, single-stream precoding transmission is employed based on the Rel. 8 codebook [6]. For the open-loop MIMO system, space-frequency block code (SFBC) using Alamouti coding [7] or large delay cyclic delay diversity (CDD) transmission is employed according to the number of transmission streams, i.e., transmit diversity or MIMO multiplexing [6]. In this section, both of these transmission modes are evaluated in order to clarify the impact due to the CRS-to-CRS collision among the serving and interfering cells. Note that only transmit diversity is employed in the serving cell since the IRC receiver can improve the cell edge user throughput, and the transmit diversity is mainly used at the cell edge due to the low Received SINR. We conduct a link level simulation that can be set to an arbitrary number of interfering cells, and evaluate the performance for the IRC receiver from the viewpoints of the output SINR after IRC reception and the user throughput.

2.2.1. CRS and Data Signal Transmission Model

In this section, a signal model is described focusing on the IRC receiver assuming the closed-loop MIMO system employing a precoding transmission. Regarding the open-loop transmit diversity employing SFBC, details of the signal model are described in [8].

Figure 2-3 illustrates the transmit frame structures assuming two transmitter antenna branches. One resource block (RB) is shown in the figure, which is the minimum assignment unit defined as 12 subcarriers × 14 OFDM symbols (one subframe). Hereafter, a synchronous network where the transmission timing of each subframe is aligned in all cells is assumed. The first two OFDM symbols are assumed to be used for control signaling and the CRS. The CRS is assumed to be multiplexed with the insertion density of 16 resource elements (REs) per RB and transmitted independently from each transmitter antenna branch.

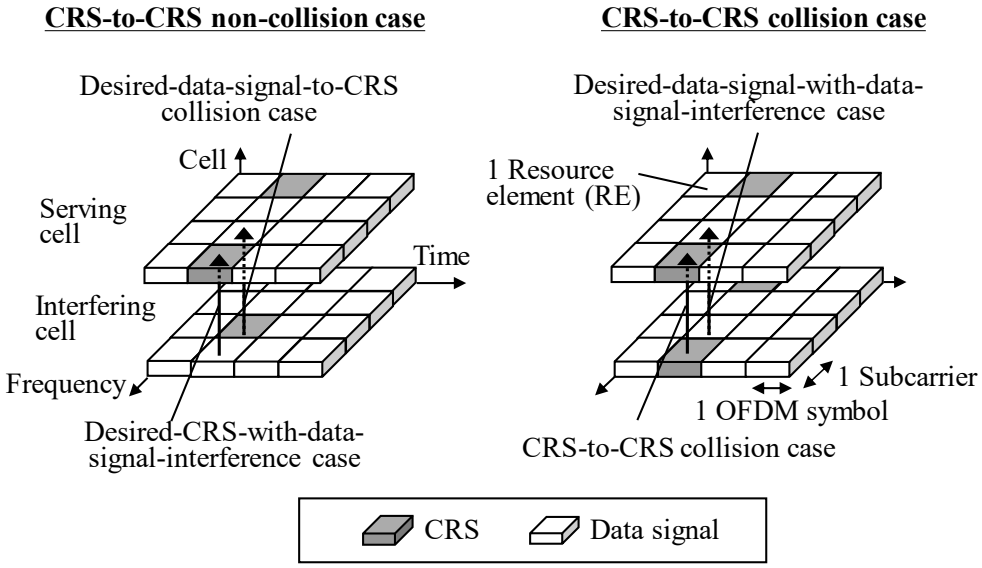

Figure 2-2. Inter-cell CRS interference

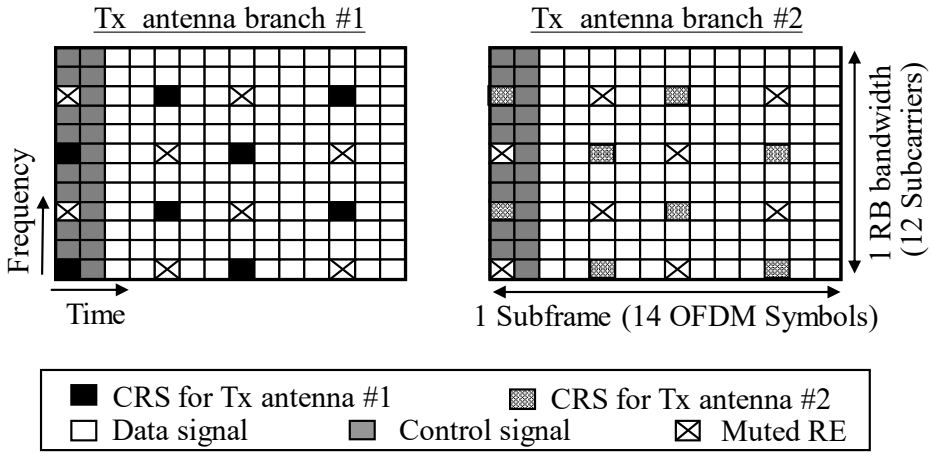

Figure 2-3. Transmit frame structure of CRS based transmission mode

The CRS is transmitted by shifting one subcarrier according to the cell ID; therefore, assuming a synchronous network, the CRSs transmitted from the interfering cells collide with those transmitted from the serving cell every three cells as illustrated in Fig. 2-2. In contrast, when there is no collision of CRSs among the three cells including the serving and dominant interfering cells, the CRSs transmitted from the interfering cells always interfere with the desired data signals from the serving cell. In the following, the signal models for each case in addition to more general cases, i.e., the desired-data-signal-with-data-signal-interference and the desired-CRS-with-data-signal-interference cases, are expressed assuming a multi-cell environment.

i) For desired-data-signal-with-data-signal-interference

As a general case, the case where the interfering data signal interferes with the desired data signal of the serving cell is assumed here. Assuming the number of receiver antenna branches as N_{Rx}, the N_{Rx}-dimensional received signal vector of the k-th subcarrier and the l-th OFDM symbol, $\mathbf{y}_{\mathrm{DtoD}}(k,l)$, is expressed as follows.

$$\mathbf{y}_{\mathrm{DtoD}}(k,l)=\sum_{q=0}^{N_{\mathrm{Cell}}-1}\mathbf{H}_q(k,l)\mathbf{W}_{\mathrm{Tx},q}(k,l)\mathbf{s}_q(k,l)+\mathbf{n}(k,l)\,, \tag{2.1}$$

where $\mathbf{H}_q(k,l)$ represents the ($N_{\mathrm{Rx}} \times N_{\mathrm{Tx}}$) channel matrix between the q-th cell and the set of user equipment (UE), $\mathbf{W}_{\mathrm{Tx},q}(k,l)$ represents the ($N_{\mathrm{Tx}} \times N_{\mathrm{Stream}}$) precoding weight matrix of the q-th cell, $\mathbf{s}_q(k,l)$ represents the N_{Stream}-dimensional information signal vector of the q-th cell, and $\mathbf{n}(k,l)$ is the N_{Rx}-dimensional noise vector. Here, N_{Stream} and N_{Cell} are the numbers of transmission streams for the UE, i.e., transmission ranks, and the total number of cells, respectively. The 0-th cell (q = 0) is defined as the serving cell for the UE. As mentioned above, N_{Tx} is assumed to be two. In the section, the total transmit data signal power per symbol, P_{Data}, is defined as $P_{\mathrm{Data}} = E[\|\mathbf{s}_q(k,l)\|^2]$. Here, $E[\cdot]$ denotes the expectation operation. Note that $\mathbf{W}_{\mathrm{Tx},q}(k,l)$ is the unitary matrix, i.e., $\mathbf{W}_{\mathrm{Tx},q}(k,l)\mathbf{W}_{\mathrm{Tx},q}^{H}(k,l)=\mathbf{I}$ where $\mathbf{I}$ is the identity matrix, when the open-loop MIMO multiplexing employing large delay CDD in LTE/LTE-Advanced [8] with two transmitter antenna branches is assumed. Furthermore, when open-loop transmit diversity employing SFBC is assumed, $\mathbf{W}_{\mathrm{Tx},q}(k,l)$ is the identity matrix and the channel matrix, $\mathbf{H}_q(k,l)$, is expressed including the SFBC [8].

ii) For desired-CRS-with-data-signal-interference

In regard to the case where the interfering data signal interferes with the received CRS of the serving cell, the received signal vector, $\mathbf{y}_{\mathrm{CtoD}}(k,l)$, is expressed as follows.

$$\mathbf{y}_{\mathrm{CtoD}}(k,l)=\mathbf{H}_0(k,l)\mathbf{d}_0(k,l)+\sum_{q=1}^{N_{\mathrm{Cell}}-1}\mathbf{H}_q(k,l)\mathbf{W}_{\mathrm{Tx},q}(k,l)\mathbf{s}_q(k,l)+\mathbf{n}(k,l)\ \ (k,l\in\mathbf{M}_{\mathrm{CRS}})\,, \tag{2.2}$$

where $\mathbf{M}_{\mathrm{CRS}}$ is the CRS RE group in the serving cell. When the N_{Rx}-dimensional channel vector regarding the m-th transmitter antenna branch is estimated based on the CRS, the following 2-dimensional CRS sequence vector, $\mathbf{d}_0(k,l)$, is used as the transmitted signals.

$$\mathbf{d}_0(k,l)=\begin{cases}\left[\sqrt{P_{\mathrm{CRS}}}d_{1,0}(k,l),0\right]^T & \textit{for Tx \#1}\\ \left[0,\sqrt{P_{\mathrm{CRS}}}d_{2,0}(k,l)\right]^T & \textit{for Tx \#2}\end{cases}, \tag{2.3}$$

where P_{CRS} is the transmit power of the CRS and $d_{m,q}(k,l)$ is the CRS sequence at the m-th transmitter antenna branch of the q-th cell. Here, P_{CRS}, is defined as $P_{\mathrm{CRS}} = E[\|\mathbf{d}_0(k,l)\|^2]$. Superscript ^{T} denotes the transpose.

iii) For CRS-to-CRS collision

As mentioned earlier, CRS-to-CRS collision occurs between the serving and interfering cells. When the CRS of the interfering cells, e.g., q = 1, is assumed to collide with one of the serving cells, the received signal vector, $\mathbf{y}_{\mathrm{CtoC}}(k,l)$, is expressed as follows.

$$\mathbf{y}_{\mathrm{CtoC}}(k,l)=\mathbf{H}_0(k,l)\mathbf{d}_0(k,l)+\mathbf{H}_1(k,l)\mathbf{d}_1(k,l)+\sum_{q=2}^{N_{\mathrm{Cell}}-1}\mathbf{H}_q(k,l)\mathbf{W}_{\mathrm{Tx},q}(k,l)\mathbf{s}_q(k,l)+\mathbf{n}(k,l)\quad(k,l\in\mathbf{M}_{\mathrm{CRS}}), \tag{2.4}$$

iv) For desired-data-signal-to-CRS collision

For the last case, it is considered that the CRS of the interfering cell, e.g., q = 1, collides with the data signal of the serving cell. The received signal vector, $\mathbf{y}_{\mathrm{DtoC}}(k,l)$, is expressed as follows.

$$\mathbf{y}_{\mathrm{DtoC}}(k,l)=\sum_{q=0,q\neq1}^{N_{\mathrm{Cell}}-1}\mathbf{H}_q(k,l)\mathbf{W}_{\mathrm{Tx},q}(k,l)\mathbf{s}_q(k,l)+\mathbf{H}_1(k,l)\mathbf{d}_1(k,l)+\mathbf{n}(k,l), \tag{2.5}$$

2.2.2. IRC Receiver Weight Matrix Using Estimated Covariance Matrix

In this section, an IRC receiver weight matrix generation scheme is described focusing on the closed-loop MIMO system. Regarding open-loop transmit diversity employing the SFBC, the IRC receiver should be considered in terms of the space and code domains [9]. Details of the receiver weight matrix generation scheme are described in [8].

2.2.2.1. IRC Receiver Weight Matrix Generation

The recovered signal vector of the data signals at the UE, $\hat{\mathbf{s}}_0(k,l)$, is detected by multiplying the ($N_{\mathrm{Stream}} \times N_{\mathrm{Rx}}$) receiver weight matrix, $\mathbf{W}_{\mathrm{Rx},0}(k,l)$, to the received signal vector, $\mathbf{y}_{\mathrm{DtoD}}(k,l)$ or $\mathbf{y}_{\mathrm{DtoC}}(k,l)$, in Eq.(2-1) or Eq.(2-5) as follows.

$$\hat{\mathbf{s}}_0(k,l)=\begin{cases}\mathbf{W}_{\mathrm{Rx},0}(k,l)\mathbf{y}_{\mathrm{DtoD}}(k,l)\\ \mathbf{W}_{\mathrm{Rx},0}(k,l)\mathbf{y}_{\mathrm{DtoC}}(k,l)\end{cases}, \tag{2.6}$$

To obtain the IRC receiver weight matrix, the RS based covariance matrix estimation scheme [4] is employed. As the RS, the CRS is assumed in this dissertation, as described in Sect. 2.2. Using the CRS sequence of the serving cell, which is known at the receiver, the covariance matrix including only the interference and noise component, $\mathbf{R}_{I+N}$, is estimated using the received CRS vector, $\mathbf{y}_{\mathrm{CtoD}}(k,l)$ or $\mathbf{y}_{\mathrm{CtoC}}(k,l)$, in Eq.(2-2) or Eq.(2-4) as follows.

$$\mathbf{R}_{I+N}=\frac{1}{N_{\mathrm{sp}}}\sum_{k,l\in\mathbf{M}_{\mathrm{CRS}}}\tilde{\mathbf{y}}(k,l)\,\tilde{\mathbf{y}}^{H}(k,l), \tag{2.7}$$

$$\tilde{\mathbf{y}}(k,l) \quad \begin{cases} \mathbf{y}_{\mathrm{CtoD}}(k,l)-\hat{\mathbf{H}}_0(k,l)\mathbf{d}_0(k,l) \\ \mathbf{y}_{\mathrm{CtoC}}(k,l)-\hat{\mathbf{H}}_0(k,l)\mathbf{d}_0(k,l) \end{cases} \quad (k,l\in\mathbf{M}_{\mathrm{CRS}}), \tag{2.8}$$

where $\hat{\mathbf{H}}_0(k,l)$ is the estimated channel matrix based on the CRS, N_{sp} is the number of CRSs for averaging in Eq.(2-7). Superscript ^{H} denotes the Hermitian transpose. Note that the UE is informed of the information of the precoding matrix in the serving cell, $\mathbf{W}_{\mathrm{Tx},0}(k,l)$, in the CRS based closed-loop MIMO system in LTE/LTE-Advanced. Using the estimated $\mathbf{R}_{\mathrm{I}+N}$ and $\hat{\mathbf{H}}_0(k,l)$, the covariance matrix, $\mathbf{R}_{yy}(k,l)$, is estimated using the following equation.

$$\mathbf{R}_{yy}(k,l)=\frac{P_{\mathrm{Data}}}{N_{\mathrm{Stream}}}\hat{\mathbf{H}}_0(k,l)\mathbf{W}_{\mathrm{Tx},0}(k,l)\mathbf{W}_{\mathrm{Tx},0}^{H}(k,l)\hat{\mathbf{H}}_0^{H}(k,l)+\mathbf{R}_{I+N}, \tag{2.9}$$

Assuming equal power allocation for each data stream, the IRC receiver weight matrix is calculated using $\mathbf{R}_{yy}(k,l)$ as follows.

$$\mathbf{W}_{\mathrm{IRC}}(k,l)=\frac{P_{\mathrm{Data}}}{N_{\mathrm{Stream}}}\left(\hat{\mathbf{H}}_0(k,l)\mathbf{W}_{\mathrm{Tx},0}(k,l)\right)^{H}\mathbf{R}_{yy}^{-1}(k,l), \tag{2.10}$$

Note that the averaging in Eq.(2.7) is usually conducted within one or a few continuous RB(s). This is because the averaging over wider time/frequency resources can mitigate the estimation error caused by the white noise when the channel matrices of the interference cells are constant within those resources. When assuming a strong frequency (or time) selective channel, however, it is expected that the channel matrices of the interference cells is not constant within the such resources. In this case, the estimation accuracy of the covariance matrix of the interference cells would be degraded due to the inconsistency of the channel, and the performance the IRC receiver expected to be degraded. Therefore, the tradeoff between the effectiveness of noise mitigation and the impact of channel selectivity needs to be considered to decide the range of averaging.

2.2.2.2. Impact on Estimation Accuracy of Covariance Matrix for CRS-to-CRS Collision

In this section, we discuss the impact on the estimation accuracy of the covariance matrix for the CRS-to-CRS collision compared to that for the desired-CRS-with-data-signal-interference.

i) For desired-CRS-with-data-signal-interference

First, the case where the data signals of the interfering cells interfere with the CRS of the serving cell is assumed. Using the RS based estimation scheme expressed in Eq.(2-7) and Eq.(2-8), the covariance matrix that only includes the interference and noise, $\mathbf{R}_{\mathrm{I}+N}$, for the closed- and open-loop MIMO systems can be estimated in principle by using the received CRS vector, $\mathbf{y}_{\mathrm{CtoD}}(k,l)$ in Eq.(2-2) as follows.

$$\begin{cases} \mathbf{R}_{I+N} \cong \sum_{q=1}^{N_{\text{Cell}}-1} \dfrac{P_{\text{Data}}}{N_{\text{Stream}}} \mathbf{H}_q \mathbf{W}_{\text{Tx},q} \mathbf{W}_{\text{Tx},q}^H \mathbf{H}_q^H + \sigma^2 \mathbf{I} & \textit{for closed-loop} \\ \mathbf{R}_{I+N} \cong \sum_{q=1}^{N_{\text{Cell}}-1} \dfrac{P_{\text{Data}}}{2} \mathbf{H}_q \mathbf{H}_q^H + \sigma^2 \mathbf{I} & \textit{for open-loop} \end{cases}, \tag{2.11}$$

where σ^2 is the noise power. Note that the channel fluctuations in the time and frequency domains are assumed to be negligible within 1 RB and the description of (k,l) is omitted for simplicity. Furthermore, regarding the open-loop MIMO multiplexing and transmit diversity, $\mathbf{W}_{\text{Tx},q} \mathbf{W}_{\text{Tx},q}^H = \mathbf{I}$ and $\mathbf{W}_{\text{Tx},q} = \mathbf{I}$ are considered, respectively. Each data signal power is also assumed to be $P_{\text{Data}}/2$ for both 1 and 2-stream transmissions.

ii) For CRS-to-CRS collision

In contrast, the CRS-to-CRS collision among the serving and interfering cells is assumed. Substituting the received CRS vector, $\mathbf{y}_{\text{CtoC}}(k,l)$, in Eq.(2-4) into Eq.(2-7) and Eq.(2-8), the estimated covariance matrix that includes only the interference and noise becomes the following expression in principle.

$$\begin{cases} \mathbf{R}_{I+N} \cong \dfrac{P_{\text{CRS}}}{2} \mathbf{H}_1 \mathbf{H}_1^H \\ \qquad + \sum_{q=2}^{N_{\text{Cell}}-1} \dfrac{P_{\text{Data}}}{N_{\text{Stream}}} \mathbf{H}_q \mathbf{W}_{\text{Tx},q} \mathbf{W}_{\text{Tx},q}^H \mathbf{H}_q^H + \sigma^2 \mathbf{I} & \textit{for closed-loop} \\ \mathbf{R}_{I+N} \cong \dfrac{P_{\text{CRS}}}{2} \mathbf{H}_1 \mathbf{H}_1^H + \sum_{q=2}^{N_{\text{Cell}}-1} \dfrac{P_{\text{Data}}}{2} \mathbf{H}_q \mathbf{H}_q^H + \sigma^2 \mathbf{I} & \textit{for open-loop} \end{cases}, \tag{2.12}$$

Note that this equation can be formulated when the number of CRSs for each transmitter antenna branch is the same as that illustrated in Fig. 2-3.

When comparing Eq.(2-11) and Eq.(2-12), the property of the estimated covariance matrix is changed due to the CRS-to-CRS collision when $\mathbf{W}_{\text{Tx},q}$ is not the unitary matrix, i.e., $\mathbf{W}_{\text{Tx},q} \mathbf{W}_{\text{Tx},q}^H \neq \mathbf{I}$, for the closed-loop MIMO system. Since a change in the property of the covariance matrix means that the accuracy of the covariance matrix estimation becomes degraded, the performance for the IRC receiver is expected to be degraded in this system. On the other hand, regarding the open-loop MIMO system, no degradation of the performance for the IRC receiver is expected since the property of the estimated covariance matrix is not changed under the assumption $P_{\text{Data}} = P_{\text{CRS}}$.

2.2.2.3. Impact on Effect of Suppressing Interference for Desired-Data-Signal-to-CRS Collision

Considering the desired-data-signal-to-CRS collision expressed in Eq.(2-5), the CRSs transmitted from the interfering cells interfere with the data signals transmitted from the serving cell, i.e.,

non-precoded interference signals affect the desired data signals. The IRC receiver can suppress the interference of data signals transmitted from the interfering cells. Therefore, especially in the closed-loop MIMO system employing precoding, the effect of suppressing the interference for the IRC receiver is expected to degrade due to the different properties of the interference signals, i.e., precoded or non-precoded signals. However, the number of desired data signals that incur interference from the CRSs transmitted from one interfering cell is limited, i.e., only 12 RE/RB under the assumptions of the CRS insertion density as illustrated in Fig. 2-3 and a synchronous network. Therefore, the impact on the IRC receiver due to the inter-cell interference of the CRS is expected to be small compared to that due to the CRS-to-CRS collision.

2.2.3. Simulation Conditions

To investigate the impact on the IRC receiver due to the CRS interference, the output SINR and the throughput performance for the IRC receiver are evaluated. In the next section, the output SINR and throughput performance levels are evaluated for both CRS-to-CRS collision and CRS-to-CRS non-collision cases as illustrated in Fig. 2-2. Note that each case includes the following cases and influences as described in the previous sections.

- CRS-to-CRS collision case:
  Includes both the CRS-to-CRS collision case as in Sect. 2.2.1 iii) and the desired-data-signal-with-data-signal-interference case as in Sect. 2.2.1 i). The former case impacts the estimation accuracy of the covariance matrix as described in Sect. 2.2.2.2. The latter case impacts the effect of suppressing interference as described in Sect. 2.2.2.3.
- CRS-to-CRS non-collision case:
  Includes both the desired-CRS-with-data-signal-interference case as in Sect. 2.2.1 ii) and the desired-data-signal-to-CRS collision case as in Sect. 2.2.1 iv). In addition to the CRS-to-CRS collision case, the former case impacts the estimation accuracy of the covariance matrix as described in Sect. 2.2.2.2. The latter case impacts the effect of suppressing interference as described in Sec. 2.2.2.3.

Here, the number of the interfering cells is assumed to be two, i.e., the three-cell model is assumed. For the CRS-to-CRS collision case, the CRSs transmitted from the most dominant interfering cell collide with the CRSs transmitted from the serving cell. In contrast, for the CRS-to-CRS non-collision case , it is assumed that there are no collisions of CRSs among the three cells.

Regarding the output SINR, since we assume that only transmit diversity, i.e., single-stream transmission, is employed in the serving cell, a single output SINR is obtained. For calculating the output SINR, the following formula is used when the closed-loop MIMO system is assumed.

$$\mathrm{SINR}=\frac{\mathbf{W}_{\mathrm{Rx}}P\mathbf{H}_0\mathbf{W}_{\mathrm{Tx},0}\mathbf{W}_{\mathrm{Tx},0}^H\mathbf{H}_0^H\mathbf{W}_{\mathrm{Rx}}^H}{\mathbf{W}_{\mathrm{Rx}}\left(\sum_{q=1}^{N_{\mathrm{cell}}-1}P\mathbf{H}_q\mathbf{W}_{\mathrm{Tx},q}\mathbf{W}_{\mathrm{Tx},q}^H\mathbf{H}_q^H+\sigma_N^2\mathbf{I}\right)\mathbf{W}_{\mathrm{Rx}}^H}, \tag{2.13}$$

Where σ_N^2 indicates noise power. Here, the description of (k,l) is omitted for simplicity. When the open-loop MIMO multiplexing is assumed, $\mathbf{W}_{\mathrm{Tx},q}\mathbf{W}_{\mathrm{Tx},q}^H$ is the identity matrix in this dissertation due to the assumption of the two transmitter antenna branches. Furthermore, if open-loop transmit diversity employs the SFBC, the channel matrix, $\mathbf{H}_q(k,l)$, is expressed including the SFBC.

For the performance evaluation, a link level simulation employing the multi cells is conducted. Note that a link level simulation is performed between each UE and its serving cell as well as the neighboring cells in this simulation.

The numbers of transmitter and receiver antenna branches are assumed to be two and two, respectively. Therefore, the spatial degree of freedom is one when transmit diversity is assumed. Fifty consecutive RBs, i.e., 9 MHz, are assigned to the UE in the serving cell. However, the assignment granularity of each UE in the interfering cells is assumed to be six consecutive RBs. Furthermore, 50 consecutive RBs are all assigned to 9 UEs in the interfering cells. In the evaluation, although the insertion density of the CRS is 16 RE/RB as illustrated in Fig. 2-3, the CRSs located in the data signal region are only used for the RS based covariance matrix estimation in order to exclude the impact of the interference of control signals. This is because a synchronous network is assumed. The covariance matrix is estimated within 1 RB. Therefore, the number of averaging samples, N_{sp}, equals 12 in Eq.(2-7). The channel estimation scheme for the CRS is assumed to be the 2-dimensional MMSE channel estimation scheme [10]. For the MMSE channel estimation filter, a uniform delay power spectrum within the cyclic prefix length of 4.69 μs is assumed in the frequency domain, and a uniform Doppler power spectrum with the maximum Doppler frequency of 5.55 Hz is assumed in the time domain. The total data signal power per symbol, P_{Data}, is assumed to be same as the CRS power, P_{CRS}.

For the throughput evaluation, hybrid automatic repeat request (ARQ) with incremental redundancy is employed and the maximum number of retransmissions is assumed to be four. Outer-loop link adaptation [11] is employed with the target BLER of 10%. Furthermore, MIMO multiplexing with two-stream transmission is used in the interfering cells in addition to the transmit diversity for the practical throughput evaluation. The probability of transmit diversity is assumed to be 80% every 6 RBs assigned to each UE in the interfering cells.

The assumption for the closed-loop MIMO system is that the two transmitter antenna codebooks defined in [6] are used for precoding transmission. Regarding the serving cell, based on the estimated channel matrix using the CRS, the UE selects the precoding weight matrix, which maximizes the received SINR from the codebook, and then the selected precoding weight matrix

Table 2-1. Simulation parameters

Carrier frequency / System bandwidth	2 GHz / 10 MHz
Resource allocation	50 RBs
MIMO antenna configuration	2 x 2 (uncorrelated)
Channel model (RMS delay spread)	9-path EVA channel model (357 ns)
Maximum Doppler frequency	5.55 Hz
Modulation and coding scheme (MCS)	QPSK (R = 0.11 – 0.61) 16QAM (R = 0.33 – 0.54) 64QAM (R = 0.39 – 0.93)
MCS transmission granularity on interfering cells	Randomly changing every 1 ms Frequency granularity: 6 RBs
Channel estimation	2D-MMSE channel estimation
Hybrid ARQ (Round trip delay)	Incremental Redundancy (8 ms)
Scheduling / Feedback delay	8 ms / 5 ms

information at the UE is fed back to the serving cell. In this evaluation, the precoding granularity is assumed to be the whole bandwidth, i.e., 50 RBs, in the frequency domain and every subframe, i.e., 1 ms, in the time domain. Furthermore, we assume that there is no feedback error. Note that the precoding weight matrix is randomly selected from the codebook for every subframe in the interfering cells for simplicity. Regarding the open-loop MIMO multiplexing employing the large delay CDD, the precoding weight matrix is defined in [6]. In the evaluation, the performance for not only the IRC receiver but also the conventional maximal ratio combining (MRC) receiver, which is equal to the MMSE receiver assuming transmit diversity, is evaluated for comparison. The other simulation parameters are given in Table 2-1.

2.2.3. Link Evaluation Results

2.2.3.1. Output SINR Performance Evaluation

In the output SINR evaluation, transmit diversity is employed at all the cells and the received signal-to-interference power ratios (SIRs) for the interfering cells are assumed to be 0 dB and 6 dB. Furthermore, the average received signal-to-noise power ration (SNR) is assumed to be 10 dB.

i) CDF of output SINR

First, to investigate which impact is the dominant degrading factor, i.e., the CRS-to-CRS collision case or the CRS-to-CRS non-collision case, the cumulative distribution function (CDF) of the output SINR of each RE within 50 RBs is evaluated.

Figures 2-4(a) and (b) show the CDF results of the output SINR for open- and closed-loop transmit diversity, respectively. Focusing on open-loop transmit diversity in Fig. 2-4(a), the performance for the IRC receiver is almost the same regardless of the CRS-to-CRS collision and

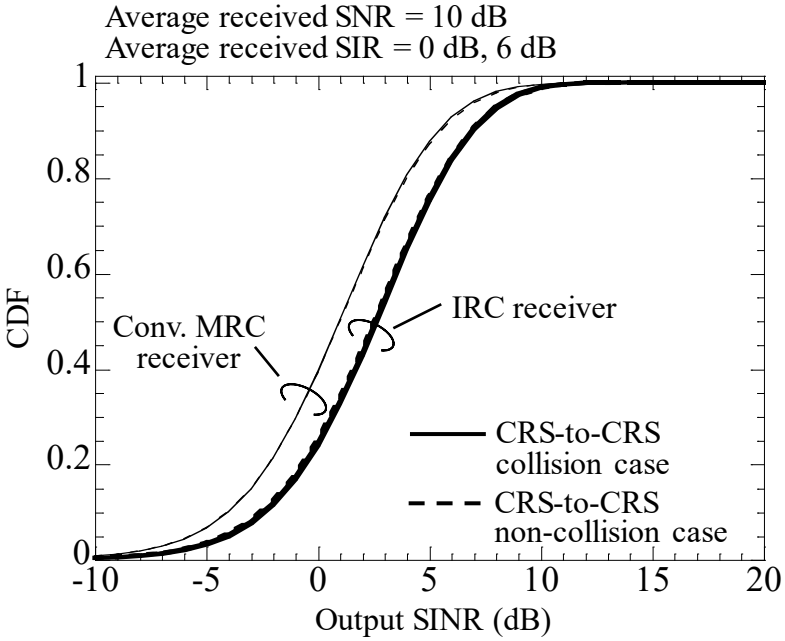

(a) Open-loop transmit diversity using SFBC

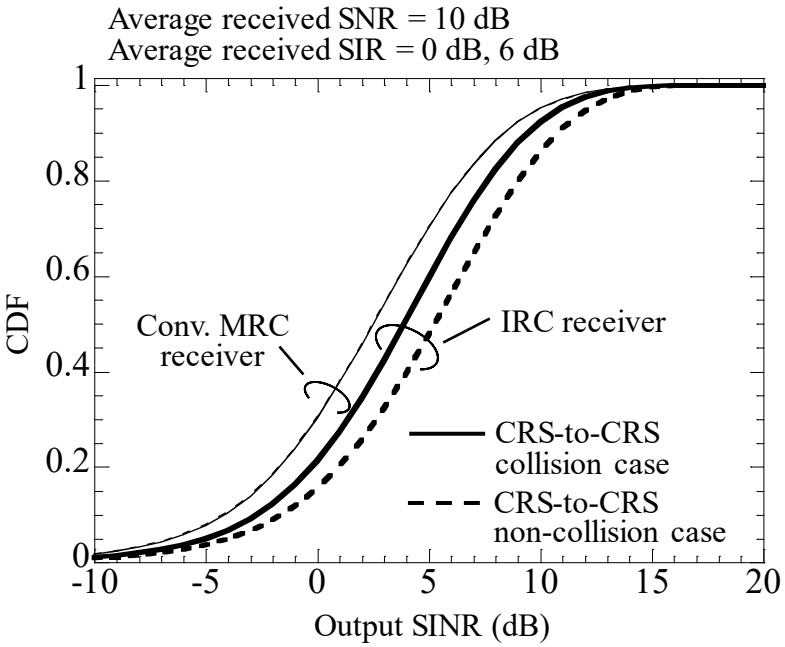

(b) Closed-loop transmit diversity using precoding

Figure 2-4. CDF of output SINR

CRS-to-CRS non-collision cases. Therefore, we can say that the impacts of the CRS-to-CRS collision and CRS-to-CRS non-collision cases, i.e., the estimation accuracy of the covariance matrix and the effect of suppressing the interference, are negligible when open-loop transmit diversity is assumed. However, focusing on closed-loop transmit diversity in Fig. 2-4(b), the performance for the CRS-to-CRS collision case is degraded compared to that for the CRS-to-CRS non-collision case. Therefore, it is clear that the impact on the estimation accuracy of the covariance matrix for the CRS-to-CRS collision case is dominant compared to the impact on the effect of suppressing interference for the CRS-to-CRS non-collision case when closed-loop transmit diversity is assumed. To investigate the reasons for these phenomena, the average output SINR for each subcarrier is evaluated in the following sections.

ii) Average output SINR for each subcarrier focusing on open-loop transmit diversity

To investigate the reason why the impacts of the CRS-to-CRS collision and CRS-to-CRS non-collision cases are negligible for open-loop transmit diversity, the output SINR performance is evaluated focusing on the OFDM symbol where the CRS is not transmitted. This evaluation clarifies the impact of the estimation accuracy of the covariance matrix due to the CRS-to-CRS collision case. Note that when assuming the CRS-to-CRS non-collision case as mentioned in Sect. 2.2.3, only the case where the interfering data signal interferes with the desired CRS can be considered.

Figure 2-5(a) shows the performance results of the average output SINR for each subcarrier within 3 RBs extracted from 50 RBs assuming the open-loop transmit diversity. In this dissertation, we define the average output SINR per subcarrier on a logarithmic scale for 10,000 subframes in an i.i.d. fading channel. From the results in Fig. 2-5(a), the performance for the IRC receiver is almost the same regardless of the CRS-to-CRS collision and CRS-to-CRS non-collision cases since the property of the estimated covariance matrix, $\mathbf{R}_{I+N}$, does not change for either case, which is discussed in Sect. 2.2.2.2. Additionally, to clarify the impact on the effect of suppressing interference for the desired-data-signal-to-CRS collision, i.e., the CRS-to-CRS non-collision case, we evaluate the average output SINR focusing on the OFDM symbol where the CRS is transmitted. Figure 2-5(b) shows the performance results of the average output SINR for each subcarrier in the above case. Note that the CRSs are transmitted every three subcarriers; therefore, there are no performance results for the subcarrier indices of $3k$ ($k \geq 0$). From the results in Fig. 2-5(b), the performance for the IRC receiver is almost the same regardless of the CRS-to-CRS collision case, CRS-to-CRS non-collision case, or the previous evaluation results. Therefore, from these results, we can say that the impacts on the IRC receiver due to the CRS-to-CRS collision and CRS-to-CRS non-collision cases are negligible when assuming the open-loop transmit diversity. for the CRS-to-CRS non-collision case. The reason for this phenomenon is considered to be that the channel estimation accuracy Note that the performance fluctuation

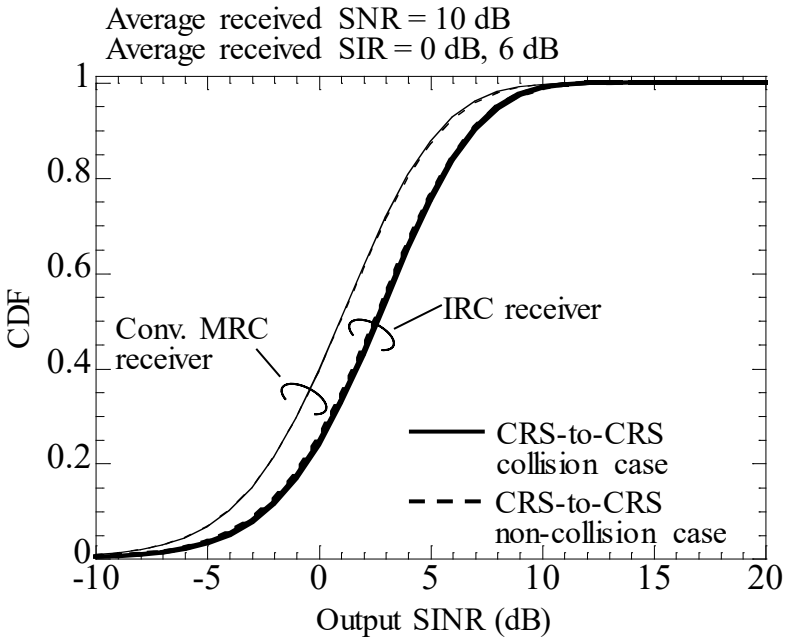

(a) OFDM symbol in CRS non-transmission

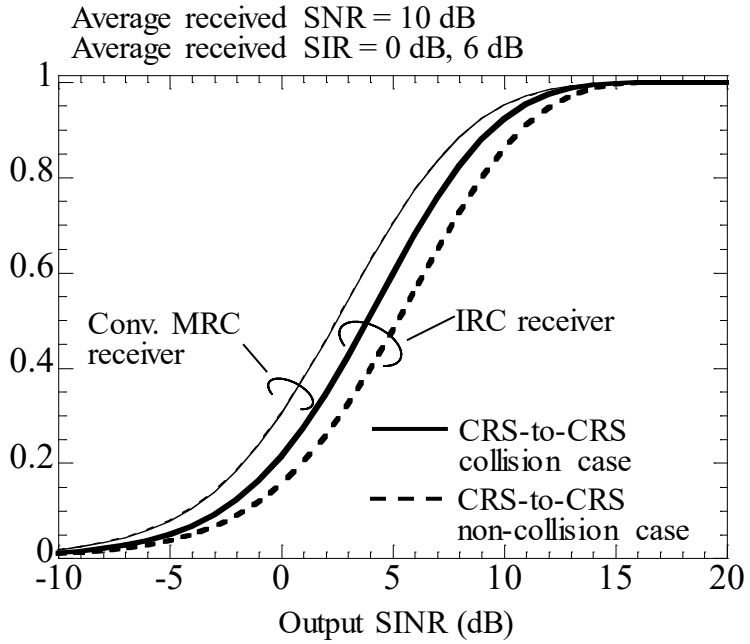

(b) OFDM symbol in CRS transmission

Figure 2-5. Average output SINR for each subcarrier (open-loop transmit diversity)

for the CRS-to-CRS collision case is large compared to that fluctuates based on the CRS from the serving cell since the CRS sequence does not change among subframes, i.e., the CRS from the serving cell suffers from the same CRS interference signal among all subframes.

iii) Average output SINR for each subcarrier focusing on closed-loop transmit diversity

To investigate the reason why the impact of the CRS-to-CRS collision is larger than that for the non-CRS-to-CRS collision case for closed-loop transmit diversity, we evaluate the average output SINR considering the same evaluation assumptions described in the previous section except for open-loop transmit diversity.

Figures 2-6(a) and (b) show the performance results of the average output SINR for each subcarrier within 3 RBs extracted from 50 RBs focusing on the OFDM symbol where the CRS is not transmitted and transmitted, respectively. Focusing on the results in Fig. 2-6(a), the performance for the CRS-to-CRS collision case is degraded compared to that for the CRS-to-CRS non-collision case. This is because the property of the estimated covariance matrix is changed due to the CRS-to-CRS collision as formulated in Eq.(2-11) and Eq.(2-12), i.e., the estimated covariance matrix does not include the precoding weight matrix for the CRS-to-CRS collision case as described in Sect. 2.2.2.2. However, when comparing the results for the IRC receiver and MRC receiver, a gain from the IRC receiver can be achieved for all cases. Note that the reason why the performance for the IRC receiver is periodical every RB, i.e., every 12 subcarriers, is that the covariance estimation period is assumed to be 1 RB in this evaluation.

In contrast, focusing on the results in Fig. 2-6(b), the performance for the IRC receiver assuming the CRS-to-CRS non-collision case is degraded especially for subcarrier indices ($3k$ + 1). This is because the CRS transmitted from the most dominant interfering cell (SIR = 0 dB) interferes with the desired data signals. When comparing the performance results for the CRS-to-CRS collision case, the results for subcarrier indices ($3k$ + 1) assuming the CRS-to-CRS non-collision case are severely degraded. Therefore, for only the REs that collide with the CRS from the interfering cell, it is clear that there is a large impact on the effect of suppressing the interference for the CRS-to-CRS non-collision case due to the CRS interference on the desired data signals. However, based on the previous CDF results of the output SINR in Fig. 2-4(b), we can say that this impact on the IRC receiver due to the inter-cell interference of the CRS is small compared to that due to the CRS-to-CRS collision, i.e., the degradation of the covariance matrix estimation accuracy, when closed-loop transmit diversity is assumed. We consider that this is because the number of desired data signals that incur interference from the CRSs transmitted from one interfering cell is limited, which is expected as described in Sect. 2.2.2.3.

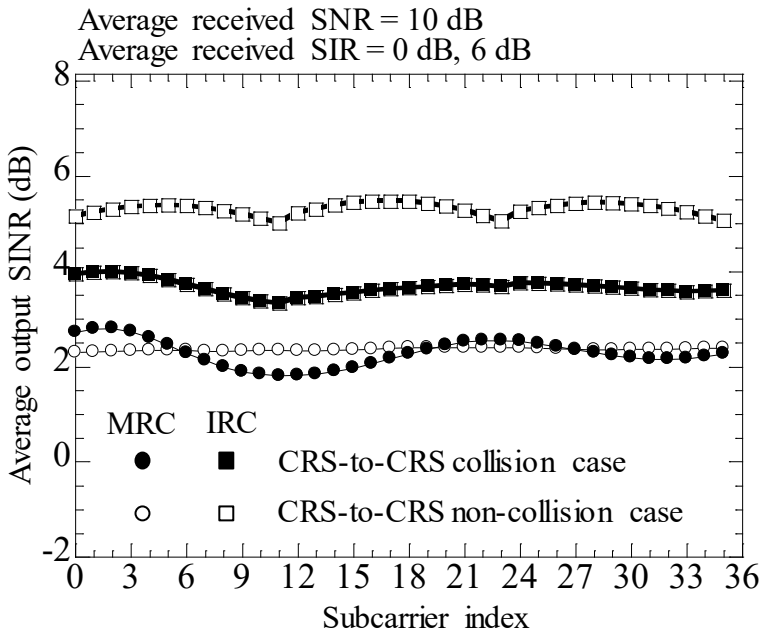

(a) OFDM symbol in CRS non-transmission

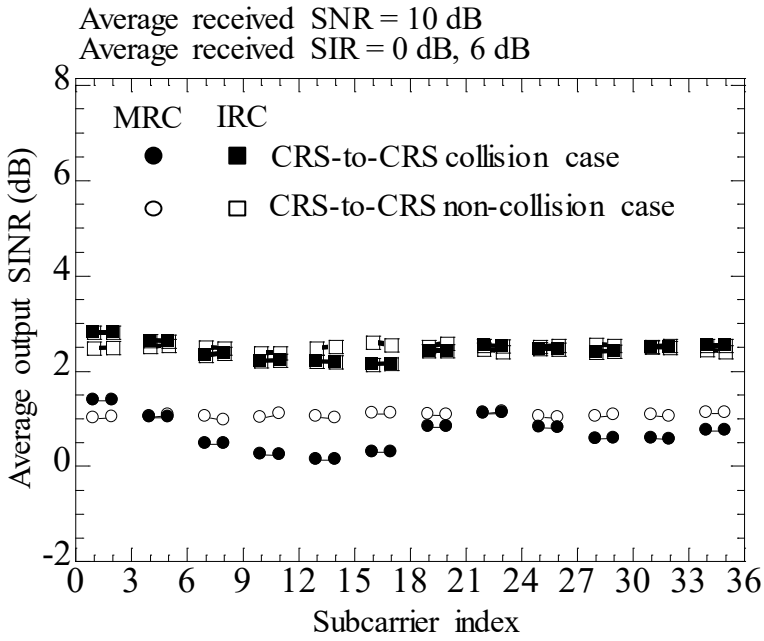

(b) OFDM symbol in CRS transmission

Figure 2-6. Average output SINR for each subcarrier (closed-loop transmit diversity)

2.2.3.2. Throughput Performance Evaluation

The throughput performance is evaluated in this section. Figures 2-7(a) and (b) show the performance results for the IRC and MRC receiver assuming open- and closed-loop transmit diversity, respectively. Note that the average received SIRs and SNR are assumed to be the same as those for the output SINR evaluation. In regard to the open-loop MIMO system in Fig. 2-7(a), the results show that the gain from the IRC receiver compared to that for the MRC receiver is almost the same regardless of the CRS-to-CRS collision and CRS-to-CRS non-collision cases, which corresponds to the above discussion. Furthermore, regarding the closed-loop MIMO system in Fig. 2-7(b), the gain from the IRC receiver in the CRS-to-CRS collision case is degraded compared to the gain in the CRS-to-CRS non-collision case. The gain however, can be achieved even when the CRS-to-CRS collision case is assumed.

To confirm the previous observations in various environments, i.e., various average received SNRs and SIRs, we additionally evaluated the throughput performance. In the additional evaluation, the average received SNR is assumed to be from 0 dB to 30 dB under the assumption of the average received SIR for each interfering cell of 0 dB and 6 dB, respectively. Figures 2-8(a) and (b) show the results of the throughput versus the average received SNR for open- and closed-loop transmit diversity, respectively. Focusing on the low SNR region for both results, the gain from the IRC receiver is reduced compared to that in the middle and high SNR regions regardless of the CRS-to-CRS collision case or the CRS-to-CRS non-collision case. This is because the effect of the null beamforming at the IRC receiver is degraded due to the noise-limited environment. However, assuming the case where the average received SNR is over 0 dB, the tendency of the throughput performance corresponds to the previous observations. Specifically, although the gain from the IRC receiver is almost the same regardless of the CRS-to-CRS collision and CRS-to-CRS non-collision cases assuming open-loop transmit diversity, the gain from the IRC receiver for the CRS-to-CRS collision case is degraded compared to that for the CRS-to-CRS non-collision case assuming closed-loop transmit diversity. Furthermore, we confirmed that a gain is achieved even for the CRS-to-CRS collision case when the average received SNR is over 0 dB.

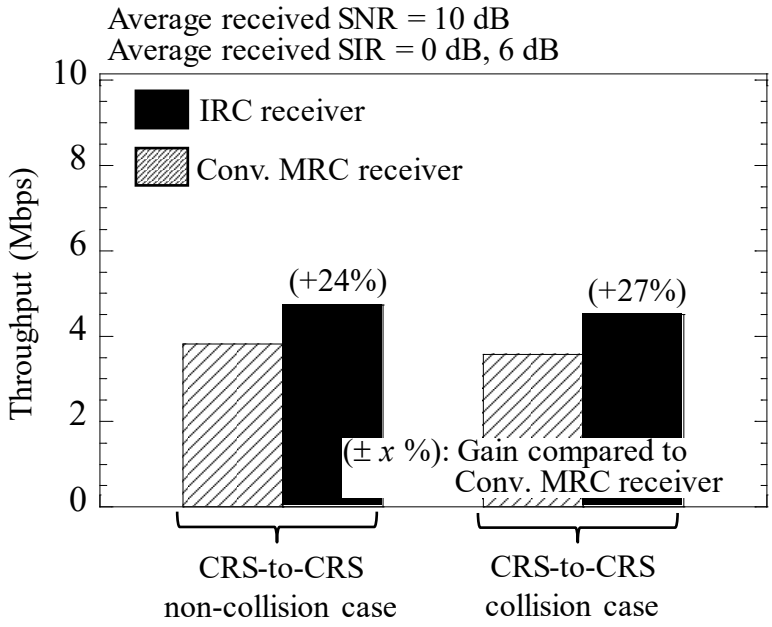

(a) Open-loop transmit diversity using SFBC

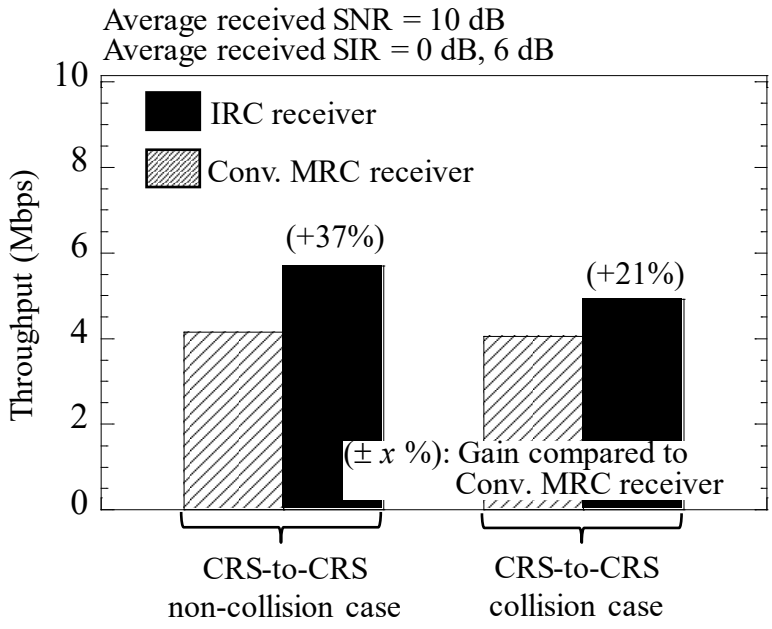

(b) Closed-loop transmit diversity using precoding

Figure 2-7. Throughput performance.

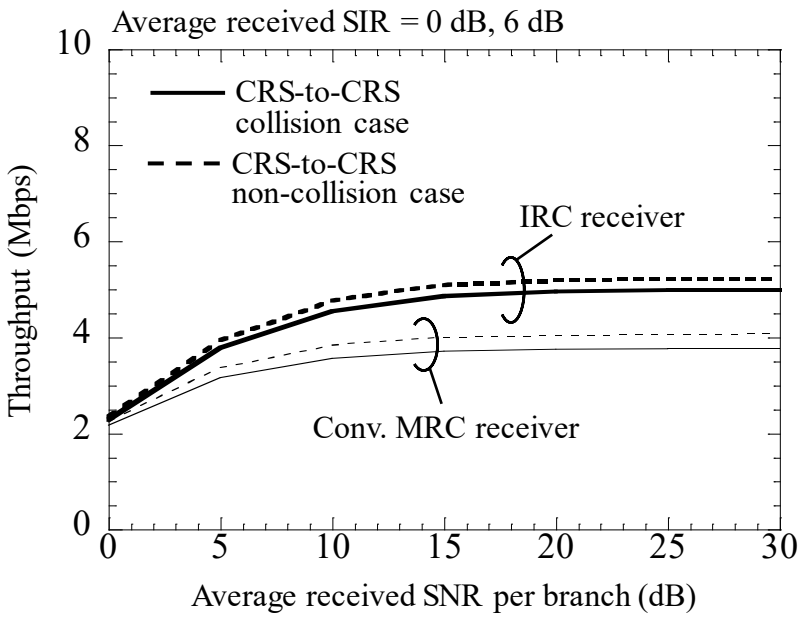

(a) Open-loop transmit diversity using SFBC

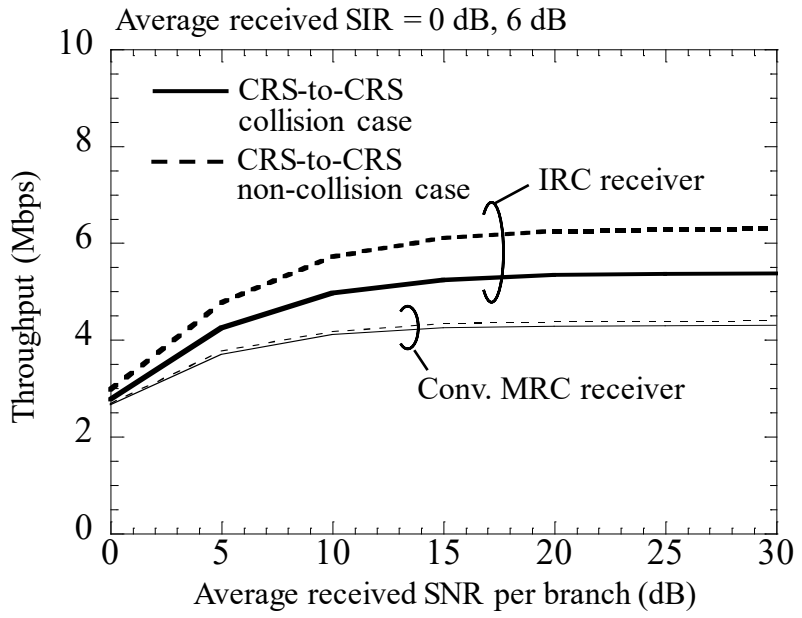

(b) Closed-loop transmit diversity using precoding

Figure 2-8. Throughput vs. average received SNR.

Finally, we evaluated the throughput performance when the average received SIR for the dominant interfering cell is assumed to be from -3 dB to 6 dB under the assumption of the average received SIR for the other interfering cell of 6 dB and the average received SNR of 10 dB. In this evaluation, the case where the received signal power from the interfering cell is stronger than that of the serving cell is also considered, i.e., SIR of less than 0 dB. This is because a handover margin called a hysteresis is considered in this dissertation to avoid an excess number of handovers, i.e., a ping-pong effect in which the user is handed back and forth several times from one base station to the other when the user moves around the cell boundary. Note that this handover hysteresis is assumed to be set to 3 dB as an example case in this dissertation.

Figures 2-9(a) and (b) show the results of the throughput versus the average received SIR for the dominant interfering cell, assuming open- and closed-loop transmit diversity, respectively. The results show that the performance tendency also corresponds to the previous observations regardless of the average received SIR for the dominant interfering cell.

Based on all the results, we can say that the gain from the IRC receiver is achieved even for the CRS-to-CRS collision case when the transmitter and receiver antenna branches are assumed to be two and two, respectively, although the impact on the estimation accuracy of the covariance matrix for the CRS-to-CRS collision case is dominant compared to that on the effect of suppressing interference for the CRS-to-CRS non-collision case assuming closed-loop transmit diversity.

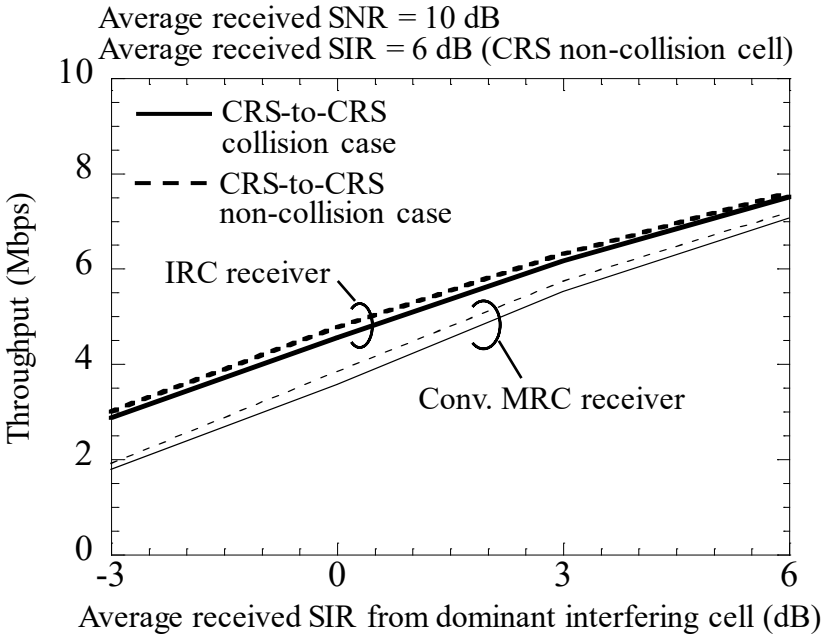

(a) Open-loop transmit diversity using SFBC

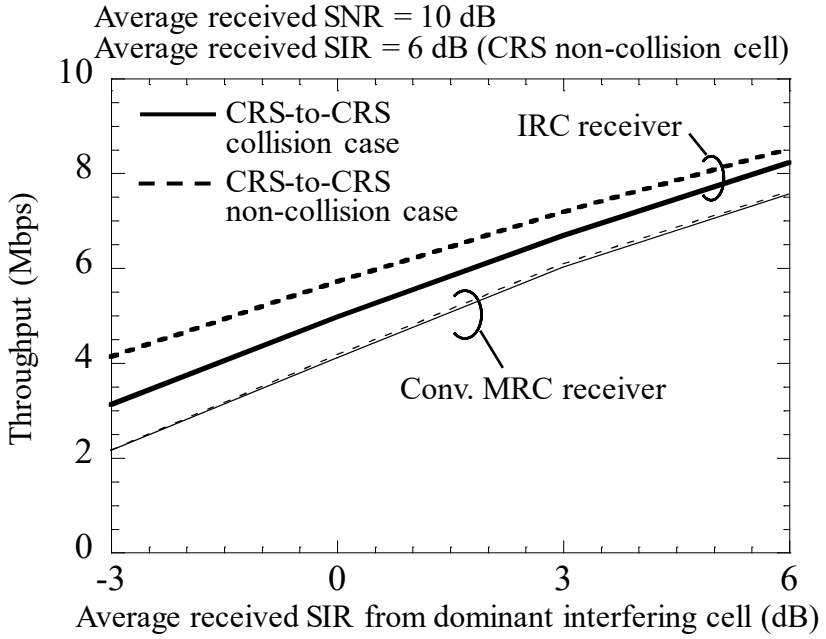

(b) Closed-loop transmit diversity using precoding

Figure 2-9. Throughput vs. average received SIR from dominant interfering cell

2.3. System Level Analysis

In the previous section, the link evaluation results of the IRC receiver are provided. From the results, it is expected that the IRC receiver can achieve better system capacity compared with the conventional receiver. Further performance improvement is expected by utilization the IRC receiver together with other techniques, e.g. CoMP transmission technique, as described in Chap. 1. To analyze the system capacity of such a combination of the IRC receiver and other technique, the link performance modeling is developed for the IRC receiver in this section.

2.3.1. Link Performance Modeling

First, overall procedure of the link performance modeling for the conventional receiver is described in this section. As the interface between the link and system level simulations, the BLER versus the average SINR performance has been widely used [12]-[14]. Therefore, the actual SINR should be modeled in the system level simulation. Figure 2-10 illustrates a methodology for the system level evaluation using link performance. At the system level, multiple UEs are distributed in the assumed multi-cell deployment. Based on the position of the UE, the channel matrix is generated for each UE including the effect of distance-dependent path loss, shadowing, and multipath fading. When MIMO transmission and reception techniques, e.g., precoding transmission and IRC reception, are assumed, the output SINR of the n-th transmission stream for the k-th subcarrier and the l-th OFDM symbol, $SINR_{\mathrm{out},n}(k,l)$, after reception processing is required [13]. This is calculated using the following formula.

$$SINR_{\mathrm{out},n}(k,l)=\frac{\frac{P_{\mathrm{Data}}}{N_{\mathrm{Stream}}}\mathbf{w}_{\mathrm{Rx},n}(k,l)\mathbf{G}_0(k,l)\mathbf{G}_0^H(k,l)\mathbf{w}_{\mathrm{Rx},n}^H(k,l)}{\mathbf{w}_{\mathrm{Rx},n}(k,l)\left(\sum_{q=1}^{N_{\mathrm{cell}}-1}\frac{P_{\mathrm{Data},q}}{N_{\mathrm{Stream}}}\mathbf{G}_q(k,l)\mathbf{G}_q^H(k,l)+\sigma_N^2\mathbf{I}\right)\mathbf{w}_{\mathrm{Rx},n}^H(k,l)}, \tag{2.14}$$

Here, $\mathbf{G}_q(k,l)$ represents the ($N_{\mathrm{Rx}} \times N_{\mathrm{Stream}}$) composite channel matrix defined as $\mathbf{H}_q(k,l)\mathbf{W}_{\mathrm{Tx},q}(k,l)$ between the q-th cell and the UE. Term $\mathbf{w}_{\mathrm{Rx},n}(k,l)$ is the n-th row vector of the ($N_{\mathrm{Stream}} \times N_{\mathrm{Rx}}$) receiver weight matrix of the serving cell, $\mathbf{W}_{\mathrm{Rx},0}$. Term $P_{\mathrm{Data},q}$ is the transmission power of the data signal in the q-th cell. From this formula, the actual receiver weight matrix including the estimation errors must be calculated to obtain the actual output SINR.

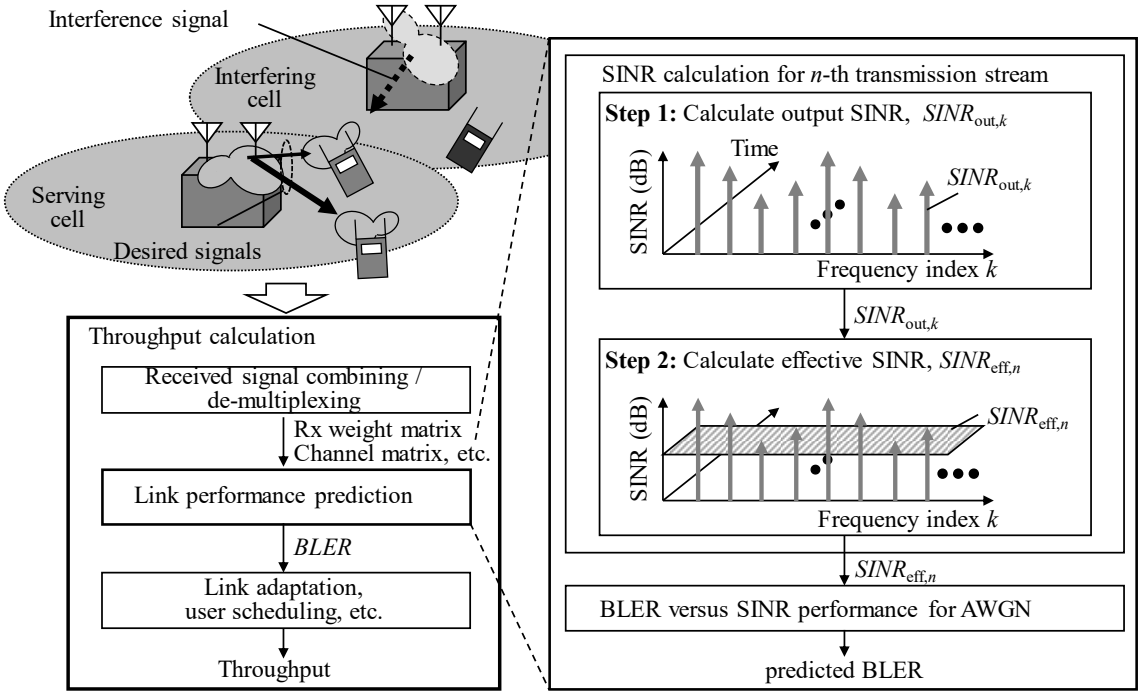

Figure 2-10. Outline of link to system mapping scheme

To address the frequency selective fading channel, the effective SINR of the n-th transmission stream, $SINR_{\text{eff},n}$, within the transmission bandwidth must be translated from $SINR_{\text{out},n}(k,l)$ using a model function, f. Once $SINR_{\text{eff},n}$ is calculated for each transmission stream, it can be used to find the block error probability for different modulation and coding schemes (MCSs) from the BLER performance for additive white Gaussian noise (AWGN) in the link level simulation. Using the block error probability, the throughput performance can be calculated in the system level simulation.

As a model function, f, Exponential Effective SINR Mapping (EESM) or Mutual Information based Exponential SINR Mapping (MIESM) is widely utilized. It was shown that MIESM has greater prediction accuracy especially when assuming a higher modulation order, but both schemes are sufficiently accurate to predict the link performance [15, 16]. Therefore, we focus on EESM in this dissertation. The model function for EESM is basically derived from Chernoff bound of bit error probability for BPSK (Binary Phase Shift Keying) over AWGN channel without any channel coding scheme. For a certain subcarrier, it is well known that the bit error probability for BPSK over AWGN channel assuming SNR r and a symbol distance 1, $P_e(1,r)$, is described as below.

$$P_e(1,r)=Q\left(\sqrt{2r}\right), \tag{2.15}$$

where $Q(x)$ is the Q-function, which is the probability that a standard normal random variable X takes a value larger than $x > 0$ defined as below.

$$Q(x)=\frac{1}{\sqrt{2\pi}}\int_{x}^{\infty}\exp\left(-\frac{t^2}{2}\right)dt\,. \tag{2.16}$$

It is also well known that the Q-function can be upper bounded by Chernoff bound as follows.

$$Q(x) \le \exp\left(-\frac{x^2}{2}\right). \tag{2.17}$$

Therefore, the Eq. (2-15) is upper bounded as follows:

$$P_e(1,r) \le \exp(-r)\,. \tag{2.18}$$

Without channel coding scheme, the BLER can be considered as a probability of at least one error over N_{subcar} subcarriers with corresponding SNR r_k. The probability is described as follows:

$$BLER=1-\prod_{k=1}^{N_{subcar}}\left(1-P_e(1,r_k)\right), \tag{2.19}$$

where N_{subcar} represents the total number of allocated subcarriers k. Applying Eq.(2-18) to Eq.(2-19) followed by expanding the polynomial and discarding the second order items, the following Eq.(2-20) can be obtained:

$$BLER \approx \sum_{k=1}^{N_{subcar}}\exp(-r_k)\,. \tag{2.20}$$

The goal of EESM is find an equivalent SNR, SNR_{eff}, which has the same BLER as Eq.(2-20) over AWGN channel, i.e.,

$$N_{subcar}\exp\left(-SNR_{eff}\right)=\sum_{k=1}^{N_{subcar}}\exp(-r_k)\,. \tag{2.21}$$

From Eq.(2.21), we can finally obtain the following equation.

$$SNR_{eff}=-\ln\left(\frac{1}{N_{subcar}}\sum_{k=1}^{N_{subcar}}\exp(-r_k)\right). \tag{2.22}$$

By similar approach, the effective SNR for QPSK (Quadrature Phase Shift Keying) can be obtained as follows:

$$SNR_{eff} = -2\ln\left(\frac{1}{N_{subcar}}\sum_{k=1}^{N_{subcar}}\exp\left(-\frac{r_k}{2}\right)\right). \quad (2.23)$$

For higher order modulation such as 16QAM, however, the same approach is not straightforward, then the generalized EESM is proposed as follows [14]:

$$SNR_{eff} = -\beta_{opt}\ln\left(\frac{1}{N_{subcar}}\sum_{k=1}^{N_{subcar}}\exp\left(-\frac{r_k}{\beta_{opt}}\right)\right), \quad (2.24)$$

where the parameter β_{opt} is training parameter that can be adjusted to minimize prediction error. The value of β_{opt} is optimized by link level simulation according to the following criteria.

$$MSE_{t,\beta} \cong \left|\log_{10} BLER^{t}_{actual} - \log_{10} BLER^{t}_{predicted,\beta}\right|^2, \quad (2.25)$$

$$\beta_{opt} = \arg\min_{\beta}\frac{1}{N_{Trial}}\sum_{t=1}^{N_{Trial}} MSE_{t,\beta}, \quad (2.26)$$

where $BLER^{t}_{actual}$ represents the actual BLER performance with a given modulation order in trial t, and $BLER^{t}_{predicted,\beta}$ represents the predicted BLER performance by given β in trial t. Term N_{Trial} represents total number of trials for the training process. Note that $BLER^{t}_{predicted,\beta}$ is calculated by mapping the effective SNR in Eq.(2.24) to the AWGN curve.

For the current mobile communication system, on the other hand, channel coding scheme such as turbo coding is usually employed, and it is not straightforward to directly derive the effective SNR including the effectiveness of channel coding by closed form. For such system, therefore, the same approach in Eqs.(2.24)-(2.26) can be utilized to derive the effective SNR, and the parameter β can adjust the impact of the channel coding scheme. The parameter β is derived for each MCS and transmission MIMO stream, hence the effective SINR after channel equalizing and transmission signal decomposition can be calculated as follows [17]:

$$SINR_{\mathrm{eff},n} = -\beta_{MCS,rank}\ln\left(\frac{1}{N_{subcar}}\sum_{k=1}^{N_{subcar}}\exp\left(-\frac{SINR_{out,n}(k,l)}{\beta_{MCS,rank}}\right)\right), \quad (2.27)$$

where $\beta_{MCS,\ rank}$ is a training parameter for the given MCS and rank. Note that rank means the number of transmission MIMO streams, and the OFDM symbol index l is an arbitrary value.

2.3.2. IRC Receiver for System Level Evaluation

In order to estimate the BLER including the channel coding gain for the IRC receiver, the output

SINR after IRC reception including an effect of interference suppression, i.e. the output SINR in Eq. (2.14) when the IRC receiver weight is applied, needs to be modeled. Furthermore, the output SINR after IRC reception should include estimation errors to evaluate the accurate system capacity by the system level simulation. Therefore, to model the output SINR for the IRC receiver, two modeling schemes are required: covariance matrix estimation error modeling and channel estimation error modeling. Regarding the former, the scheme using the complex Wishart distribution was proposed in [18, 19]. It was shown that the covariance matrix can be approximated accurately assuming a frequency flat fading channel by this scheme. However, when assuming a frequency selective fading channel, there is a problem in that the accuracy of this modeling scheme is expected to degrade since the frequency selectivity is not considered in this scheme. Regarding the latter, i.e., the channel estimation error, a scheme using statistics of the mean square error (MSE) of the estimated channel coefficients was proposed in [20]. However, since this scheme does not consider the channel fading fluctuations in the time and frequency domains, there is a problem in that the accuracy of this modeling scheme is also expected to degrade. Therefore, this dissertation investigates and proposes modeling schemes to address the above problems. One modeling scheme is for the covariance matrix. It averages the conventional approximation using the complex Wishart distribution in the frequency domain. The other is an accurate modeling scheme for the channel estimation error derived according to the ideal channel response of all cells and a channel estimation filter. To clarify the effectiveness of the proposed schemes, we conduct a multi-cell link level simulation assuming two-cell and three-cell model environments, and evaluate the performance of the IRC receiver employing the proposed modeling schemes from the viewpoints of the output SINR and BLER performance.

2.3.2.1. Signal Model and IRC Receiver Weight Generation

As descried in Sect. 2.2, various transmission modes and RS structures are supported in LTE/LTE-Advanced. When considering CRS-based transmission mode, the performance gain of the IRC receiver is slightly degraded in the CRS-to-CRS collision case due to inadequate interference covariance as shown in the previous section. When considering DMRS-based covariance estimation, on the other hand, such problem is not occurred since the DMRS is transmitted with the same transmit precoding as the data signal, while CRS is transmitted without any transmit precoding. Therefore, collision/non-collision of DMRS within the cells does not have an impact on the performance of the IRC receiver. Hence, for the sake of the simplicity of the analysis, hereafter we assume DMRS-based transmission mode.

i) Signal model

Assuming the number of receiver antenna branches is N_{Rx}, the N_{Rx}-dimensional received signal vector of the k-th subcarrier and the l-th OFDM symbol, $\mathbf{y}(k,l)$, is expressed as follows.

$$\mathbf{y}(k,l)=\sum_{q=0}^{N_{Cell}-1}\mathbf{G}_q(k,l)\mathbf{s}_q(k,l)+\mathbf{n}(k,l)\,. \tag{2.28}$$

The recovered signal vector at the UE, $\hat{\boldsymbol{s}}_0(k,l)$, is detected by using the receiver weight matrix, $\mathbf{W}_{\mathrm{Rx},0}(k,l)$, as follows.

$$\hat{\mathbf{s}}_0(k,l)=\mathbf{W}_{\mathrm{Rx},0}(k,l)\mathbf{y}(k,l)\,, \tag{2.29}$$

ii) IRC receiver weight generation with estimation errors

The IRC receiver weight matrix, $\mathbf{W}_{\mathrm{IRC}}(k,l)$, is expressed as follows.

$$\mathbf{W}_{\mathrm{IRC}}(k,l)=\frac{P_{\mathrm{Data}}}{N_{\mathrm{Stream}}}\hat{\mathbf{G}}_0^H(k,l)\left(\hat{\mathbf{G}}_0(k,l)\hat{\mathbf{G}}_0^H(k,l)+\hat{\mathbf{R}}_{I+N}(k,l)\right)^{-1}, \tag{2.30}$$

where $\hat{\mathbf{G}}_0(k,l)$ is the estimated channel matrix of the serving cell using DMRS that estimates $\mathbf{G}_0(k,l)$ without the precoding matrix information, and $\hat{\mathbf{R}}_{I+N}(k,l)$ is the estimated covariance matrix that includes only interference and noise. Using $\mathbf{W}_{\mathrm{IRC}}(k,l)$ as $\mathbf{W}_{\mathrm{Rx},0}(k,l)$, the recovered signal vector is detected while suppressing the interference signals. Assuming the ($N_{\mathrm{Rx}} \times N_{\mathrm{Stream}}$) estimation error matrix to be $\mathbf{Z}_{\mathrm{c}}(k,l)$ due to the DMRS, the estimated channel matrix of the serving cell, $\hat{\mathbf{G}}_0(k,l)$, can be expressed as follows.

$$\hat{\mathbf{G}}_0(k,l) = \mathbf{G}_0(k,l) + \mathbf{Z}_{\mathrm{c}}(k,l)\,, \tag{2.31}$$

In regard to the covariance matrix that includes only interference and noise, the DMRS-based covariance matrix estimation scheme [19] is employed. Applying this scheme, the estimated covariance matrix, $\hat{\mathbf{R}}_{I+N}(k,l)$, can be expressed as follows in principle.

$$
\begin{aligned}
\hat{\mathbf{R}}_{I+N}(k,l) &= E\left[(\mathbf{y}(k,l)-\hat{\mathbf{G}}_0(k,l)\mathbf{d}_0(k,l))(\mathbf{y}(k,l)-\hat{\mathbf{G}}_0(k,l)\mathbf{d}_0(k,l))^H\right] \\
&= E\left[\mathbf{y}(k,l)\mathbf{y}^H(k,l)\right]-E\left[\mathbf{y}(k,l)\mathbf{d}_0^H(k,l)\hat{\mathbf{G}}_0^H(k,l)\right] \\
&\quad -E\left[\hat{\mathbf{G}}_0(k,l)\mathbf{d}_0(k,l)\mathbf{y}^H(k,l)\right]+E\left[\hat{\mathbf{G}}_0(k,l)\mathbf{d}_0(k,l)\mathbf{d}_0^H(k,l)\hat{\mathbf{G}}_0^H(k,l)\right] \\
&= E\left[\left(\sum_{q=0}^{N_{\text{Cell}}-1}\mathbf{G}_q(k,l)\mathbf{s}_q(k,l)+\mathbf{n}(k,l)\right)\left(\sum_{q=0}^{N_{\text{Cell}}-1}\mathbf{G}_q(k,l)\mathbf{s}_q(k,l)+\mathbf{n}(k,l)\right)^H\right] \\
&\quad -E\left[\left(\sum_{q=0}^{N_{\text{Cell}}-1}\mathbf{G}_q(k,l)\mathbf{s}_q(k,l)+\mathbf{n}(k,l)\right)\mathbf{d}_0^H(k,l)\left(\mathbf{G}_0^H(k,l)+\mathbf{Z}_{\text{c}}(k,l)\right)^H\right] \\
&\quad -E\left[\left(\mathbf{G}_0^H(k,l)+\mathbf{Z}_{\text{c}}(k,l)\right)\mathbf{d}_0(k,l)\left(\sum_{q=0}^{N_{\text{Cell}}-1}\mathbf{G}_q(k,l)\mathbf{s}_q(k,l)+\mathbf{n}(k,l)\right)^H\right] \\
&\quad +E\left[\left(\mathbf{G}_0^H(k,l)+\mathbf{Z}_{\text{c}}(k,l)\right)\mathbf{d}_0(k,l)\mathbf{d}_0^H(k,l)\left(\mathbf{G}_0^H(k,l)+\mathbf{Z}_{\text{c}}(k,l)\right)\right] \\
&= \sum_{q=0}^{N_{\text{Cell}}-1}\mathbf{G}_q(k,l)E\left[\mathbf{s}_q(k,l)\mathbf{s}_q^H(k,l)\right]\mathbf{G}_q^H(k,l)+E\left[\mathbf{n}(k,l)\mathbf{n}^H(k,l)\right] \\
&\quad -\mathbf{G}_0(k,l)E\left[\mathbf{d}_0(k,l)\mathbf{d}_0^H(k,l)\right]\mathbf{G}_0^H(k,l)-\mathbf{G}_0(k,l)E\left[\mathbf{d}_0(k,l)\mathbf{d}_0^H(k,l)\right]\mathbf{G}_0^H(k,l) \\
&\quad +\mathbf{G}_0(k,l)E\left[\mathbf{d}_0(k,l)\mathbf{d}_0^H(k,l)\right]\mathbf{G}_0^H(k,l)+E\left[\mathbf{Z}_{\text{c}}(k,l)\mathbf{d}_0(k,l)\mathbf{d}_0^H(k,l)\mathbf{Z}_{\text{c}}(k,l)\right] \\
&= \sum_{q=1}^{N_{\text{Cell}}-1}\frac{P_{\text{Data},q}}{N_{\text{Stream}}}\mathbf{G}_q(k,l)\mathbf{G}_q^H(k,l)+\frac{P_{\text{Data}}}{N_{\text{Stream}}}E\left[\mathbf{Z}_{\text{c}}(k,l)\mathbf{Z}_{\text{c}}^H(k,l)\right]+\sigma_N^2\mathbf{I}.
\end{aligned}
\tag{2.32}
$$

where $\mathbf{d}_0(k,l)$ is the DMRS sequence of the serving cell and $E[\|\mathbf{d}_0(k,l)\|^2]=P_{\text{Data}}$. Note that the subcarrier index and OFDM symbol index belong to $\mathbf{M}_{\text{DMRS}}$, which is the DMRS RE group of the serving cell. Furthermore, we assume that the data signal vectors of different cells, $\mathbf{s}_q(k,l)$, the DMRS sequence vector of the serving cell, $\mathbf{d}_0(k,l)$, and the noise vector, $\mathbf{n}(k,l)$, are uncorrelated. Furthermore, $E[\mathbf{s}_q(k,l)\mathbf{s}_q^H(k,l)]=(P_{\text{Data}}/N_{\text{Stream}})\mathbf{I}$, $E[\mathbf{d}_0(k,l)\mathbf{d}_0^H(k,l)]=(P_{\text{Data}}/N_{\text{Stream}})\mathbf{I}$, and $E[\mathbf{n}(k,l)\mathbf{n}^H(k,l)]=\sigma_N^2\mathbf{I}$ are defined in the derivation. In a practical application, the number of averaged samples is limited. Therefore, $\hat{\mathbf{R}}_{I+N}(k,l)$ is averaged using multiple DMRS resource elements (REs) as follows.

$$
\bar{\mathbf{R}}_{I+N}=\frac{1}{N_{\text{sp}}}\sum_{k,l\in\mathbf{M}_{\text{DMRS}}}\left(\mathbf{y}(k,l)-\hat{\mathbf{G}}_0(k,l)\mathbf{d}_0(k,l)\right)\left(\mathbf{y}(k,l)-\hat{\mathbf{G}}_0(k,l)\mathbf{d}_0(k,l)\right)^H. \tag{2.33}
$$

Note that N_{sp} is the number of averaged samples (DMRSs) within a resource block (RB) or continuous RBs. When applying this estimation scheme, the IRC receiver utilizes the same covariance matrix that includes only interference and noise within some RBs. Therefore, the maximum gain from the IRC receiver cannot be achieved. However, from the cell-edge user throughput evaluation results summarized in [6], the IRC receiver can achieve enough performance gain as shown in Sect. 2.2.3.2.

In the system level simulation, the estimated covariance matrix, $\bar{\mathbf{R}}_{I+N}$, and the channel estimation error, $\mathbf{Z}_c$, must be modeled since the actual data signals and DMRSs are not generated. Both modeling schemes are described in the next section.

2.3.1.3. Covariance Matrix Estimation Error Modeling

i) Conventional method assuming frequency flat fading channel

As the covariance matrix estimation error modeling scheme, a scheme using the complex Wishart distribution was proposed in [18, 19]. In [19], the scheme for applying the complex Wishart distribution for DMRS based covariance matrix estimation was proposed assuming a frequency flat fading channel. From the Eq.(2-33), we can see that the covariance matrix of the interference cells, $\hat{\mathbf{R}}_{I+N}(k,l)$, is derived by summing the channel covariance matrix of the q-th cell, $\mathbf{G}_q(k,l)\mathbf{G}_q^H(k,l)$. Therefore, when assuming a frequency flat fading channel, i.e., the channel covariance matrix is constant within the DMRS samples for averaging, it can be approximated using the complex Wishart distribution with N_{sp} degrees of freedom as follows.

$$\bar{\mathbf{R}}_{I+N} = \frac{1}{N_{\text{sp}}} W_{N_{Rx}}\left(\hat{\mathbf{R}}_{I+N}(k,l), N_{\text{sp}}\right), \tag{2.34}$$

where $W_{N\text{Rx}}\left(\hat{\mathbf{R}}_{I+N}(k,l), N_{\text{sp}}\right)$ is a random matrix that obeys the N_{Rx}-variate complex Wishart distribution with scale matrix $\hat{\mathbf{R}}_{I+N}(k,l)$ and N_{sp} degrees of freedom. Furthermore, $W_{N\text{Rx}}\left(\hat{\mathbf{R}}_{I+N}(k,l), N_{\text{sp}}\right)$ can be modeled using the Bartlett decomposition [21] as follows.

$$W_{N_{Rx}}\left(\hat{\mathbf{R}}_{I+N}(k,l), N_{\text{sp}}\right) = \mathbf{QAA}^H\mathbf{Q}^H, \tag{2.35}$$

where $\mathbf{Q}$ is calculated using the Cholesky decomposition of $\hat{\mathbf{R}}_{I+N}(k,l)$. Term $\mathbf{A}$ is the lower-triangle matrix generated according to the complex Wishart distribution as follows.

$$\mathbf{A} = \begin{bmatrix} \sqrt{c_1/2} & 0 & \cdots & \\ n_{21} & \sqrt{c_2/2} & \cdots & \vdots \\ \vdots & \vdots & \ddots & \\ n_{N_{\text{Rx}}1} & n_{N_{\text{Rx}}2} & \cdots & c_N \quad /2 \end{bmatrix}, \tag{2.36}$$

where c_i follows the Chi-square distribution, i.e., $c_i \sim$ $_{\text{sp}} - i + 1))$,and n_{ij} follows a complex Gaussian random variable, i.e., $n_{ij} \sim$.

Following the approximation in Eq.(2.34), the estimated covariance matrix is modeled assuming that the frequency flat fading channel model, i.e., scale matrix, $\hat{\mathbf{R}}_{I+N}(k,l)$, is the same regardless of the subcarrier and OFDM indices. Therefore, when a frequency selective fading channel is assumed, the accuracy of this modeling scheme is expected to degrade.

i) Proposed method assuming frequency selective fading channel

To address the problem of a frequency selective fading channel, we propose a modified scheme based on the complex Wishart distribution. In this scheme, the approximation in Eq.(2.34) is applied to each DMRS RE and averaged in the frequency domain as follows.

$$\bar{\mathbf{R}}_{I+N}=\frac{1}{N_{\text{freq}}}\sum_{u=1}^{N_{\text{freq}}}\frac{N_{\text{freq}}}{N_{\text{sp}}}W_{N_{\text{Rx}}}\left(\hat{\mathbf{R}}_{I+N}(k_u,l_v),N_{\text{sp}}/N_{\text{freq}}\right),\ (k_u,l_v\in\mathbf{M}_{\text{DMRS}}), \tag{2.37}$$

where N_{freq} is the number of the DMRSs in the frequency domain, and the k_u-th subcarrier ($1 \le u \le N_{\text{freq}}$) and the l_v-th OFDM symbol ($1 \le v \le N_{\text{time}}$: number of the DMRSs in the time domain) represent the DMRS RE position. Using the Cholesky decomposition of $\hat{\mathbf{R}}_{I+N}(k_u,l_v)$ as $\mathbf{Q}_u$ the lower-triangle matrix generated according to the complex Wishart distribution as $\boldsymbol{A}_u$, Eq.(2.32) can be modeled using the Bartlett decomposition as follows.

$$\bar{\mathbf{R}}_{I+N}=\frac{1}{N_{\text{sp}}}\sum_{u=1}^{N_{\text{freq}}}\mathbf{Q}_u\mathbf{A}_u\mathbf{A}_u^H\mathbf{Q}_u^H\ , \tag{2.38}$$

Since the fluctuations of the estimated covariance matrix in the frequency domain are included in the modeling result from Eq.(2.38), the accuracy of the modeling is expected to be improved compared to the conventional method.

2.3.1.4. Channel Estimation Error Modeling

In this section, the modeling scheme of the channel estimation error, $\mathbf{Z}_{\text{c}}$, is discussed. First, we investigate the second-order statistic of $\mathbf{Z}_{\text{c}}$, i.e., $E[\mathbf{Z}_{\text{c}}(k,l)\mathbf{Z}_{\text{c}}^H(k,l)]$ in Eq.(2.32), to model the channel estimation error. Term $E[\mathbf{Z}_{\text{c}}(k,l)\mathbf{Z}_{\text{c}}^H(k,l)]$ is expressed using its coefficient, $z_{ij}(k,l)$, as follows.

$$E\left[\mathbf{Z}_{\text{c}}(k,l)\mathbf{Z}_{\text{c}}^H(k,l)\right]=\sum_{j=1}^{N_{\text{Stream}}}\begin{bmatrix} E\left[\left|z_{1j}(k,l)\right|^2\right] & \cdots E\ z_{j}\ k,l)z_{N_{\text{Rx}}j}^*(k,l)\right] \\ \vdots & \ddots \quad \vdots \\ E\left[z_{N_{\text{Rx}}j}(k,l)z_{1j}^*(k,l)\right]\cdots & E\left[z_{N_{\text{Rx}}j}(k,l)\right|^2\right] \end{bmatrix}, \tag{2.39}$$

It is assumed that the elements of $\mathbf{Z}_{\text{c}}$ as AWGN, i.e., $z_{ij}(k,l) \sim$ $\mathbb{I}[|z_{ij}(k,l)|^2])$. Therefore, there are two parameters to model the channel estimation error, i.e., the auto-covariance, $E[|z_{ij}(k,l)|^2]$, and cross-covariance, $E[z_{ij}(k,l)z_{i'j}^*(k,l)]$ $(i \ne i')$. To derive these parameters, the scheme using the MSE statistic of the estimated channel coefficients based on a channel estimation filter was proposed in [20]. This scheme is described as Method 1 hereafter. Furthermore, we propose another modeling scheme according to the ideal channel response of all cells and a channel estimation filter to model the fluctuations in the estimation error due to the channel fading fluctuations in the time and frequency domains. This scheme is referred to as Method 2 hereafter.

i) Method 1 - using MSE statistic of estimated channel coefficients

In this dissertation, the channel estimation is performed using a channel estimation filter, e.g., 2-dimensional MMSE channel estimation filter [22]. When N_{RS} is the number of DMRSs for estimating the channel coefficient and the N_{RS}-dimensional channel estimation filter vector for estimating the channel coefficient for the k-th subcarrier and the l-th OFDM symbol is defined as $\boldsymbol{w}_{\mathrm{CE}}(k,l)$, the auto-covariance of the estimation error in Eq.(2.40), i.e., the MSE of the estimated channel coefficient, is derived as follows.

$$\begin{aligned} E\left[\left|z_{ij}(k,l)\right|^2\right] &= E\left[\left|g_{0,ij}(k,l) - \mathbf{w}_{CE}^T(k,l)\tilde{\mathbf{g}}_{RS\ ij}\right|^2\right] \\ &= P_g + \mathbf{w}_{CE}^T(k,l)\boldsymbol{\Phi}\mathbf{w}_{CE}^*(k,l) - \boldsymbol{\theta}^T\mathbf{w}_{CE}^*(k,l) - \mathbf{w}_{CE}^T(k,l)\boldsymbol{\theta}^* \end{aligned}, \tag{2.40}$$

where P_{g} is the average channel amplitude, $g_{0,ij}(k,l)$ is the channel coefficient of the k-th subcarrier and the l-th OFDM symbol between the i-th receiver antenna branch and the j-th transmission stream at the serving cell. Term $\tilde{\mathbf{g}}_{\ ij}$ is the N_{RS}-dimensional estimated channel vector based on the least square between the i-th receiver antenna branch and the j-th transmission stream at the serving cell consisting of the estimated channel coefficients at the DMRS RE. Terms Φ and $\boldsymbol{\theta}^T$ are the auto-covariance matrix of $\tilde{\mathbf{g}}_{\ ij}$ and the cross-covariance vector between $g_{0,ij}(k,l)$ and $\mathbf{g}_{\mathrm{RS},0,ij}$, respectively.

$$\boldsymbol{\Phi} = E\left[\mathbf{g}_{RS,0,ij}\mathbf{g}_{RS,0,ij}^H\right] + \left(\sigma_I^2 + \frac{\sigma_N^2}{P_g}\right)\mathbf{I}, \tag{2.41}$$

$$\boldsymbol{\theta}^T = E\left[g_{0,ij}(k,l)\mathbf{g}_{RS,0,ij}^H\right], \tag{2.42}$$

Here, $\mathbf{g}_{\mathrm{RS},0,ij}$ is the N_{RS}-dimensional ideal channel vector of the serving cell comprising the channel coefficients at the DMRS RE. Term σ_I^2 is the average received interference signal power. Note that the interference signals are assumed to be whitened sufficiently. Therefore, non-diagonal elements of the covariance matrix of the interference signal are assumed to be zero, i.e., $\sigma_I^2\mathbf{I}$. This is because the transmitted signals, i.e., data signals, reference signals, and control signals are assumed to be scrambled using a length-31 Gold sequence specified according to the cell ID [6], which is a pseudo-random sequence with a low cross-correlation [23]. More preciously, Eq.(2.30) is derived from $\tilde{\mathbf{g}}_{RS\ ij}$ which is the estimated channel vector based on multiplying the DMRS sequence of the serving cell. In this case, the interference signals are also multiplied by the DMRS sequence of the serving cell. Therefore, non-diagonal elements of the covariance matrix of the interference signal are whitened sufficiently due to the different Gold sequences between the serving and interfering cells. Terms Φ and $\boldsymbol{\theta}^T$ are calculated using the channel

model and the maximum Doppler frequency, i.e., using the statistic of the channel coefficients.

The cross-covariance in Eq.(2.39), i.e., $E[z_{ij}(k,l)z_{i'j}^{*}(k,l)]$ $(i \neq i')$, is expressed using the correlation coefficient between the receiver antenna branches, ρ_{Rx}, as follows.

$$E\left[z_{ij}(k,l)z_{i'j}^{*}(k,l) \right] = \rho_{\mathrm{RX}} E\left[\left| z_{ij}(k,l) \right|^{2} \right], \tag{2.43}$$

From Eq.(2.40) and Eq.(2.41), the auto-covariance and cross-covariance of the channel estimation error include only the statistic of the channel and the channel estimation filter; therefore, this modeling scheme does not correspond to the fluctuations in the estimation error in the time and frequency domains.

ii) Method 2 (proposed) - modeling error according to channel fluctuations

We propose Method 2 that uses the ideal channel response of all cells to model the fluctuations in the estimation error in the time and frequency domains. Specifically, the auto-covariance and the cross-covariance of the estimation error for Method 1 shown in Eq.(2.40) and Eq.(2.43) are replaced by Eq.(2.44) and Eq.(2.45). Note that the interference signals are assumed to be whitened sufficiently by the scrambling sequence for deriving Eq.(2.44) and Eq.(2.45); therefore, the terms regarding the interference signals are expressed as a diagonal matrix.

$$\begin{aligned} &E\left[\left| z_{ij}(k,l) \right|^{2} \right] = \left| g_{0,ij}(k,l) \right|^{2} \\ &+\mathbf{w}_{CE}^{T}(k,l)\left(\mathbf{g}_{RS,0,ij}\mathbf{g}_{RS,0,ij}^{H} + \sum_{q=1}^{N\mathrm{Cell}-1} diag\left(\left| g_{q,ij}(k_1,l_1) \right|^{2}, \cdots \ g_{q\ ij}\ k_{N\mathrm{RS}}, l_{N\mathrm{RS}} \right|^{2} \right) + \frac{\sigma_N^2}{P}\mathbf{I} \right) \mathbf{w}_{CE}^{*}(k,l), \\ &-g_{0,ij}(k,l)\mathbf{g}_{RS,0,ij}^{H}\mathbf{w}_{CE}^{*}(k,l) - \mathbf{w}_{CE}^{T}(k,l)\mathbf{g}_{RS,0,ij}g_{0,ij}^{*}(k,l) \end{aligned} \tag{2.44}$$

$$\begin{aligned} &E\left[z_{ij}(k,l)z_{i'j}^{*}(k,l) \right] = g_{0,ij}(k,l)g_{0,i'j}^{*}(k,l) \\ &+\mathbf{w}_{CE}^{T}(k,l)\left(\mathbf{g}_{RS,0,ij}\mathbf{g}_{RS,0,i'j}^{H} + \sum_{q=1}^{N\mathrm{Cell}-1} diag\left(g_{q,ij}(k_1,l_1)g_{q,i'j}^{*}(k_1,l_1), \cdots \ g_{q\ ij}\ k_{N\mathrm{RS}}, l_{N\mathrm{RS}} \right) g_{q,i'j}^{*}(k_{N\mathrm{RS}},l_{N\mathrm{RS}}) \right) + \frac{\sigma_N^2}{P}\mathbf{I} \mathbf{w}_{CE}^{*}(k,l), \\ &-g_{0,ij}(k,l)\mathbf{g}_{RS,0,i'j}^{H}\mathbf{w}_{CE}^{*}(k,l) - \mathbf{w}_{CE}^{T}(k,l)\mathbf{g}_{RS,0,ij}g_{0,i'j}^{*}(k,l) \end{aligned} \tag{2.45}$$

In the following, we show the derivation of those equations. First, $\mathbf{Z}_c(k,l)$ is expressed using the channel coefficient of the serving cell, $g_{0,ij}(k,l)$, the channel estimation filter, $\mathbf{w}_{\mathrm{CE}}$, and the estimated channel vector of the serving cell, $\tilde{\mathbf{g}}_{RS\ \ ij}$.

$$\mathbf{Z}_{\mathrm{c}}(k,l) = \begin{bmatrix} g_{0,00}(k,l) - \mathbf{w}_{CE}^{T}(k,l)\tilde{\mathbf{g}}_{RS} & \cdots & g_{\ \ N} & k\ l & \mathbf{w}_{CE}^{T}\ k\ l\ \tilde{\mathbf{g}}_{RS\ \ \ N} \\ \vdots & \ddots & & & \vdots \\ g_{0,N_{\mathrm{Rx}}0}(k,l) - \mathbf{w}_{CE}^{T}(k,l)\tilde{\mathbf{g}}_{RS\ \ N} & \cdots & g_{\ N\ \ N} & k\ l & \mathbf{w}_{CE}^{T}\ k\ l\ \tilde{\mathbf{g}}_{RS\ \ N\ \ N} \end{bmatrix}, \tag{2.46}$$

From Eq.(2.43), the second order statistic of $\mathbf{Z}_c(k,l)$, i.e., $E[\mathbf{Z}_{\mathrm{c}}(k,l)\mathbf{Z}_{\mathrm{c}}^{H}(k,l)]$, is expressed as follows.

$$E\left[\mathbf{Z}_c(k,l)\mathbf{Z}_c{}^H(k,l)\right]$$
$$=\sum_{j=1}^{N_{\text{Stream}}}\begin{bmatrix} E\left[\left|g_{0,0j}(k,l)-\mathbf{w}_{CE}^T(k,l)\tilde{\mathbf{g}}_{RS\ \ j}\right.\right. & \cdots & E\ g_{\ j}\ k\ l\ \ \mathbf{w}_{CE}^T\ k\ l\ \tilde{\mathbf{g}}_{RS\ \ j}\ g_{\ j}\ k\ l\ \ \mathbf{w}_{CE}^T\ k\ l\ \tilde{\mathbf{g}}_{RS\ \ j}{}^H \\ \vdots & \ddots & \vdots \\ E\left[\left(g_{0,\text{Rx}\,j}(k,l)-\mathbf{w}_{CE}^T(k,l)\tilde{\mathbf{g}}_{RS\ \ j}\right.\right. g_{\ j}\ k\ l\ \ \mathbf{w}_{CE}^T\ k\ l\ \tilde{\mathbf{g}}_{RS\ \ j}{}^H\Big] & \cdots & E\left[\left|g_{0,\text{Rx}\,j}(k,l)-\mathbf{w}_{CE}^T(k,l)\tilde{\mathbf{g}}_{RS\ \ j}\right.\right. \end{bmatrix}, \tag{2.47}$$

The diagonal and non-diagonal elements in Eq.(2.47) are expressed as follows.

$$\begin{aligned} &E\left[\left|g_{0,ij}(k,l)-\mathbf{w}_{CE}^T(k,l)\tilde{\mathbf{g}}_{RS\ \ ij}\right.\right] \\ &=\left|g_{0,ij}(k,l)\right|^2-g_{0,ij}(k,l)E\left[\tilde{\mathbf{g}}_{RS\ \ ij}^H\right]\mathbf{w}_{CE}(k,l) \\ &-\mathbf{w}_{CE}^T(k,l)E\left[\tilde{\mathbf{g}}_{RS\ \ ij}\ g_{\ ij}\ k\ l\ \ \mathbf{w}_{CE}^T\ k\ l\ E\tilde{\mathbf{g}}_{RS\ \ ij}\tilde{\mathbf{g}}_{RS\ \ ij}^H\right]\mathbf{w}_{CE}\ k\ l \end{aligned}, \tag{2.48}$$

$$\begin{aligned} &E\left[\left(g_{0,ij}(k,l)-\mathbf{w}_{CE}^T(k,l)\tilde{\mathbf{g}}_{RS\ \ ij}\right.\right. g_{\ i\,j}\ k\ l\ \ \mathbf{w}_{CE}^T\ k\ l\ \tilde{\mathbf{g}}_{RS\ \ i\,j}{}^H \\ &=g_{0,ij}(k,l)g_{0,i'j}^*(k,l)-g_{0,ij}(k,l)E\left[\tilde{\mathbf{g}}_{RS\ \ i\,j}^H\right]\mathbf{w}_{CE}(k,l) \\ &-\mathbf{w}_{CE}^T(k,l)E\left[\tilde{\mathbf{g}}_{RS\ \ ij}\ g_{\ i\,j}\ k\ l\ \ \mathbf{w}_{CE}^T\ k\ l\ E\tilde{\mathbf{g}}_{RS\ \ ij}\tilde{\mathbf{g}}_{RS\ \ i\,j}^H\right]\mathbf{w}_{CE}^*(k,l) \end{aligned}, \tag{2.49}$$

Here, the estimated channel vector, $\tilde{\mathbf{g}}_{RS\ \ ij}$, is expressed as follows.

$$\tilde{\mathbf{g}}_{RS\ \ ij}=\begin{bmatrix} g_{0,ij}(k_1,l_1)+\dfrac{d_0(k_1,l_1)}{\left|d_0(k_1,l_1)\right|^2}\left(\sum_{q=1}^{N_{\text{Cell}}-1}\sum_{j'=1}^{N_{\text{Stream}}}g_{q,ij'}(k_1,l_1)s_{q,j'}(k_1,l_1)+n_i(k_1,l_1)\right) \\ \vdots \\ g_{0,ij}(k_{N_{\text{sp}}},l_{N_{\text{sp}}})+\dfrac{d_0(k_{N_{\text{sp}}},l_{N_{\text{sp}}})}{\left|d_0(k_{N_{\text{sp}}},l_{N_{\text{sp}}})\right|^2}\left(\sum_{q=1}^{N_{\text{Cell}}-1}\sum_{j'=1}^{N_{\text{Stream}}}g_{q,ij'}(k_{N_{\text{sp}}},l_{N_{\text{sp}}})s_{q,j'}(k_{N_{\text{sp}}},l_{N_{\text{sp}}})+n_i(k_{N_{\text{sp}}},l_{N_{\text{sp}}})\right) \end{bmatrix}, \tag{2.50}$$

where $s_{q,j'}(k,l)$ and $n_i(k,l)$ are the transmitted symbol of the j'-th transmission stream at the q-th cell and the noise coefficient at the i-th receiver antenna branch on the k-th subcarrier and the l-th OFDM symbol, respectively. The expectation of $\tilde{\mathbf{g}}_{RS\ \ ij}$ is calculated as follows.

$$\begin{aligned} E\left[\tilde{\ }\right.&\begin{bmatrix} g_{0,ij}(k_1,l_1)+\dfrac{d_0(k_1,l_1)}{\left|d_0(k_1,l_1)\right|^2}E\left[\sum_{q=1}^{N_{\text{Cell}}-1}\sum_{j'=1}^{N_{\text{Stream}}}g_{q,ij'}(k_1,l_1)s_{q,j'}(k_1,l_1)+n_i(k_1,l_1)\right] \\ \vdots \\ g_{0,ij}(k_{N_{\text{sp}}},l_{N_{\text{sp}}})+\dfrac{d_0(k_{N_{\text{sp}}},l_{N_{\text{sp}}})}{\left|d_0(k_{N_{\text{sp}}},l_{N_{\text{sp}}})\right|^2}E\left[\sum_{q=1}^{N_{\text{Cell}}-1}\sum_{j'=1}^{N_{\text{Stream}}}g_{q,ij'}(k_{N_{\text{sp}}},l_{N_{\text{sp}}})s_{q,j'}(k_{N_{\text{sp}}},l_{N_{\text{sp}}})+n_i(k_{N_{\text{sp}}},l_{N_{\text{sp}}})\right] \end{bmatrix} \\ &=\begin{bmatrix} g_{0,ij}(k_1,l_1) \\ \vdots \\ g_{0,ij}(k_{N_{\text{sp}}},l_{N_{\text{sp}}}) \end{bmatrix} \\ &=\mathbf{g}_{\text{RS},0,ij} \end{aligned}, \tag{2.51}$$

In the derivation of Eq.(2.51), the cross-correlations between the DMRS sequence of the serving cell and the data signals from the interfering cells are assumed to be zero due to the different Gold sequences between the serving and interfering cells.

Here, we derive Eq.(2.44). The (m, m) diagonal elements of $E[\tilde{\mathbf{g}}_{RS\ \ ij}\tilde{\mathbf{g}}_{RS\ \ ij}^H$ in Eq.(2.48) are

calculated as in Eq.(2.52).

$$
\begin{aligned}
&E\left[\left|g_{0,ij}(k_m,l_m)+\frac{d_0(k_m,l_m)}{\left|d_0(k_m,l_m)\right|^2}\left(\sum_{q=1}^{N_{\mathrm{Cell}}-1}\sum_{j'=1}^{N_{\mathrm{Stream}}}g_{q,ij'}(k_m,l_m)s_{q,j'}(k_m,l_m)+n_i(k_m,l_m)\right)\right|^2\right] \\
&=\left|g_{0,ij}(k_m,l_m)\right|^2+\frac{1}{\left|d_0(k_m,l_m)\right|^2}\left(\sum_{q=1}^{N_{\mathrm{Cell}}-1}\sum_{j'=1}^{N_{\mathrm{Stream}}}g_{q,ij'}(k_m,l_m)E\left[s_{q,j'}(k_m,l_m)s_{q,j'}^*(k_m,l_m)\right]g_{q,ij'}^*(k_m,l_m)+E\left[n_i(k_m,l_m)n_i^*(k_m,l_m)\right]\right), \\
&=\left|g_{0,ij}(k_m,l_m)\right|^2+\sum_{q=1}^{N_{\mathrm{Cell}}-1}\sum_{j'=1}^{N_{\mathrm{Stream}}}\left|g_{q,ij'}(k_m,l_m)\right|^2+\frac{1}{P_0}\sigma_N^2
\end{aligned}
\tag{2.52}
$$

The (m, m') non-diagonal elements of $E[\tilde{\mathbf{g}}_{RS\ ij}\tilde{\mathbf{g}}_{RS\ ij}^H$ in Eq.(2.48) are calculated as in Eq.(2.43).

$$
\begin{aligned}
&E\left[\left(g_{0,ij}(k_m,l_m)+\frac{d_0(k_m,l_m)}{\left|d_0(k_m,l_m)\right|^2}\left(\sum_{q=1}^{N_{\mathrm{Cell}}-1}\sum_{j'=1}^{N_{\mathrm{Stream}}}g_{q,ij'}(k_m,l_m)s_{q,j'}(k_m,l_m)+n_i(k_m,l_m)\right)\right)\right. \\
&\left.\left(g_{0,ij}(k_{m'},l_{m'})+\frac{d_0(k_{m'},l_{m'})}{\left|d_0(k_{m'},l_{m'})\right|^2}\left(\sum_{q=1}^{N_{\mathrm{Cell}}-1}\sum_{j'=1}^{N_{\mathrm{Stream}}}g_{q,ij'}(k_{m'},l_{m'})s_{q,j'}(k_{m'},l_{m'})+n_i(k_{m'},l_{m'})\right)\right)^*\right], \\
&=g_{0,ij}(k_m,l_m)g_{0,ij}^*(k_{m'},l_{m'})
\end{aligned}
\tag{2.53}
$$

From Eq.(2.52) and Eq.(2.53), $E[\tilde{\mathbf{g}}_{RS\ ij}\tilde{\mathbf{g}}_{RS\ ij}^H$ is expressed as follows.

$$
E\left[\tilde{\quad}\quad\tilde{\quad}\quad_{S,0,ij}\mathbf{g}_{RS,0,ij}^H+\sum_{q=1}^{N_{\mathrm{Cell}}-1}diag\left(\left|g_{q,ij}(k_1,l_1)\right|^2\cdots\quad_{\mathrm{RS}}(k_{N_{\mathrm{RS}}},l_{N_{\mathrm{RS}}})\right|^2\right)+\frac{\sigma_N^2}{P}\mathbf{I},
\tag{2.54}
$$

By substituting Eq.(2.51) and Eq.(2.54) into Eq.(2.48), Eq.(2.44) is derived.

Next, we derive Eq.(2.45). The (m, m) diagonal elements of $E[\tilde{\mathbf{g}}_{RS\ ij}\tilde{\mathbf{g}}_{RS\ ij}^H$ in Eq.(2.49) are calculated as in Eq.(2.55).

$$
\begin{aligned}
&E\left[\left(g_{0,ij}(k_m,l_m)+\frac{d_0(k_m,l_m)}{\left|d_0(k_m,l_m)\right|^2}\left(\sum_{q=1}^{N_{\mathrm{Cell}}-1}\sum_{j'=1}^{N_{\mathrm{Stream}}}g_{q,ij'}(k_m,l_m)s_{q,j'}(k_m,l_m)+n_i(k_m,l_m)\right)\right)\right. \\
&\left.\left(g_{0,i'j}(k_m,l_m)+\frac{d_0(k_m,l_m)}{\left|d_0(k_m,l_m)\right|^2}\left(\sum_{q=1}^{N_{\mathrm{Cell}}-1}\sum_{j'=1}^{N_{\mathrm{Stream}}}g_{q,i'j'}(k_m,l_m)s_{q,j'}(k_m,l_m)+n_{i'}(k_m,l_m)\right)\right)^*\right], \\
&=g_{0,ij}(k_m,l_m)g_{0,i'j}^*(k_m,l_m)+\frac{1}{\left|d_0(k_m,l_m)\right|^2}\left(\sum_{q=1}^{N_{\mathrm{Cell}}-1}\sum_{j'=1}^{N_{\mathrm{Stream}}}g_{q,ij'}(k_m,l_m)E\left[s_{q,j'}(k_m,l_m)s_{q,j'}^*(k_m,l_m)\right]g_{q,i'j'}^*(k_m,l_m)+E\left[n_i(k_m,l_m)n_{i'}^*(k_m,l_m)\right]\right) \\
&=g_{0,ij}(k_m,l_m)g_{0,i'j}^*(k_m,l_m)+\sum_{q=1}^{N_{\mathrm{Cell}}-1}\sum_{j'=1}^{N_{\mathrm{Stream}}}g_{q,ij'}(k_m,l_m)g_{q,i'j'}^*(k_m,l_m)+\frac{1}{P_0}\sigma_N^2
\end{aligned}
\tag{2.55}
$$

The (m, m') non-diagonal elements of the second order statistic of $E[\tilde{\mathbf{g}}_{RS\ ij}\tilde{\mathbf{g}}_{RS\ ij}^H$ in Eq.(2.49) are calculated as in Eq.(2.56).

$$
\begin{aligned}
&E\left[\left(g_{0,ij}(k_m,l_m)+\frac{d_0(k_m,l_m)}{\left|d_0(k_m,l_m)\right|^2}\left(\sum_{q=1}^{N_{\mathrm{Cell}}-1}\sum_{j'=1}^{N_{\mathrm{Stream}}}g_{q,ij'}(k_m,l_m)s_{q,j'}(k_m,l_m)+n_i(k_m,l_m)\right)\right)\right. \\
&\left.\left(g_{0,i'j}(k_{m'},l_{m'})+\frac{d_0(k_{m'},l_{m'})}{\left|d_0(k_{m'},l_{m'})\right|^2}\left(\sum_{q=1}^{N_{\mathrm{Cell}}-1}\sum_{j'=1}^{N_{\mathrm{Stream}}}g_{q,i'j'}(k_{m'},l_{m'})s_{q,j'}(k_{m'},l_{m'})+n_{i'}(k_{m'},l_{m'})\right)\right)^*\right], \\
&=g_{0,ij}(k_m,l_m)g_{0,i'j}^*(k_{m'},l_{m'})
\end{aligned}
\tag{2.56}
$$

From Eq.(2.55) and Eq.(2.56), $E[\tilde{\mathbf{g}}_{RS\ ij}\tilde{\mathbf{g}}^{H}_{RS\ \ i'j'}]$ is expressed as in Eq.(2.57).

$$E\Big[\tilde{\mathbf{g}}_{RS\ \ ij}\tilde{\mathbf{g}}^{H}_{RS\ \ i'j'}\Big] = \mathbf{g}_{RS,0,ij}\mathbf{g}^{H}_{RS,0,i'j'} + \sum_{q=1}^{N_{\mathrm{Cell}}-1} diag\Big(g_{q,ij}(k_1,l_1)g^{*}_{q,i'j'}(k_1,l_1)\cdots g_{q\ ij}(k_{N_{\mathrm{RS}}},l_{N_{\mathrm{RS}}})g^{*}_{q,i'j'}(k_{N_{\mathrm{RS}}},l_{N_{\mathrm{RS}}})\Big) + \frac{\sigma_N^2}{P_g}\mathbf{I}, \quad (2.57)$$

By substituting Eq.(2.51) and Eq.(2.57) into Eq.(2.49), Eq.(2.45) is derived.

iii) Combination of Methods

Term $\boldsymbol{Z}_c$, i.e., the channel estimation error matrix, is included in both Eq.(2.31) and Eq.(2.32), i.e., the channel matrix of the serving cell and the covariance matrix including interference and noise. Therefore, there are four combinations for applying the two methods of the channel estimation error modeling. We define these four combinations as follows.

- Method 1-1: Method 1 is applied to both the channel matrix and covariance matrix.
- Method 1-2: Method 1 is applied to the channel matrix, and Method 2 is applied to the covariance matrix.
- Method 2-1: Method 2 is applied to the channel matrix, and Method 1 is applied to the covariance matrix.

Method 2-2: Method 2 is applied to both the channel matrix and covariance matrix.

2.3.3. Simulation Conditions

Figure 2-11 shows the transmit frame structure. One RB is shown in the figure. The first two OFDM symbols are assumed to be used for control signaling and the CRS. The channel state information-RS (CSI-RS) is assumed to be multiplexed in the 10th and 11th OFDM symbols. Note that the CRS is transmitted at each transmit antenna branch. The CSI-RS is transmitted using CMD every two transmit antenna branches. Here, the CRS is the reference signal used to demodulate the control signaling and perform mobility measurement. The CSI-RS is a reference signal used to obtain accurate CSI associated with each transmitter antenna branch. The DMRS, which is transmitted using CDM every two transmission streams, is assumed to be multiplexed with the insertion density of 12 RE/RB.

To clarify the validity of the modeling schemes for the IRC receiver, a multi-cell link level simulation is performed. Note that a link level simulation is performed between each UE and the neighboring cells as well as the serving cell in this simulation. In addition to the IRC receivers to which the modeling schemes are applied, the realistic IRC receiver that estimates the covariance matrix and the channel matrix of the serving cell using the DMRS is also evaluated for comparison. The numbers of the interfering cells are assumed to be one and two, i.e., two-cell and three-cell models. A synchronous network is assumed.

The simulation conditions for the serving cell are described here. As the channel model, a one-path frequency flat fading channel model and six-path exponentially decayed channel model, in which the average received power of each path is reduced by 2 dB in descending order from the first path, are assumed. In the evaluation, each path delay between adjacent paths is assumed to be the same and this path delay, i.e., RMS delay spread, is parameterized for the six-path exponentially decayed channel model. As the transmission scheme, we assumed the closed-loop transmit diversity using precoding single-stream transmission for the serving cell. The numbers of the transmitter and receiver antenna branches are assumed to be two and two, respectively; therefore, the spatial degree of freedom is one. The transmitter and receiver spatial correlations are assumed to be 0.0, i.e., uncorrelated. Therefore, ρ_{Rx} in Eq.(2.43) is assumed to be 0.0. Fifty consecutive RBs, i.e., 9 MHz, are assigned to the UE in the serving cell. The covariance matrix is estimated within 1 RB; therefore, the number of averaging samples, N_{sp}, equals 12 and the number of the DMRSs in the frequency domain, N_{freq}, equals 3. The channel estimation scheme is assumed to be the 2-dimensional MMSE channel estimation scheme [22]. For the MMSE channel estimation filter, a uniform delay power spectrum within the cyclic prefix length of 4.69 μs is assumed in the frequency domain, and a uniform Doppler power spectrum with the maximum Doppler frequency of 5.55 Hz is assumed in the time domain. As the precoding scheme, the two transmitter antenna codebooks defined in [6] are used. Based on the estimated channel matrix using the CSI-RS, the UE selects the precoding weight matrix that maximizes the received SINR from the codebook, and then the selected precoding weight matrix information at the UE is fed back to the serving cell.

Next, the simulation conditions for the interfering cells are described here. In this simulation, we assume that the conditions for the interfering cells are almost the same as those for the serving cell excluding the following three points. First, the received SIR from each interfering cell is assumed to be 0 dB for the two-cell model and 3 dB for the three-cell model. Second, in the interfering cells, we assume that the assignment unit for a UE is set to 3 RBs to reduce the control signal bits for assignment of RBs. Since the total number of RBs is set to 50 RBs, the assignment unit becomes 2 RBs at the edge of the system bandwidth. Furthermore, 9 UEs are assumed to be assigned in the interfering cells. Therefore, 6 RBs are assigned to 8 UE and 2 RBs are assigned to a UE as illustrated in Fig. 2-12. Finally, in the interfering cell, the precoding weight matrix selection must be modeled since the precoding weight matrix selection is not performed for the UE connected to the interfering cell in order to reduce the computational complexity. Therefore, we assumed that the precoding weight matrix is randomly selected from the codebook for every subframe in the interfering cells for simplicity. The other simulation conditions are given in Table 2-2.

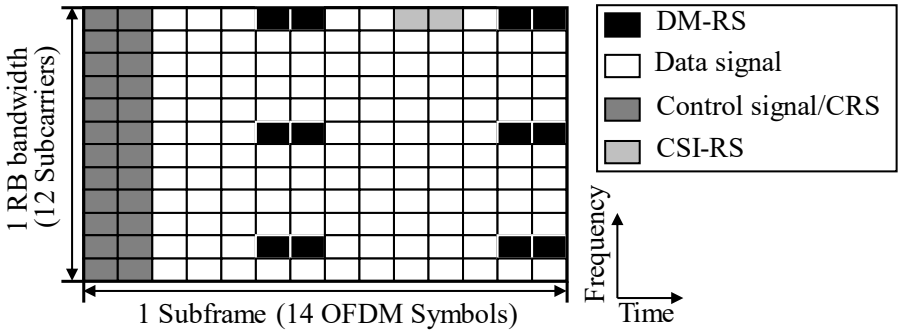

Figure 2-11. Transmission frame structure

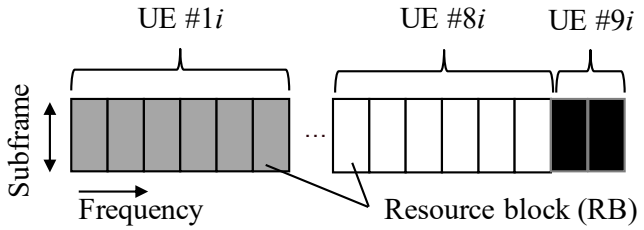

Figure 2-12. Resource allocation in the i-th interfering cell.

Table 2-2. Simulation parameters

Carrier frequency / System bandwidth	2 GHz / 10 MHz
Resource allocation size	50 RB
MIMO antenna configuration	2 x 2 (uncorrelated)
Transmission scheme	Closed-loop transmit diversity
Maximum Doppler frequency	5.55 Hz
Modulation and coding scheme (MCS) transmission granularity on interfering cells	Randomly changing every 1 ms Frequency granularity: 6 RBs
Channel estimation	2D-MMSE channel estimation

2.3.4. Validation Results of Link Performance Modeling

2.3.3.1. Evaluation of Covariance Matrix Estimation Error

To clarify the validity of the modeling schemes of the covariance matrix estimation error, which are discussed in Sec. 2.3.1.3, the CDF performance of the output SINR of each subcarrier is evaluated. Note that the time fluctuations are sufficiently small within the RB in this dissertation. In the evaluation, ideal channel estimation is assumed since only the accuracy of the covariance matrix estimation error modeling is evaluated.

Figure 2-13 shows the CDF of the output SINR performance for the two-cell model. We assume frequency flat fading and frequency selective fading channel models (RMS delay spread of 1.3 μs, which is aligned within the CP duration) with the average received SNR of 20 dB. Focusing on the frequency flat fading channel model, the results show that all the performance levels are almost the same. Therefore, both modeling schemes based on the complex Wishart distribution can accurately model the covariance matrix estimation error. However, focusing on the frequency selective fading channel model, the performance for the conventional method is severely degraded compared to that for the realistic IRC receiver. This is because the conventional method does not take into account the channel fluctuations in the frequency domain. In contrast, the performance for the proposed method achieves almost the same performance for the realistic IRC receiver even when the high frequency selective channel model is assumed.

Figures 2-14(a) and (b) show the median of the output SINR as a function of the RMS delay spread up to 1.3 μs for the average received SNR of 10 dB and 20 dB, respectively. In this evaluation, the two- and three-cell models are assumed. Furthermore, for comparison we evaluate the performance of the ideal IRC receiver, which suppresses the interference signal perfectly using the ideal covariance matrix for each RE. From the results of all the cases, the degradation in the conventional method compared to the realistic IRC receiver becomes large according to the increase in the RMS delay spread. However, the performance of the proposed method is almost the same for the realistic IRC receiver regardless of the RMS delay spread. Therefore, we can say that the proposed method is a robust modeling scheme for the covariance matrix estimation error even for a frequency selective fading channel model. Note that the improvement using the proposal method assuming the three-cell model is less than that assuming the two-cell model. This is because the impact on the covariance matrix estimation error in the two-cell model is greater than that in the three-cell model. More preciously, in the two-cell model, the IRC receiver can suppress the interfering signal effectively since the number of spatial degrees of freedom at the receiver is equal to the number of sources of interference. Therefore, the accuracy of the IRC receiver weight matrix, i.e., the covariance matrix, is very important in suppressing the interference signal. In contrast, in the three-cell model, the IRC receiver cannot suppress all

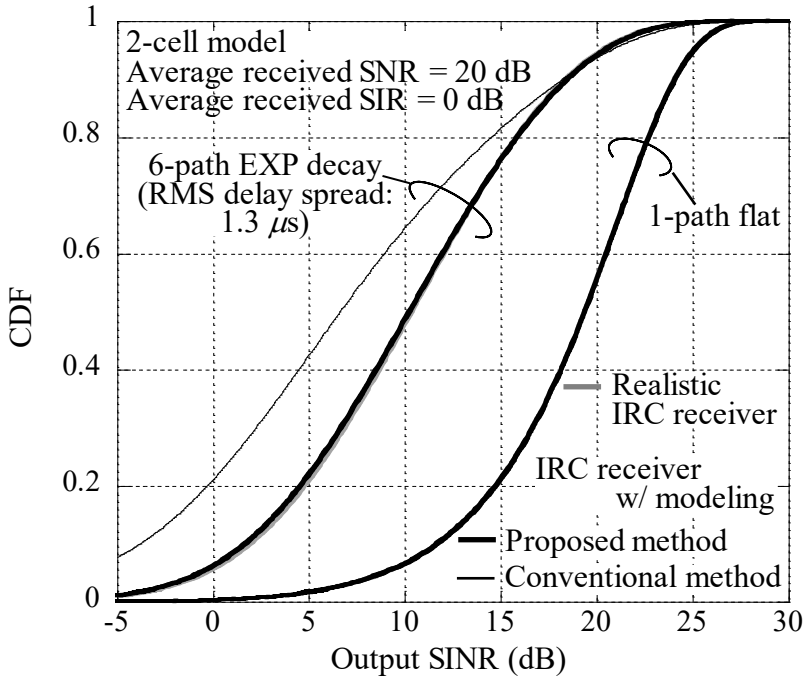

Figure 2-13. CDF of output SINR with ideal channel estimation.

the interfering signals perfectly due to a lack of the spatial degrees of freedom at the receiver. Therefore, the impact on the accuracy of the covariance matrix is relatively small compared to the two-cell model. Furthermore, the ideal IRC receiver achieves the highest performance regardless of the RMS delay spread. On the other hand, the performance of other receivers decreases according to the increase in the RMS delay spread. This is because the covariance matrix is estimated by averaging in the time and frequency domains, i.e., within 1 RB. Therefore, the estimated covariance matrix is degraded compared to the ideal covariance matrix using ideal channel matrices of all cells, due to especially the channel fluctuations in the frequency domain.

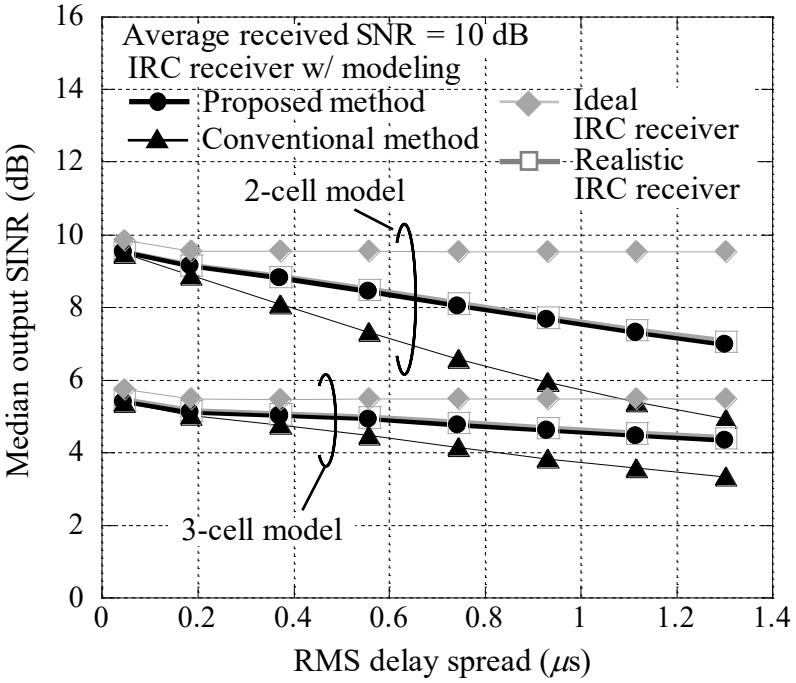

(a) Average received SNR = 10 dB

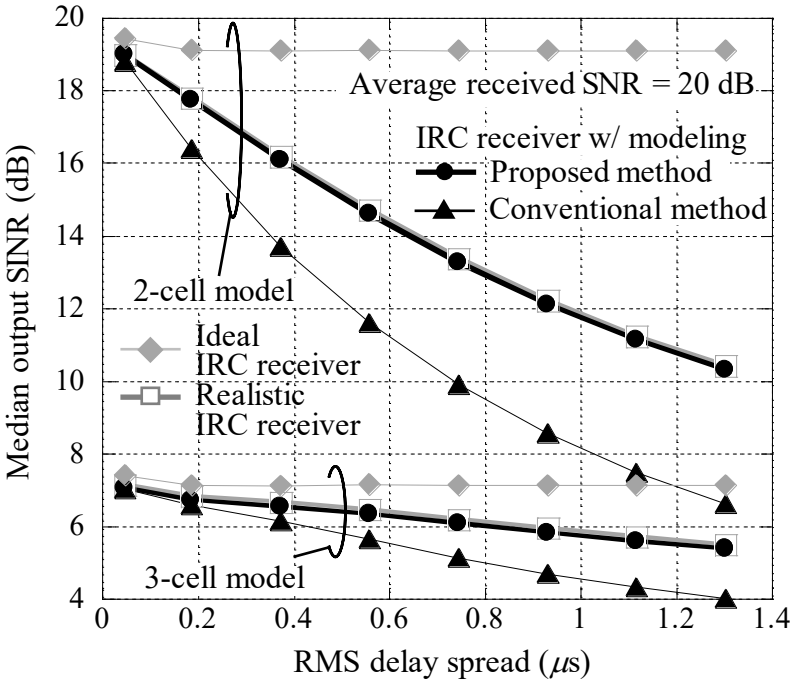

(b) Average received SNR = 20 dB

Figure 2-14. Median output SINR with ideal channel estimation

2.3.3.2. Evaluation of Channel Estimation Error

To clarify which combination of channel estimation error modeling schemes that are discussed in Sect. 2.3.1.4 can yield accurate approximations, the CDF performance of the output SINR of each subcarrier is evaluated. In the evaluation, realistic channel estimation based on the DMRS is assumed for the realistic IRC receiver. Using the results of the modeling schemes, we employ the proposed method of covariance matrix estimation error modeling. For comparison, the performance of the IRC receiver that employs only the covariance matrix estimation error modeling, i.e., when the channel estimation error is not taken into account, is also evaluated.

Figure 2-15 shows the CDF of the output SINR performance for the two-cell model. Here, the frequency flat fading channel model and average received SNR of 20 dB are assumed. The results show that when the channel estimation error is not taken into account, the output SINR performance is higher than that for the realistic IRC receiver. Therefore, the channel estimation error should be taken into account to achieve the actual IRC receiver modeling. Focusing on the results for the four modeling methods of the channel estimation error, the performance for Method 2-2, which applies the proposed channel estimation error modeling of Method 2 to both the channel matrix and the covariance matrix, is the closest to that for the realistic IRC receiver. This is because the proposed modeling scheme of the channel estimation error takes into account the error according to the channel fading fluctuations in the time and frequency domains.

Next, we focus on the performance of Method 1-1 and Method 2-1, which apply the channel estimation error modeling of Method 1 to the covariance matrix. Figures 2-16(a) and (b) show the median of the output SINR as a function of the RMS delay spread up to 1.3 μs for the average received SNRs of 10 dB and 20 dB, respectively. In this evaluation, the two- and three-cell models are assumed. The results show that the performance levels for Method 1-1 and Method 2-1 are severely degraded especially for the SNR of 20 dB assuming the two-cell model. In the two-cell model, the interference signal can be perfectly suppressed when the ideal IRC receiver weight is assumed. Therefore, it is considered that the accuracy of the covariance matrix estimation error modeling is more important than the accuracy of the channel estimation error modeling. Since Method 1 does not take into account the error according to the channel fluctuations, the impact on the modeling error of the covariance matrix becomes large. In contrast, focusing on the three-cell model, the results show that the performance levels for all receivers are less than that in the two-cell model. This is because the interference signal is not perfectly suppressed by the IRC receiver in the three-cell model due to the lack of the spatial degrees of freedom at the receiver, i.e., there are more sources of interference than spatial degrees of freedom. We focus on the performance for Method 1-2 and Method 2-2, which apply the proposed channel estimation error modeling of Method 2 to the covariance matrix. Figures 2-17(a) and (b) show the median of the output SINR as a function of the RMS delay spread up to 1.3 μs for the average received SNRs

of 10 dB and 20 dB, respectively. The results for Method 1-2 and Method 2-2 exhibit performance that is close to that for the realistic IRC receiver for all cases. Especially, the modeling error of Method 2-2 is less than that for Method 1-2 in the low RMS delay spread region. Therefore, we can say that Method 2-2 is a robust modeling scheme for the channel estimation error.

Finally, to confirm the BLER modeling base on the output SINR derived from the proposed covariance and channel matrices modeling schemes, we evaluate the BLER performance when a channel coding scheme is employed. In this case, the channel coding gain needs to be taken into account. For this purpose, there are several modeling methods such as the EESM as mentioned in Sect. 2.3.1. Therefore, to take the channel encoding/decoding into account, the EESM is employed.

In the evaluation, turbo coding with the channel coding rate of R = 0.48 or 0.61, and the constraint length of 4 is employed. Here, $\beta = 1$ is used and QPSK is assumed as the modulation scheme. This is because optimum β becomes almost 1 when the QPSK data modulation is used [12], which is the typical situation for cell-edge users. As the covariance matrix modeling scheme, the proposed scheme is applied. Regarding the channel estimation error modeling scheme, the proposed channel estimation error modeling scheme applied to both the channel matrix of the serving cell and the covariance matrix, i.e., Method 2-2 in the dissertation, and the performance for the conventional channel estimation error modeling scheme applied to both the channel matrix of the serving cell and the covariance matrix, i.e., Method 1-1 in the dissertation, are assumed.

Figure 2-18 shows the evaluation results for the BLER performance. From the results, the performance for the proposed scheme, i.e., Method 2-2, is similar to that for the realistic IRC receiver that includes the actual estimation errors. However, the performance tendency for the conventional scheme, i.e., Method 1-1, is slightly different from that for the realistic IRC receiver. Therefore, we can say that the proposed covariance matrix and channel estimation error modeling schemes can model a realistic IRC receiver accurately even when the channel encoding/decoding is taken into account.

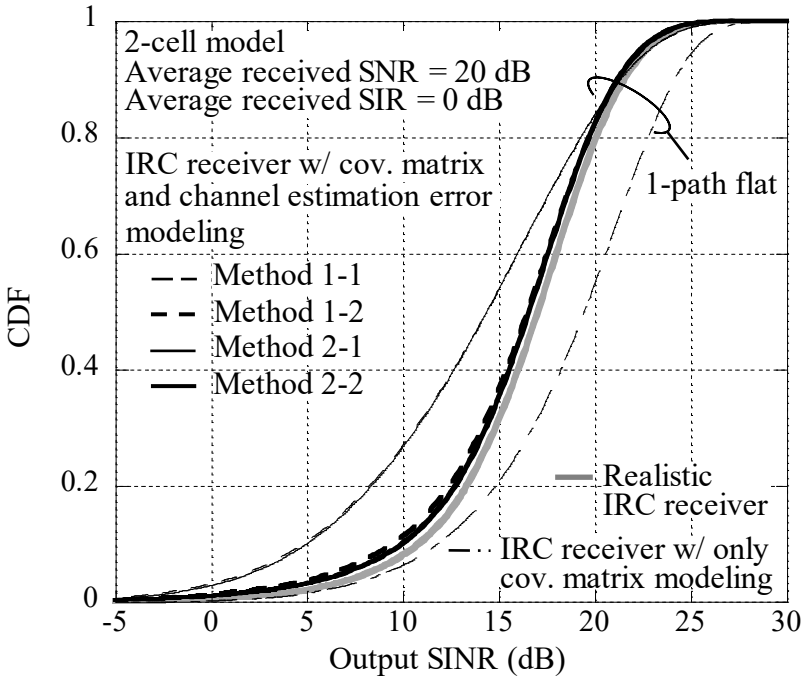

Figure 2-15. CDF of output SINR with realistic channel estimation

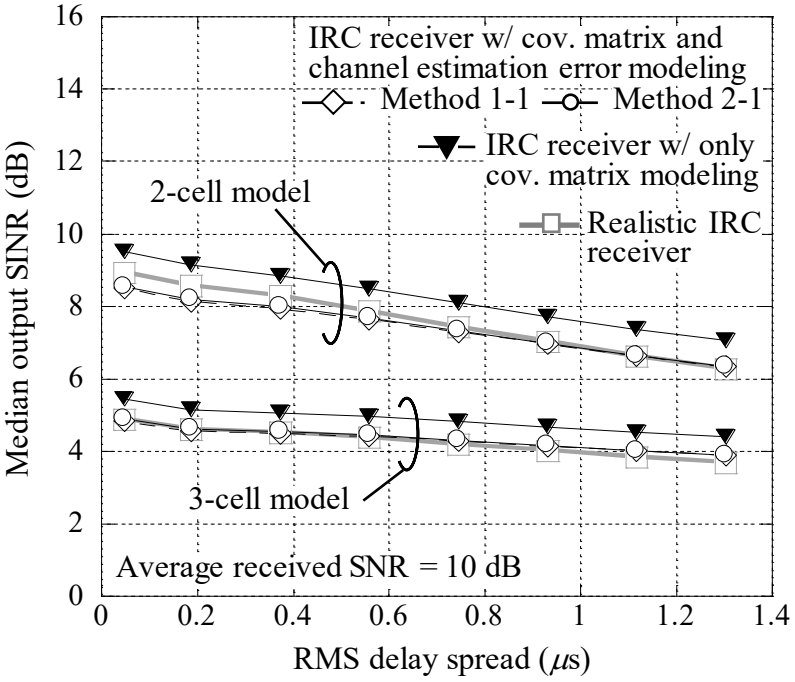

(a) Average received SNR = 10 dB

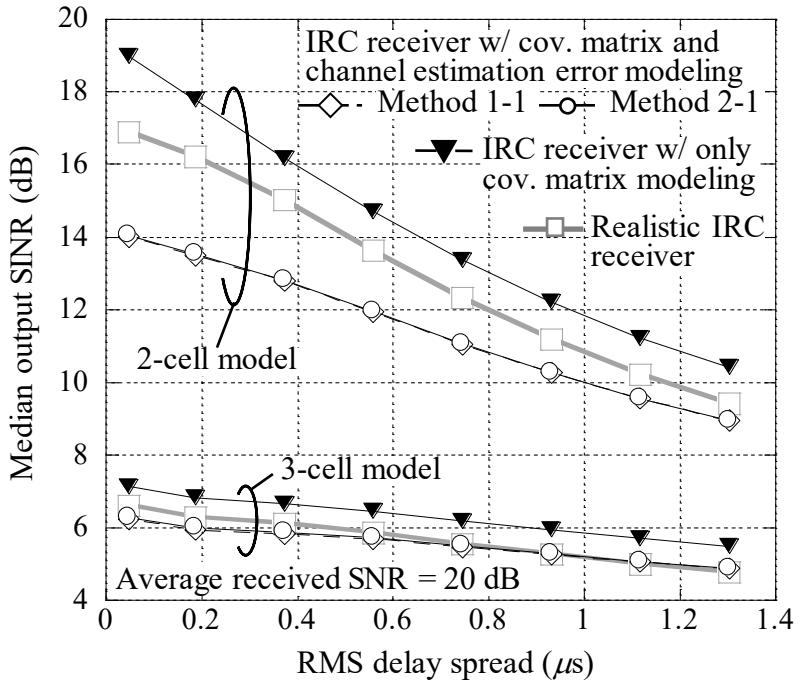

(b) Average received SNR = 20 dB

Figure 2-16. Median output SINR with realistic channel estimation using Method 1-1 and Method 2-1

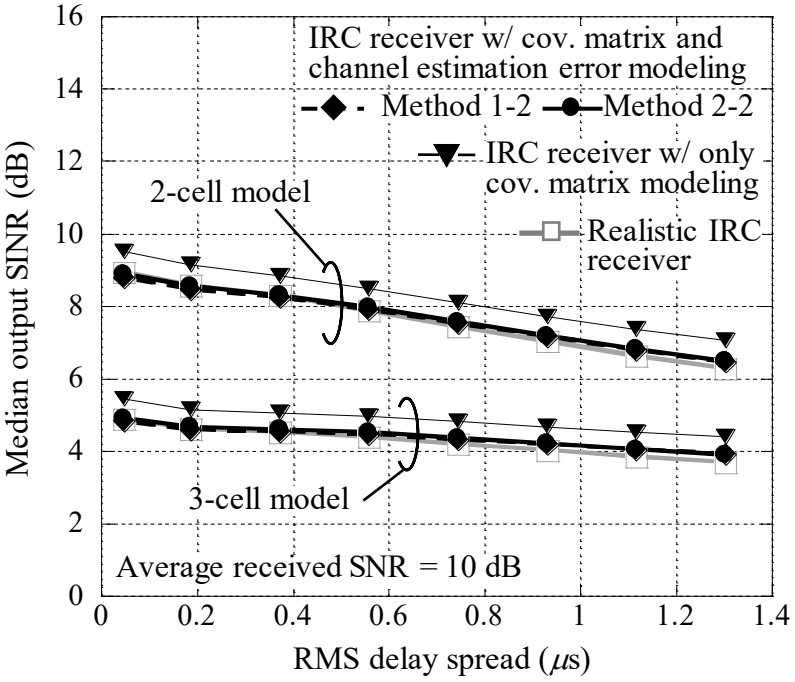

(b) Average received SNR = 10 dB

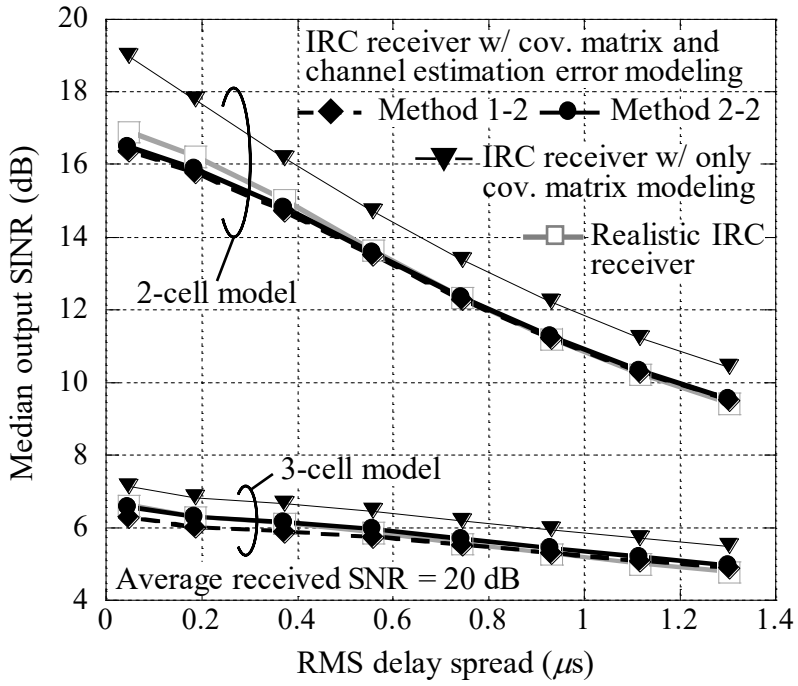

(b) Average received SNR = 20 dB

Figure 2-17. Median output SINR with realistic channel estimation using Method 1-2 and Method 2-2

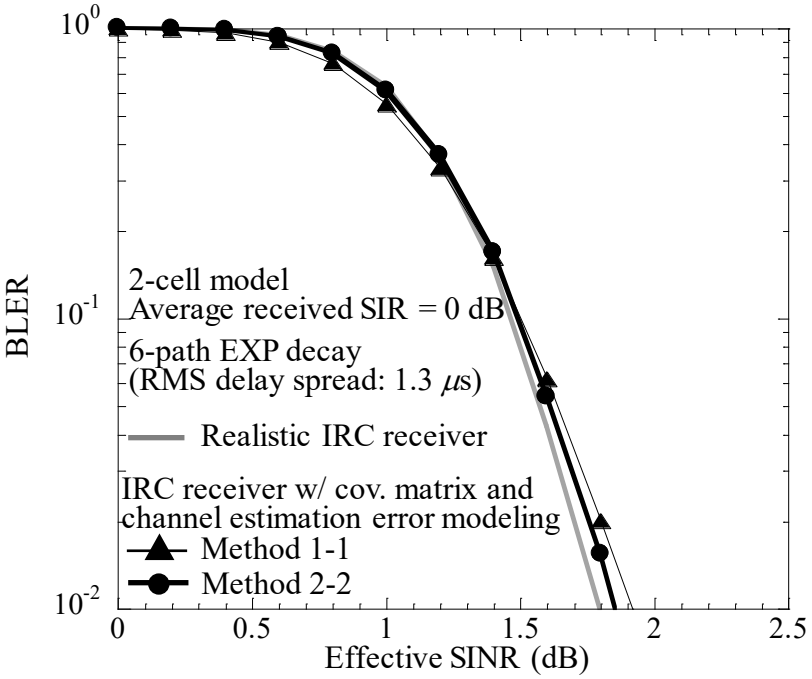

(c) QPSK, $R = 0.48$

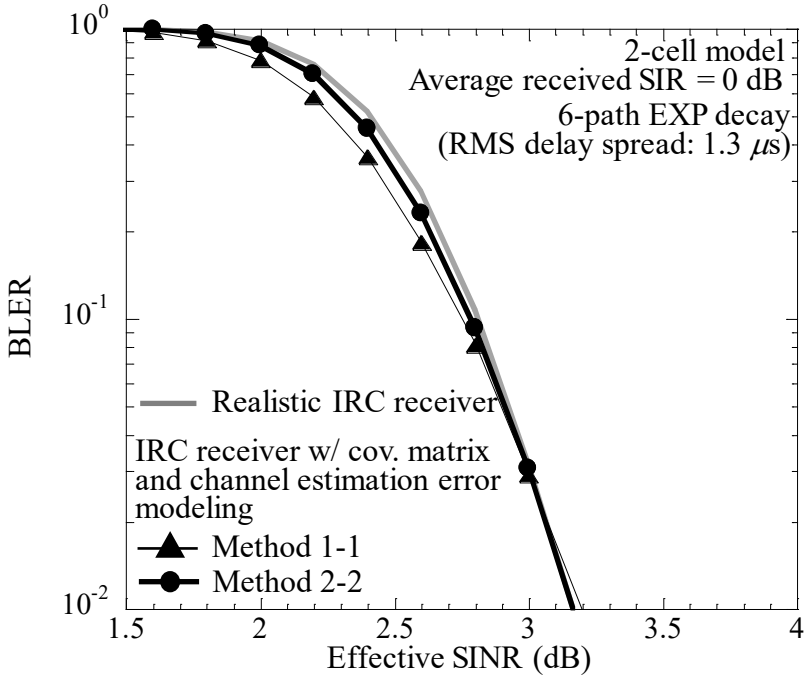

(b) QPSK, $R = 0.61$

Figure 2-18. BLER performance based on EESM (b = 1)

2.3.5. System Capacity of IRC Receiver

Based on the proposed link performance modeling, the system level analysis was conducted in [24]. Specifically, in the study, a combination of the IRC receiver and ICIC in heterogeneous network (HetNet) was evaluated. In this section, we briefly summarize the analysis in [24].

HetNet deployment employing cell range expansion (CRE) [25, 26] was assumed in this study. In this deployment, the UEs originally connect to the microcell, which have the higher received signal power than the picocells, but it is offloaded to the picocells by biasing the signal power from the picocells as illustrated in Fig. 2-19(a). The such bias is called “CRE offset”. Due to CRE, however, the UEs in picocells suffer the severe interference mainly from the microcell. Therefore, especially for the such UEs, the effect of the IRC receiver is expected to be high. On the other hand, authors also assumed the ICIC technique. In order to protect the UEs from the severe interference from the microcell, signal transmission in the microcell is stopped in some subframes as illustrated in Fig. 2-19(b). The subframe without signal transmission of the microcell is called “protected subframe”. In the protected subframe, the effect of the IRC receiver is expected to be low.

Assuming above deployment scenario, authors conducted the system level evaluation, and compared the performance of the conventional MMSE and IRC receivers. Note that the link performance modeling proposed in this dissertation (Sect. 2.3.2) was assumed for the IRC receiver. As the evaluation assumption, a 19 hexagonal macrocell site model with 3 macrocells per macrocell site was assumed, and the numbers of transmitter and receiver antenna branches are assumed to be two and two, respectively. Furthermore, the CRE offset value of 16 dB. See [24] for the detailed simulation assumption.

Figure 2-20 (a), (b) and (c) show the CDF of the user throughput for the UEs connected to the macrocell and picocells corresponding to the protected subframe ratio, i.e., 0.125, 0.5, and 0.875. Note that the ratio of UEs connected to macrocells (picocells) to all UEs is 0.348 (0.652). Based on the results, we can see that the CDF curves are shifted in parallel according to the increase in the protected subframe ratio when focusing on the user throughput for the UEs connected to the macrocell. On the other hand, when focusing on the user throughput for the UEs connected to the picocells, the gain from the IRC receiver is decreased according to the increase in the protected subframe ratio. Other detailed analysis can be seen in [24].

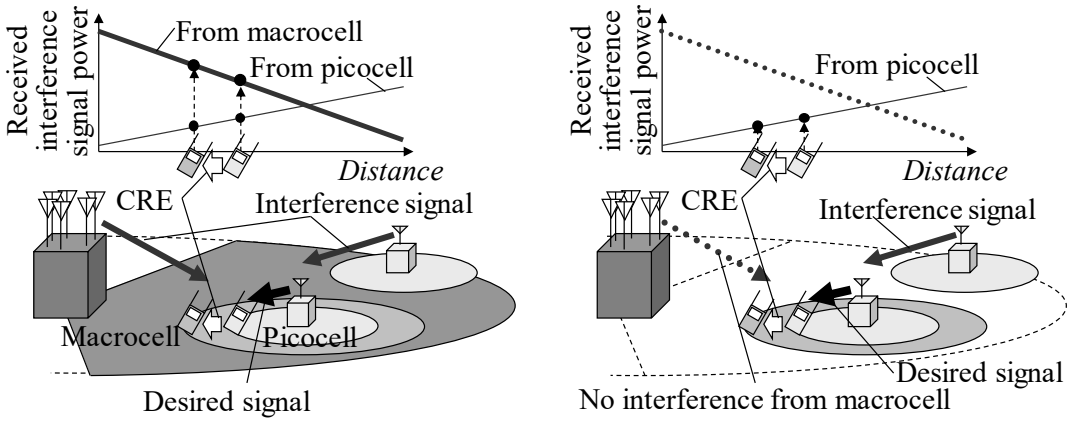

(a) CRE (b) CRE and ICIC

Figure 2-19. Inter-cell interference in heterogeneous network [24]

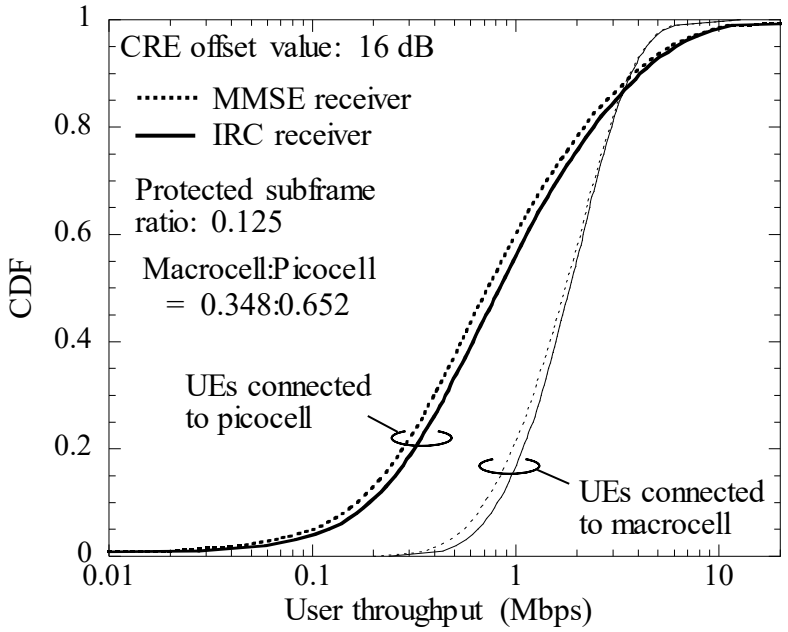

(a) Protected subframe ratio: 0.125

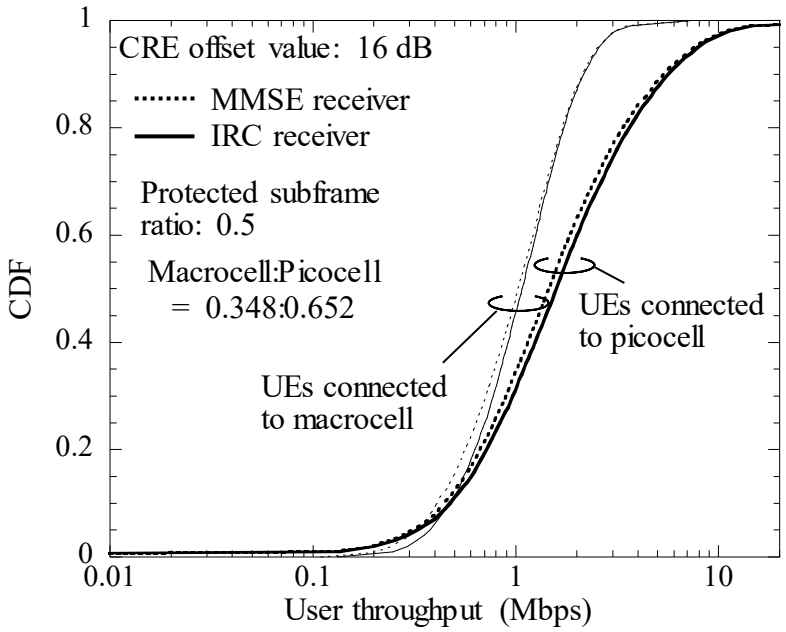

(b) Protected subframe ratio: 0.5

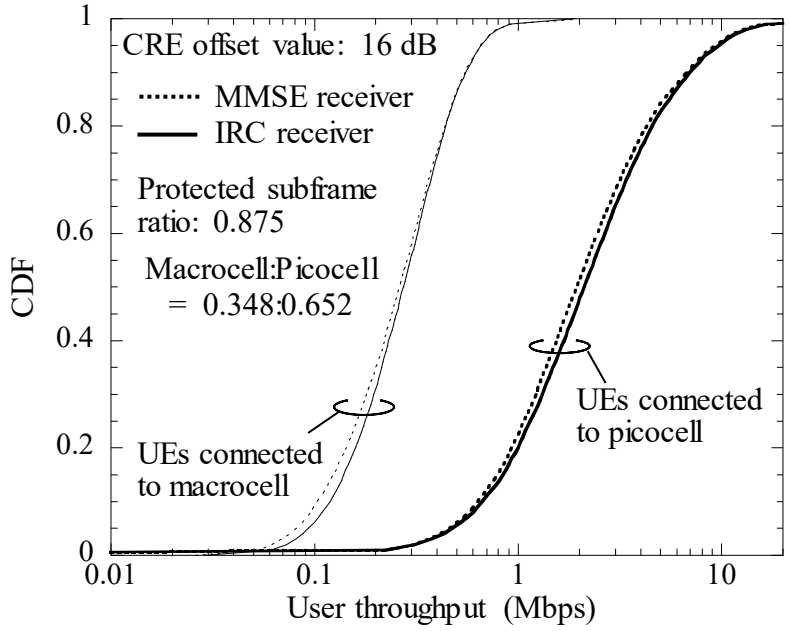

(c) Protected subframe ratio: 0.875

Figure 2-20. CDF of user throughput for UEs connected to macrocell or picocell [24]

2.4. Conclusion

This chapter provides both the link level and system level analysis.

Regarding the link level analysis, we investigated which factor, i.e., the impact of the CRS-to-CRS collision among cells or the impact of the CRS interference on the desired data signals, was dominant in both closed- and open-loop MIMO multiplexing systems. The simulation results assuming the LTE/LTE-Advanced downlink with two transmitter and receiver antenna branches showed that the impact of the CRS-to-CRS collision among cells was larger than the impact of the CRS interference on the desired data signals especially for the closed-loop system although these impacts did not seriously affect the performance of the open-loop MIMO system, from the viewpoint of the output SINR. Even when CRS-to-CRS collisions among cells occurred in the closed-loop MIMO system, the IRC receiver could improve the throughput by more than 20% compared to that for the conventional MRC receiver under the simulation assumptions in this chapter. Furthermore, this chapter provides the evaluation results of the throughput performance assuming various average received SNRs and SIRs. The results showed that the observations for the impact of inter-cell interference of the CRS are verified in various environments from the viewpoint of the throughput performance.

Regarding the system level analysis, especially we proposed the link performance modeling of the IRC receiver including the effect of the covariance matrix and channel estimation error assuming DMRS based transmission mode. As the modeling scheme of the covariance matrix, we proposed a scheme that averages the conventional approximation using the complex Wishart distribution in the frequency domain to address frequency selective fading. Furthermore, we proposed a modeling scheme that models the channel estimation error according to the ideal channel response of all cells and a channel estimation filter to address channel fading fluctuations. The results of simulations assuming the LTE/LTE-Advanced downlink with two transmitter and receiver antenna branches showed that the proposed modeling scheme for the covariance matrix estimation error accurately approximates the performance of a realistic IRC receiver, which estimates the covariance matrix and channel matrix of the serving cell based on the DMRS, even in a frequency selective fading channel. Furthermore, the results also showed that the proposed modeling scheme for the channel estimation error is a robust scheme in RMS delay spread of a channel model compared to the scheme using the MSE statistic of the estimated channel coefficients based on a channel estimation filter. Based on the proposed link performance modeling, the system capacity of the IRC receiver can be accurately evaluated by the system level simulation.

References

[1] 3GPP, TR 36.829 (V11.0.0), “Enhanced performance requirement for LTE UE,” March 2012.

[2] X. Wang and H. V. Poor, “Iterative (Turbo) soft interference cancellation and decoding for coded CDMA,” *IEEE Trans. Commun.*, vol. 47, pp. 1046-1061, July 1999.

[3] T. Abe and T. Matsumoto, “Space-time turbo equalization in frequency selective MIMO channels,” *IEEE Trans. Veh. Technol.*, pp. 469-475, May 2003

[4] 3GPP, R1-111562, Renesas Mobile Europe Ltd., “Interference aware receiver modeling at system level,” May 2011.

[5] Y. Ohwatari, N. Miki, T. Asai, T. Abe, and H. Taoka, “Performance of advanced receiver employing interference rejection combining to suppress inter-cell interference in LTE-Advanced downlink,” *in Proc. VTC2011-Fall*, Sept. 2011.

[6] 3GPP, TS36.211 (V10.2.0), “Physical channels and modulation,” June 2011.

[7] S. M. Alamouti, “A simple transmit diversity technique for wireless communications,” *IEEE J. Select. Areas Commun.*, vol. 16, no. 8, pp. 1451-1458, Oct. 1998.

[8] 3GPP, R4-121552, NTT DOCOMO, “Test coverage for improved minimum performance requirements for E-UTRA,” March 2012.

[9] A. F. Naguib, N. Seshadri, and A. R. Calderbank, “Applications of space–time block codes and interference suppression for high capacity and high data rate wireless systems,” *in Proc. Asilomar Conf. Computers, Signals and Systems*, pp. 1803–1810, Nov. 1998.

[10] P. Hoeher, S. Kaiser, and P. Robertson, “Two-dimensional pilot-symbol-aided channel estimation by Wiener filtering,” *in Proc. ICASSP’97*, pp. 1845-1848, Apr. 1997.

[11] J. Lee, R. Arnott, K. Hamabe, and N. Takano, “Adaptive modulation switching level control in high speed downlink packet access transmission,” *in Proc. 3G Mobile Communication Technologies 2002*, pp. 156-159, May 2002.

[12] K. Brueninghaus, D. Astély, T. Sälzer, S. Visuri, A. Alexiou, S. Karger, and G.-A. Seraji, “Link performance models for system level simulations of broadband radio access systems,” *in Proc. IEEE PIMRC2005*, pp. 2306–2311, Sept. 2005.

[13] V. Pauli, I. Viering, C. Buchner, E. Saad, G. Liebl, A. Klein, "Efficient link-to-system level modeling for accurate simulations of MIMO-OFDM systems," *in Proc. IEEE ICC2009*, pp. 1-6, June 2009.

[14] 3GPP, TR 25.892 (V6.0.0), “Feasibility study for orthogonal frequency division multiplexing (OFDM) for UTRAN enhancement,” June 2004.

[15] M. Moisio, and A. Oborina, “Comparison of effective SINR mapping with traditional AVI approach for modeling packet error rate in multi–state channel,” *in Proc. Next Generation Teletraffic and Wired/Wireless Advanced Networking*, June 2006.

[16] X. He, K. Niu, Z. He, and J. Lin, “Link layer abstraction in MIMO-OFDM system,” *IEEE International Workshop on Cross Layer Design*, Sept. 2007.

[17] 3GPP, R1-031303, Ericsson, “System-level evaluation of OFDM - further considerations,” Nov. 2003.

[18] 3GPP, R1-111031, Nokia and Nokia Siemens Networks, “On advanced UE MMSE receiver modelling in system simulations,” Feb. 2011.

[19] 3GPP, R1-111562, Renesas Mobile Europe Ltd, “Interference aware receiver modeling at system level,” May 2011.

[20] 3GPP, R4-120375, Huawei and HiSilicon, “Discussion on advanced receiver modelling for system level performance evaluation,” Feb. 2012.

[21] W. B. Smith and R. R. Hocking, "Algorithm AS 53: Wishart variate generator." *Journal of the Royal Statistical Society C (Applied Statistics)*, vol.21, no.3, pp.341-345, 1972.

[22] P. Hoeher, S. Kaiser, and P. Robertson, “Two-dimensional pilot-symbol-aided channel estimation by Wiener filtering,” *in Proc. ICASSP’97*, pp. 1845-1848, Apr. 1997.

[23] R. Gold, "Optimal binary sequences for spread spectrum multiplexing," *IEEE Trans. on Information Theory*, vol. 13(4), pp. 619–621, Oct. 1967.

[24] Y. Ohwatari, A. Morimoto, N. Miki and Y. Okumura, “Investigation on interference rejection combining receiver in heterogeneous networks for LTE-Advanced downlink,” *in Proc. SPAWC*, Jun. 2013.

[25] A. Damnjanovic, J. Montojo, Y. Wei, T. Ji, T. Luo, M. Vajapeyam,T. Yoo, O. Song, and D. Malladi, “A survey on 3GPP heterogeneous, networks,” *in Proc. IEEE Wireless Communications*, vol. 18, no. 3, pp. 10 –21, June 2011.

[26] V. Chandrasekhar, J. Andrews, and A. Gatherer, “Femtocell networks: A survey,” *IEEE Comm. Mag.*, vol. 46, no. 9, pp. 59 –67, Sept. 2008.

Chapter 3. Non-Orthogonal Multiple Access

3.1. Introduction

In the LTE/LTE-Advanced downlink, OFDM based radio acces was adopted as a multiple access scheme. This type of orthogonal multiple access (OMA) scheme is a reasonable choice for achieving good system-level throughput performance in packet-domain services with simple single-user detection. When considering advanced multi-user detection however, there is room for achieving higher performance using non-orthogonal multiple access (NOMA) [1].

In NOMA, multiple UEs are multiplexed in the power dimension, and the inter-user interference due to such non-orthogonal user multiplexing is mitigated by advanced multi-user detection technology as shown in Fig. 3-1. From an information-theoretical point of view, it is well-known that NOMA using such a kind of superposition coding at the transmitter and multi-user detection at the UE side not only outperforms OMA, but is also optimal in the sense of achieving the capacity region of the downlink broadcast channel [2]. Up to now, several studies have reported that NOMA can significantly outperform OMA, e.g., in [1, 3-6].

Recently, the 3GPP has also investigated the performance of NOMA in the LTE/LTE-Advanced downlink [7], and the specification of NOMA was completed targeting a high traffic load case in LTE Release 14, called LTE-Advanced Pro [8]. As a realistic multi-user detection technology (referred to as “receiver” hereafter), the following two receivers have been studied in [7].

i) R-ML (Reduced complexity-Maximum Likelihood detector)

ii) CWIC (Codeword Level Interference Canceller)

In the R-ML, the desired and interfering signals are jointly detected under the maximum likelihood (ML) criteria, and some complexity-reduction algorithms such as QRM-MLD [9] are applied. In the CWIC, successive interference cancellation, which performs channel equalization/signal decomposition, channel decoding/re-encoding, and replica signal subtraction

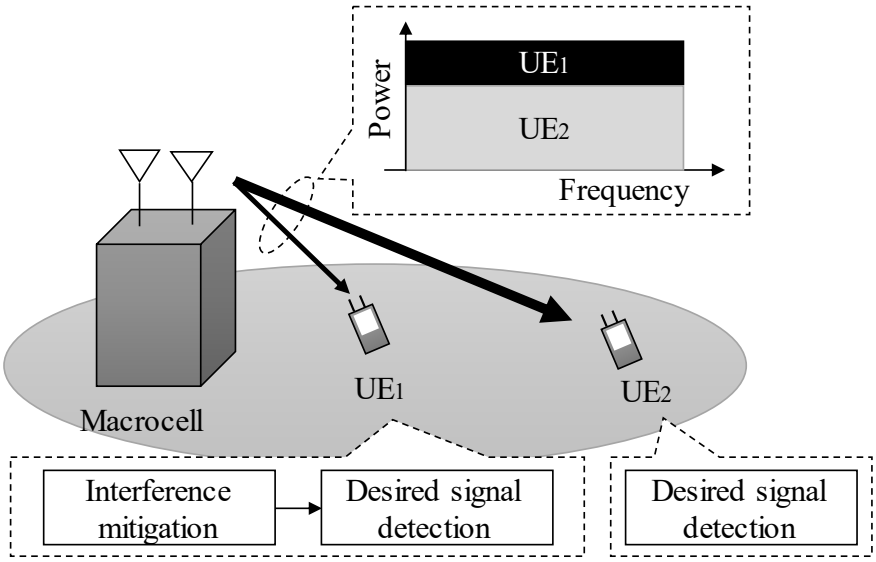

Figure 3-1. Non-orthogonal multiple access (NOMA)

processes for interference signal(s), is applied. In [10-11], it has been shown that the block error rate (BLER) performance of the R-ML is almost the same as that for the CWIC in NOMA by the link level simulation when the same precoder is applied to multiplexed UEs for the R-ML. From the system performance perspective, on the other hand, other aspects must be taken into account as reported in [12]. For the CWIC, information on channel coding of the interfering MS(s) needs to be known by the receiver and control signaling overhead is increased. Furthermore, in order to minimize the increase in the control signal overhead and receiver complexity, the codewords of multiplexed UEs must share the same scheduled resources, which reduces the scheduling flexibility. On the other hand, for the R-ML, information on channel coding of the interfering UE is not required and the same level of scheduling flexibility as that for OMA is retained. One potential disadvantage for the R-ML is that only the UEs using the same precoder can be multiplexed to achieve a similar BLER to that for the CWIC. Details regarding these aspects are described in Sect. 3.2. Hence, the R-ML has some advantages (and a disadvantage) over the CWIC as given in Table 3-1. To verify the impact of these aspects, system level throughput performance of the R-ML in NOMA should be investigated.

In order to evaluate the system level performance, as described in the previous sections, a system level simulation is typically utilized [13-15]. For the system level simulation, a link performance modeling, which is the BLER estimation (prediction) from the SINR, is a key technology to ensure the accuracy of the evaluation. The EESM [16] or MIESM schemes [17] are typically utilized as conventional link performance modeling for the conventional MMSE receiver in OMA. As a further enhancement of these schemes, various modeling schemes for the

Table 3-1. Receiver comparison in NOMA

Attributes	R-ML	CWIC
Signaling overhead	Low	Middle ~ High
User scheduling flexibility	Flexible	Not flexible
Transmission precoder assignment	Not flexible (Only same among users)	Flexible

R-ML and CWIC in OMA have been proposed, e.g., in [18-20]. For the link performance modeling for NOMA, the worst case model was proposed to emulate error propagation by the CWIC in [3]. However, the effect of the imperfect inter-user interference mitigation due to the R-ML cannot be taken into account by the worst case model. Furthermore, a link performance modeling for the R-ML in NOMA was proposed in [12]. However, ideal channel estimation is assumed in the paper, and how to model the channel estimation error is not clear. Hence, we still have room for improvement in the link performance modeling for the R-ML.

In this section, we firstly propose a new link performance modeling for the R-ML in NOMA considering both the effect of imperfect inter-user interference mitigation and channel estimation. Second, we present system capacity analysis, i.e. the system level throughput performance of the R-ML in NOMA, and show that it is higher than that for the CWIC in the LTE downlink of NOMA due to the scheduling flexibility.

3.2. Signal Transmission Model for NOMA

3.2.1. Signal Transmission Model

As shown in Fig. 3-1, multiple UEs are multiplexed in the power dimension in NOMA. Assuming that the number of receiver antenna branches is N_{Rx}, the N_{Rx}-dimensional received signal vector of the k-th subcarrier and the l-th OFDM symbol for user u, $\mathbf{y}_u(k,l)$, is expressed as follows.

$$\mathbf{y}_u(k,l) = \mathbf{H}_u \sum_{j=1}^{N_{user}} \sqrt{p_j}\,\mathbf{W}_{\mathrm{Tx},j}\mathbf{s}_j + \mathbf{n}, \tag{3.1}$$

where $\mathbf{H}_u$, $\mathbf{W}_{\mathrm{Tx},j}$, and $\mathbf{s}_j$ represent a (N_{Rx} x N_{Tx}) channel matrix, (N_{Tx} x N_{Stream}) transmission precoding matrix, and N_{Stream}-dimensional transmission signal vector of user u or j, respectively. Note that we omit the subcarrier index k and the OFDM symbol index l for simplicity. Terms N_{Tx}, N_{Stream}, and N_{user} represent the number of transmission antenna branches, transmission streams and multiplexed users, respectively. Term $\mathbf{n}$ represents the N_{Rx} -dimensional noise vector including inter-cell interference signals and thermal noise, and p_j represents the transmission power of user

j and it is constrained by $\sum_{j=1}^{N_{user}} p_j = 1$. Note the inter-cell interference(s) is not explicitly expressed in this equation for simplicity, and it is assumed to be included in the noise vector, **n**. In this dissertation, we assume $N_{Rx} = N_{Tx} = N_{user} = 2$, and N_{Stream} can be set to maximally two. In addition, we assume $p_1 \le p_2$ and inter-user interference mitigation is applied for only user 1 (UE_1).

3.2.2. Transmission Precoder Restriction for R-ML

For the R-ML, the same transmission precoder should be applied to multiplexed users in order to achieve a high throughput performance. In this section, we show the details of this aspect.

In the R-ML, the desired and interfering signals, i.e., multiple $\mathbf{s}_j$ for all users are jointly detected based on the ML criteria. Since the dimension of each $\mathbf{s}_j$ is maximally N_{Stream}, at most $N_{Sream} \times N_{users}$ data streams are received at the R-ML. Hence, when assuming $N_{Sream} \times N_{users} > N_{Rx}$, the performance of the R-ML is severely degraded due to the lack of spatial degrees of freedom. To maintain the performance of the R-ML, the same transmission precoder, $\mathbf{W}_{\mathrm{Tx}}$, can be applied to all users as shown in Eq. (3-2).

$$\begin{aligned} \mathbf{y}_u(k,l) &= \mathbf{H}_u \sum_{j=1}^{N_{user}} \sqrt{p_j}\mathbf{W}_{\mathrm{Tx}j}\mathbf{s}_j + \mathbf{n} \\ &= \mathbf{H}_u \mathbf{W}_{\mathrm{Tx}} \sum_{j=1}^{N_{user}} \sqrt{p_j}\mathbf{s}_j + \mathbf{n} \\ &= \mathbf{H}_u \mathbf{W}_{\mathrm{Tx}} \hat{\mathbf{s}} + \mathbf{n} \end{aligned}, \tag{3.2}$$

where $\hat{\mathbf{s}} = \sum_{j=1}^{N_{user}} \sqrt{p_j}\mathbf{s}_j$, and the dimension of $\hat{\mathbf{s}}$ is maximally N_{Stream}. When assuming that $\hat{\mathbf{s}}$ is detected by the R-ML, clearly the performance can be maintained because $N_{Stream} \le N_{Rx}$. We note that joint modulation among the multiplexed users was proposed in [10-11] to improve the performance of the R-ML. More specifically, the coded bits from multiplexed users are jointly modulated such that the signal constellation of $\hat{\mathbf{s}}$ becomes Gray code as shown Figs. 3-2 and 3-3. In the following, we assume such joint modulation to improve the performance of the R-ML. However, the transmission precoder restriction, i.e., a user can be multiplexed only with the users that have the same optimal precoding matrix, could degrade the system level throughput performance due to a lack of flexibility in the user-multiplexing. On the other hand, the CWIC does not have the transmission precoder restriction. Without this restriction, the CWIC can maintain the detection performance thanks to the channel decoding process for the interference signals and intentionally introduce a transmission power difference for each user.

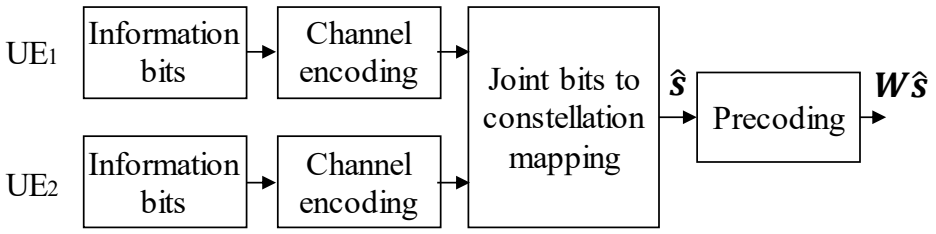

Figure 3-2. Joint modulation among multiplexed users

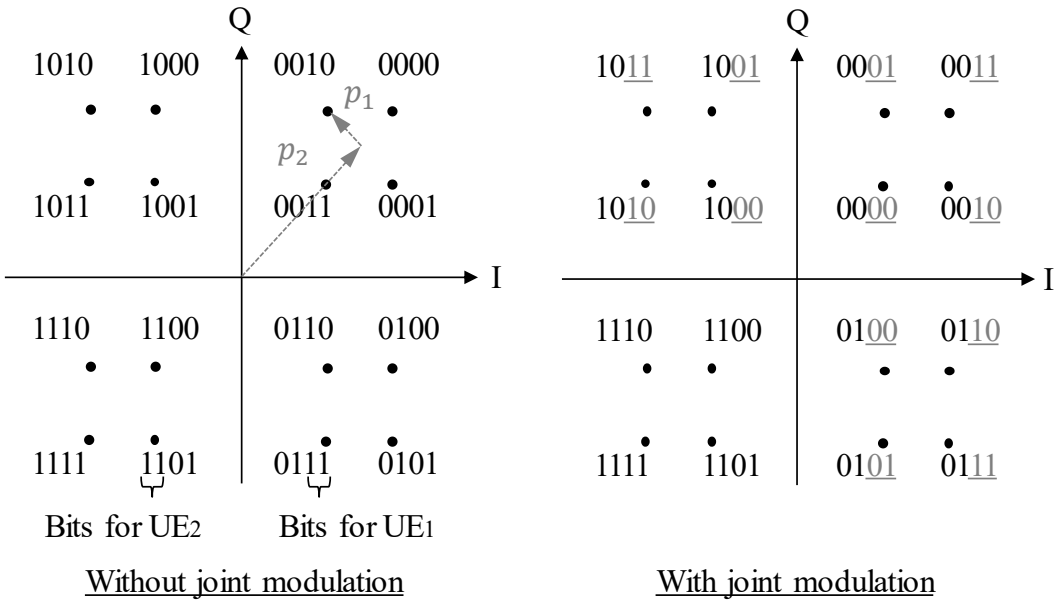

Figure 3-3. Example of joint signal constellation (QPSK for both UEs).

3.2.3. Scheduling Flexibility and Signaling Overhead

As described in Sect. 3.1, the CWIC requires channel decoding and re-encoding processes for interfering user(s), whereas R-ML does not require such processes. Consequently, the CWIC requires more signaling information than the R-ML as shown in Table 3-2. Note that similar aspects were also pointed out in [12]. In NOMA, the optimal pair of multiplexed users is expected to vary dynamically given the channel environment of each user. Hence, dynamic configuration of user pairings should be allowed in order to improve the system level throughput performance of NOMA. To do this, the information in Table 3-2 should be signaled to the desired user in a dynamic manner, e.g., using the Physical layer Downlink Control CHannel (PDCCH) in the LTE [21]. In this case, the amount of signaling overhead of the CWIC becomes too large to ignore compared to the R-ML. One way to reduce the signaling overhead of the CWIC is resource alignment among multiplexed users as shown in Fig. 3-4(a). Since the allocated resources of each

Table 3-2. Example of required signaling Information

Required Information for Cancellation	R-ML	CWIC
Transmission power ratio	○	○
Modulation order of paired user(s)	○	○
Code rate of paired user(s)	×	○
Redundancy version of paired user(s)	×	○
Resource allocation of paired user(s)	×	○
Transmission precoder of paired user(s)	×	○

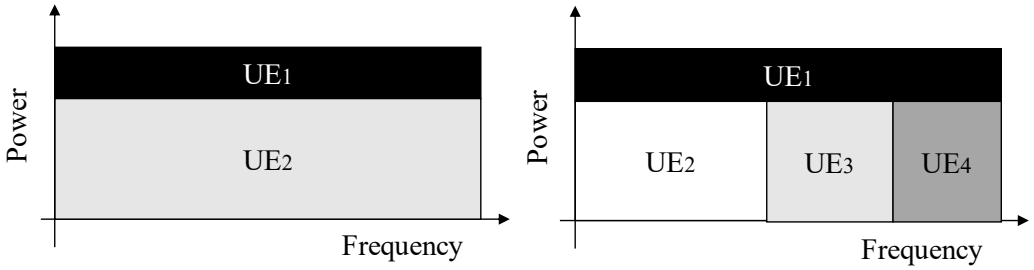

(a) Wideband scheduling with resource alignment

(b) Subband scheduling with wideband power allocation

Figure 3-4. Scheduling methodologies

user are aligned, signaling information for only one interfering user is required. On the other hand, since the signaling overhead of the R-ML is very low, the same level of scheduling flexibility as that for OMA is retained as shown in Fig. 3-4(b). Details of the subband scheduling methodology for NOMA are described in Sect.3.4.2. In this case, since multiple users can be allocated to each subband, the performance of NOMA can be improved due to the frequency selective scheduling gains.

3.3. Link Performance Modeling for NOMA

As described above, in terms of scheduling flexibility and transmission precoder assignment, the R-ML has some advantages/disadvantage over the CWIC. In order to evaluate the impact of these aspects, the system level throughput performance of the R-ML should be investigated. In this section, we propose a link performance modeling for the R-ML to conduct a system level evaluation. Note that the general description of link performance modeling is shown in Sect. 2.3.1.

3.3.1. Proposal Link Performance Modeling for R-ML

For the link performance modeling for the CWIC in NOMA, the worst case model was proposed to emulate error propagation in [3]. In this model, the signal for the high power UE (UE2) is first decoded by the conventional link performance at the low power UE (UE1). If such a signal can be correctly decoded, the output SINR of UE1 is calculated assuming an ideal inter-user interference canceller. Hence, for the R-ML, this model cannot be utilized because the residual inter-user interference after the R-ML processing cannot be taken into account. In [12], on the other hand, an MIESM based scheme for the R-ML in NOMA was proposed. By utilizing this scheme, the residual inter-user interference can be accurately modeled. However, ideal channel estimation was assumed in this study, and how to model the channel estimation error is not clear. In general, modeling of the channel estimation error is a very important to evaluate the realistic performance of NOMA. Therefore, we propose a modified EESM for the R-ML in this section. The proposed scheme can model the link performance of the R-ML together with channel estimation error in a simple scheme.

The goal is to predict the BLER performance of the R-ML in NOMA. The key issue is how to calculate the output SINR of the R-ML. It is well known that there is some difficulty in the calculation of the output SINR of the R-ML, e.g., [18-19]. Hence, in these studies, it was proposed that the output SINR of the R-ML in OMA is calculated using the SINRs of the MMSE receiver and the ideal inter-stream/cell interference canceller. The SINRs are interpreted as lower and upper bounds of the SINR of the R-ML, and an internally dividing point between those SINRs is selected to fit the actual performance of the R-ML using a link level simulation. In OMA, such an approach is reasonable since the efficiency of the inter-stream/cell interference mitigation by the R-ML is diverse according to the channel environment. In NOMA, however, the R-ML has basically similar efficiency in terms of the inter-user interference mitigation capability as the ideal inter-user interference canceller (ideal IC) [10]. Therefore, we propose the following simplified link performance modeling scheme for the R-ML in NOMA using only the output SINR of the ideal IC as follows.

Step 1) Calculate the output SINR of the ideal IC as follows.

$$SINR_{out,k,u,n}^{ideal} = \frac{p_u \mathbf{w}_{Rx,u,n}^{ideal} \mathbf{g}_{u,n} \mathbf{g}_{u,n}^H \mathbf{w}_{Rx,u,n}^{ideal\ H}}{\mathbf{w}_{Rx,u,n}^{ideal} \left(\sum_{n'=1,n' \neq n}^{N_{Stream}} p_u \mathbf{g}_{u,n'} \mathbf{g}_{u,n'}^H + \sigma_N^2 \mathbf{I} \right) \mathbf{w}_{Rx,u,n}^{ideal\ H}}, \tag{3.3}$$

$$\boldsymbol{w}_{Rx,u,n}^{ideal} = p_u \boldsymbol{g}_{u,n}^H \left(p_u \boldsymbol{G}_u \boldsymbol{G}_u^H + \sigma_N^2 \boldsymbol{I} \right)^{-1}. \tag{3.4}$$

Where $\mathbf{G}_u = \mathbf{H}_u \mathbf{W}_{\mathrm{Tx},u}$, and $\boldsymbol{g}_{u,n}$ represents the n-th column of $\mathbf{G}_u$. Terms. Note that the output SINR

of the MMSE receiver in NOMA can be calculated using Eqs.(3.5)-(3.6).

$$SINR_{out,k,u,n} = \frac{p_u \mathbf{w}_{MMSE,u,n} \mathbf{g}_{u,n} \mathbf{g}_{u,n}^H \mathbf{w}_{MMSE,u,n}^H}{\mathbf{w}_{MMSE,u,n} \left(\sum_{n'=1,n' \neq n}^{N_{Stream}} p_u \mathbf{g}_{u,n'} \mathbf{g}_{u,n'}^H + \sum_{u'=1,u' \neq u}^{N_{user}} p_{u'} \mathbf{G}_u \mathbf{G}_u^H + \sigma_N^2 \mathbf{I} \right) \mathbf{w}_{MMSE,u,n}^H}, \tag{3.5}$$

$$\mathbf{w}_{MMSE,u,n} = p_u \mathbf{g}_{u,n}^H \left(\sum_{j=1}^{N_{user}} p_j \mathbf{G}_u \mathbf{G}_u^H + \sigma_N^2 \mathbf{I} \right)^{-1}, \tag{3.6}$$

When assuming that the inter-user interference is perfectly canceled by the ideal IC, Eqs.(3.5)-(3.6) can be written as Eqs. (3.3)-(3.4).

Step 2) Optimize the training parameter, $\beta_{MCS,\ rankcombi,pu}$, for each combination of MCS, rank and transmission power ratio.

In NOMA, the following rank combination of multiplexed users can be considered.

- Rank (1-1): rank 1 for UE1, rank 1 for UE2
- Rank (1-2): rank 1 for UE1, rank 2 for UE2
- Rank (2-1): rank 2 for UE1, rank 1 for UE2
- Rank (2-2): rank 2 for UE1, rank 2 for UE2

In each rank combination, the R-ML has a different efficiency for inter-user interference mitigation. Furthermore, transmission power p_u also has an impact on the performance of the R-ML. Therefore, training parameter β should be optimized for each combination of MCS, rank and transmission power ratio.

Step 3) Calculate the effective SINR of the R-ML as follows.

$$SINR_{\text{eff},\ u,n} = -\beta_{MCS,\ rankcombi,pu} \ln \left(\frac{1}{N_{subcar}} \sum_{k=1}^{N_{subcar}} \exp \left(-\frac{SINR_{out,k,u,n}^{ideal}}{\beta_{MCS,\ rankcombi,pu}} \right) \right). \tag{3.7}$$

In Step 2, training parameter $\beta_{MCS,\ rankcombi,pu}$ is optimized by the following criteria similar to the conventional EESM.

$$\text{MSE}_{t,\beta} \cong \left| \log_{10} \text{BLER}_{\text{R-ML}}^t - \log_{10} \text{BLER}_{predicted,\beta}^t \right|^2, \tag{3.8}$$

$$\beta_{MCS,\ rankcombi,pu} = \arg\min_{\beta} \frac{1}{N_{Trial}} \sum_{t=1}^{N_{Trial}} \text{MSE}_{t,\beta}, \tag{3.9}$$

where $\text{BLER}_{\text{R-ML}}^t$ represents the actual BLER performance of the R-ML receiver including or not

including channel estimation error with a given MCS, rank combination and transmission power, and $\mathrm{BLER}^{t}_{predicted,\beta}$ represents the predicted BLER performance by mapping the effective SINR in Eqs. (3-3)-(3-4) and (3-7) to the AWGN curve in the trial *t*. In the proposed scheme, we can simply use the output SINR of the ideal IC in Steps 1 and 3 instead of the output SINR of the MMSE receiver. The difference in performance between the R-ML and ideal IC can be compensated by $\beta_{MCS,\ rankcombi,pu}$ trained in Step 2.

3.3.2. Validation Results of Link Performance Modeling

In this section, we show the accuracy of the link performance modeling described in Section 3.3.1 based on the link level simulation. In this evaluation, we assume the closed-loop single user MIMO system defined in LTE downlink, i.e. transmission mode (TM) 4 [25], as the baseline OMA scheme. The following combination of rank and transmission precoder index [21] is assumed.

- Case 1: Rank (1-1) with codebook index 0 for both users
- Case 2: Rank (2-1) with codebook index 1 for UE1 and 0 for UE2
- Case 3: Rank (2-2) with codebook index 1 for both users

In Case 2, we note that the first column of transmission precoder index 1 for UE1 is the same as transmission precoder index 0 for UE2 with power scaling of $1/\sqrt{2}$. In this case, joint modulation such as Eq. (3-2) can be applied to the first transmission stream. The modulation order of the interfering user is set to QPSK and the transmission power ratio for UE1, i.e., p_1 is set to 0.14, 0.23, and 0.36 as examples. For the proposed EESM for the R-ML, $\beta_{MCS,\ rankcombi,pu}$ is adjusted such that $\mathrm{BLER}^{t}_{predicted,\beta}$ is well aligned with $\mathrm{BLER}^{t}_{\text{R-ML}}$ =0.1. Other parameters are summarized in Table 3-3.

Figures 3-5, 3-6 and 3-7 show the validation results for UE1 when assuming QPSK, 16QAM and 64QAM respectively. Note that the modulation order used in these figures is an example, and any modulation order can be utilized for each case. In the figures, the gray line indicates the reference AWGN curve and the other black lines represent the predicted BLER performance of the R-ML. To investigate the impact of the channel estimation, we show the results with both ideal and realistic channel estimation (2-dimensional MMSE channel estimation [22]). The beta values used in Figs. 3-5 to 3-7 are shown in Table 3-4. Figure 3.5 shows that the proposed scheme accurately models the link performance of the R-ML in an ideal channel estimation case, and the

Table 3-3. Link level assumptions for validation

Parameters	Values
System bandwidth	10 MHz
MIMO antenna configuration	2-by-2 (Uncorrelated)
Transmission mode for each user	Closed loop spatial multiplex
Channel model (Doppler frequency)	6-path TU channel model (5 Hz)
Channel estimation	Ideal / 2D MMSE
Number of control symbols	2 OFDM symbol
Number of CRS ports	2 CRS ports
Receiver	R-ML (QRM-MLD)
Joint modulation	On

prediction error due to channel estimation error is at most 0.2 dB. On the other hand, Figs. 3-6 and 3-7 show that there is no significant difference between the ideal and realistic channel estimation cases. This is because the channel estimation errors in these cases are not large since the MCS levels are high, i.e., the operating SINR region is high. However, Fig. 3-7 also shows that some prediction error remains even for the ideal channel estimation. For EESM, it is known that there is some prediction error in the higher modulation order and code rate case, e.g. [23]. However, since the prediction error is quite small (at most 0.2 dB), we conclude that the proposed link performance modeling can accurately predict the BLER performance of the R-ML in NOMA.

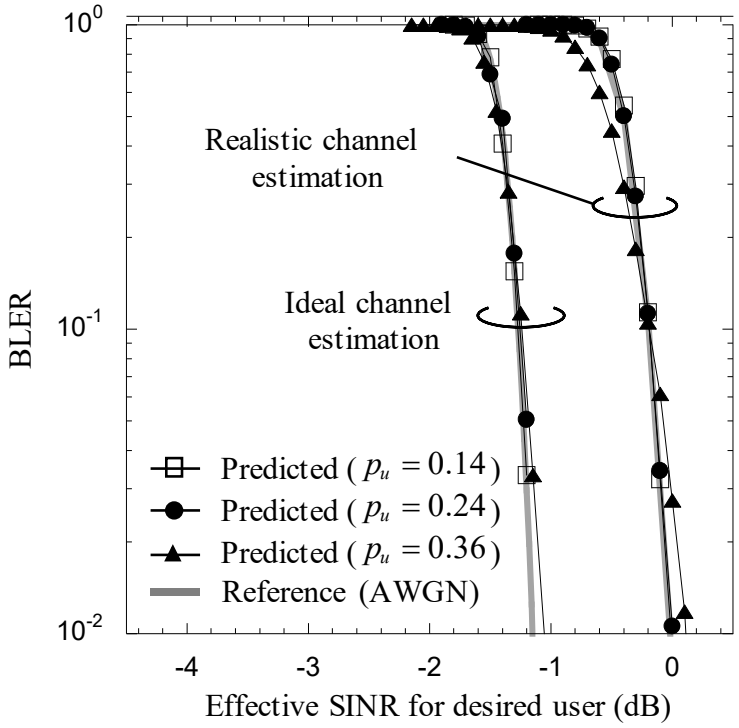

Figure 3-5. Validation results (Case 1 with QPSK/R = 0.33)

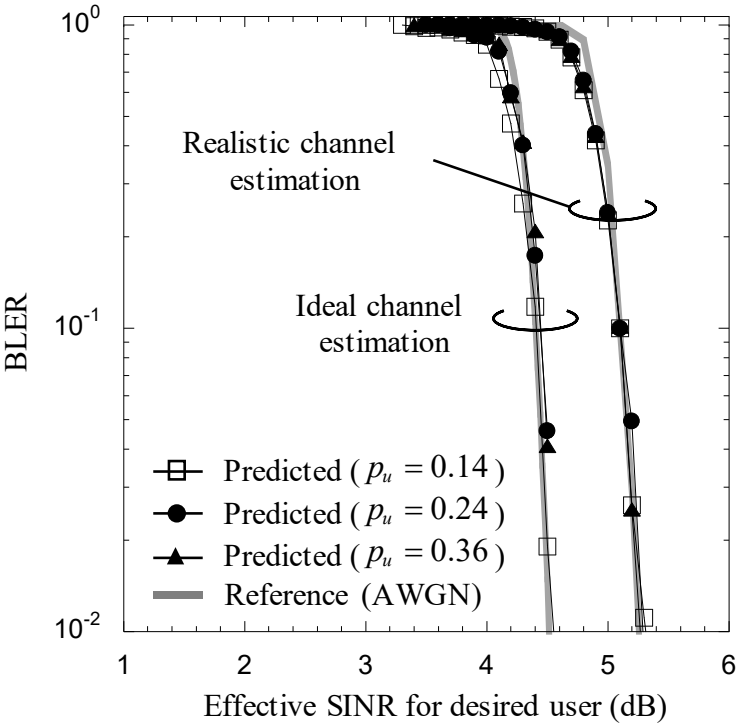

Figure 3-6. Validation results (Case 2 with 16QAM/R = 0.36)

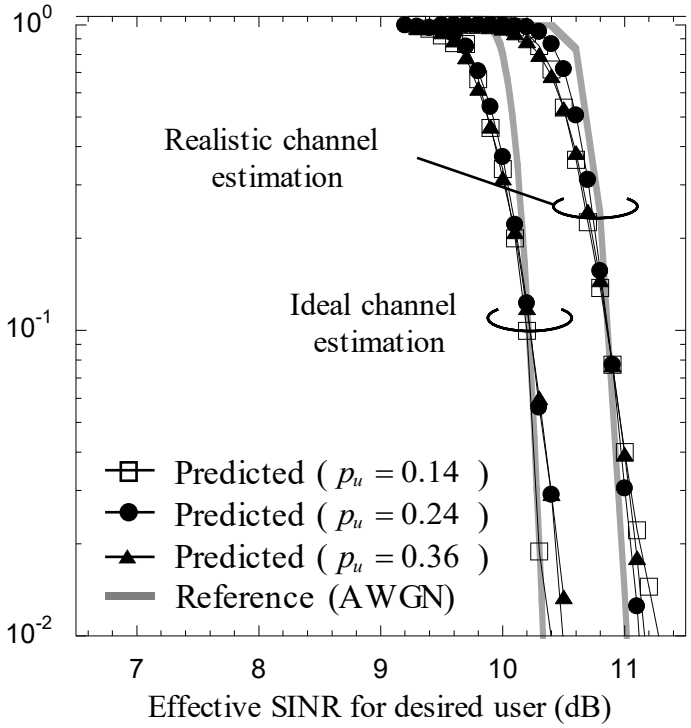

Figure 3-7. Validation results (Case 3 with 64QAM/R = 0.46)

Table 3-4. Beta values in validation results

	Figure 3-5		Figure 3-6		Figure 3-7	
Channel estimation/ Power ratio	**Ideal**	**Realistic**	**Ideal**	**Realistic**	**Ideal**	**Realistic**
0.14	1.1	1.8	3.2	3.8	8.5	10
0.23	1.1	1.0	3.6	3.9	8.5	10
0.36	1.1	0.51	3.6	3.5	6.5	6.6

3.4. System Level Analysis

In this section, we show the system level throughput performance of the R-ML in NOMA based on the link performance modeling proposed in Sect. 3.3. As described in Section 3.2, the R-ML can enable flexible scheduling as shown in Fig. 3-4(b) for NOMA. In this section, we describe details of the scheduling methodology and system level evaluation results for the R-ML.

3.4.1. Scheduling Methodology

First, we assume CRS based transmission mode, TM4 [21], as the baseline OMA scheme. In TM4, adaptive modulation and coding scheme (AMC), adaptive transmission precoding and transmission rank adaptation were adapted based on the feedback channel state indicator (CSI), which includes channel quality indicator (CQI), precoding matrix indicator (PMI), and rank indicator (RI). Once the RI, PMI, and CQI reported from the UEs are available, the base station (BS) can conduct resource allocation to its served UEs by using the proportional fair (PF) scheduling algorithm [24] for both OMA and NOMA. For simplicity, the multiplexing order of superposition coding is assumed to be two with only one layer per UE. As shown below, for NOMA, dynamic switching of NOMA and OMA is allowed.

1. Start from the first subband (i.e., Subband #1)
2. Select one of the pair of users as (UE_1, UE_2) from the serving cell. A single user is selected for OMA. For NOMA, define a combination for the rank of the paired UEs as (m-n), where m denotes the rank for NOMA UE1 with interference mitigation (low power UE), and n denotes the rank for NOMA UE2 without interference mitigation (high power UE). As described in Section 3.3, there are several different combinations of rank for NOMA paired UEs. It is also noted that the combination of the precoder among paired NOMA UEs is checked when the same precoder case is assumed. We note that rank combination (1-2) is excluded. This is because it would be difficult for low power UE1 to decode jointly the desired and interference signals in such a rank combination.
3. Select one of the transmission power sets from the predetermined multiple transmission power sets for paired NOMA UEs where the predetermined transmission power sets (p_1, p_2) = (0.14, 0.86), (0.17, 0.83), (0.23, 0.77), (0.36, 0.64), which were optimized by link and system level simulation in advance. Specifically, utilizing excessively large numbers of power sets in the scheduling process incurs significant signaling overhead. Therefore, in order to minimize the signaling overhead, the values are heuristically selected to achieve similar system capacity when assuming the full flexible case, i.e., the power sets (p_1, p_2) =

(0.01, 0.99), (0.02, 0.98), …, (0.49, 0.51). Note that full transmission power is assumed for the OMA case.

4. Calculate the scheduling SINRs for NOMA using the reported CQI assuming OMA and the power set of (p_1, p_2). Computation of the scheduling SINR for NOMA UEs is based on an approximation of the received SINR after power-domain multiplexing as follows.
   i. Scheduling SINR of NOMA for low power UE_1: p_1 x CQI_{UE1}
   ii. Scheduling SINR of NOMA for high power UE_2: p_2 / (p_1 + CQI_{UE2})
   iii. Scheduling SINR of OMA for UE_j: CQI_{UEj}

   We note that UE_1 and UE_2 are selected such that CQI_{UE1} is always higher than CQI_{UE2}. We also assume that the transmission power, p_1, for UE_1 is always lower than that, p_1, for UE_2. Then, UE_1 is assumed to apply ideal IC to remove the interference from the other user, while UE_2 directly decodes its own signal.
5. Calculate the multi-user PF metric using the following formula.

$$Metric_{PF} = \sum_{j \in \mathbf{U}} \left(\frac{\tau(j|\mathbf{U},\mathbf{P})}{T(j)} \right), \tag{3.7}$$

   where **U** denotes the candidate user set. Terms $T(j)$ and $\tau(j|\mathbf{U},\mathbf{P})$ denote the average throughput and instantaneous throughput of UE_j, respectively. Term **P** denotes the allocated power sets.
6. Repeat Steps 2-5 with all of the combinations of candidate transmission power sets (p_1, p_2) and user sets (UE_1, UE_2). Similarly, also compute the PF metric of OMA.
7. Select the transmission power and user sets with the highest PF metric in Step 6. Note that the PF metrics for both OMA and NOMA are compared and selected.
8. Perform Steps 1 to 7 on the remaining subbands.

When Step 8 is finished, transmission power sets are optimized in each subband, and thus the transmission power for a paired UE may be different for different subbands. Also, a paired UE (OMA or NOMA) and the need for interference mitigation are different for the scheduled subbands. For example, for UE3, subband #4 is required to cancel the interference from UE2, while the subbands #5, #6, and #8 are not required as shown in Fig. 3-8. These assumptions may increase the complexity of the decoding process on the receiver side depending on the receiver assumption. Thus, in our evaluation, alignment for the users and transmission power sets are further conducted to mitigate the complexity using the following steps.

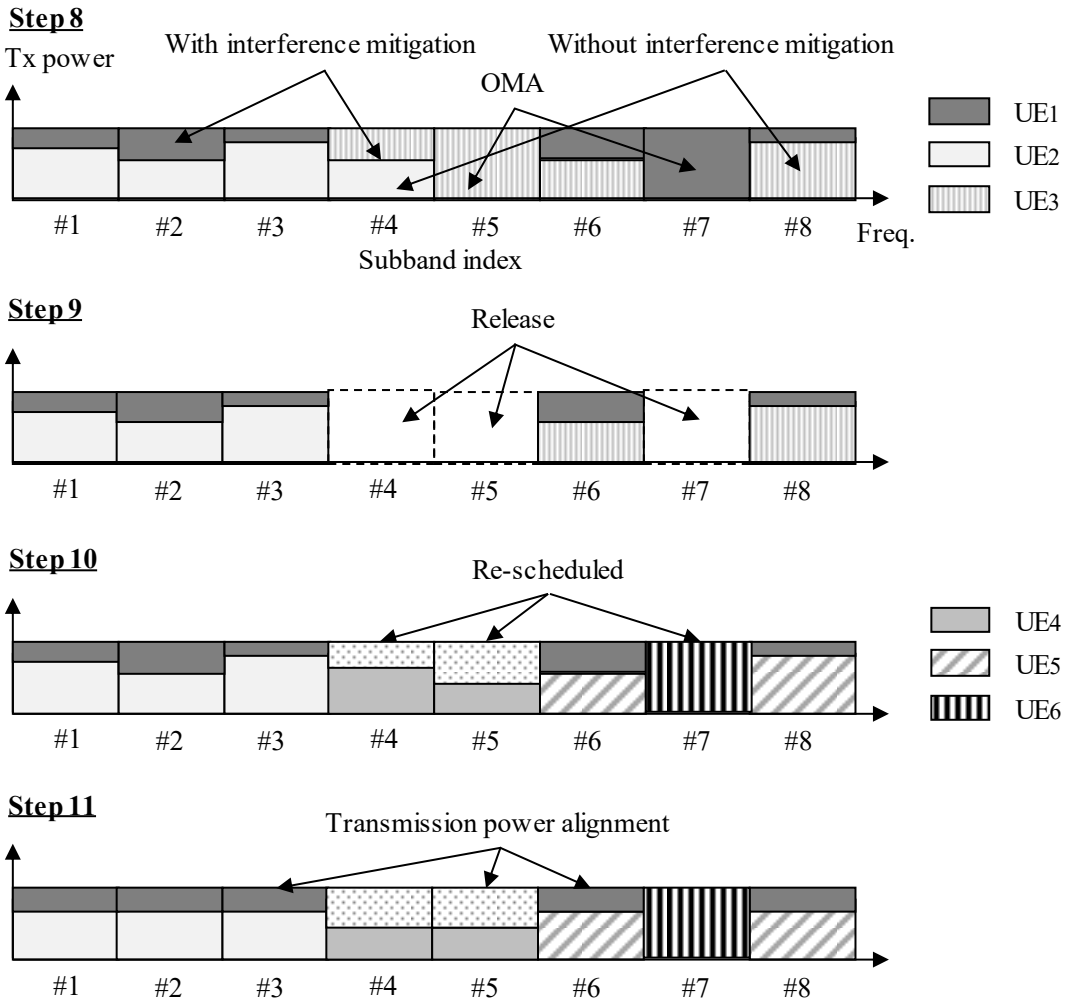

Figure 3-8. Scheduling process

9. Check and count the number of subbands whether or not interference mitigation is required or not for each scheduled user. Note that this step is performed sequentially for paired UEs (NOMA) or UEs (OMA) determined after Steps 1-8 in order of the PF metric.

   i. For a UE of interest, if the number of subbands requiring interference mitigation is the largest, those subbands are retained as the scheduled subbands requiring interference mitigation and other subbands for this UE are released. For example, for UE_1, subbands #1, #2, #3, #6 and #8 are selected.

   ii. For a UE of interest, if the number of subbands not requiring interference mitigation is the largest, those subbands are retained as the scheduled subbands not requiring interference mitigation and other subbands for this UE are released.

iii. For a UE of interest, if the number of subbands not having a paired UEs is the largest, those subbands are retained as the scheduled subbands not having a paired UEs, i.e., OMA subbands, and other subbands for this UE are released.

10. Repeat Steps 2-9 for the released subband. If no subband is released in Step 9, this means that all scheduled UEs or UE pairs are aligned on different
11. Align the transmission power sets for each user in the scheduled subband. Specifically, optimal transmission power sets for each user are exhaustively searched to achieve the highest PF metric. Note that different transmission powers are not allocated to different subbands of the same UE. With this restriction, the transmission power set is uniquely determined by each user. It is also noted that the power optimization is conducted, separately (i.e., subbands #1, #2, #3, #6, #8 and subbands #4, #5 in Fig. 3-8, separately).

3.4.2. System Evaluation Results

The simulation parameters are given in Table 3-5. In this evaluation, the scheduling methodology described in Section 3.4.1 is applied to the R-ML with subband scheduling. For the comparison, the ideal IC is also evaluated as the upper bound of the CWIC, but wideband scheduling is applied to the ideal IC as described in Section 3.2.3. The R-ML/ideal IC is applied to only low power UEs (UE1) to deal with the inter-user interference. The link performance modeling for the R-ML is provided in Section 3.3. For the ideal IC, the output SINR is calculated using Eqs. (3.3)-(3.4), and Eq. (2.28) is applied to derive the effective SINR. In the evaluation, FTP traffic model 1 [25] is assumed, and the cell-average, 95th percentile (95%tile), 50%tile, and 5%tile of the system level throughput performance are evaluated. In addition, resource utilization of each case is also provided.

Tables 3-6 and 3-7 give the system level throughput performance of the ideal IC and R-ML with subband scheduling, respectively. Furthermore, Table 3-8 indicates the performance of the R-ML with wideband scheduling to investigate the impact of the scheduling scheme on the R-ML. Note that the scheduling scheme for OMA is the same as NOMA in these tables, i.e., wideband scheduling is utilized in Tables 3-6 and 3-8 and subband scheduling in Table 3-7. For the ideal IC and R-ML with wideband scheduling, the offered traffic load (packet arrival rate) is set to 10.5, 11.5, and 12.0 UE/s. For the R-ML with subband scheduling, the packet arrival rate is set to 12.0, 13.5, and 14.5 UE/s, which is equal to or higher than that for the ideal IC. Tables 3-6 to 3-8 indicate that NOMA can provide a significant performance gain compared to OMA using the superposed user multiplexing. For example, the cell-average gain of 20% (5%tile gain of 30%) can be achieved for the packet arrival rate = 12.0 UE/s in the ideal IC case. On the other hand, we can see that the absolute system level throughput performance of the ideal IC and R-ML with

Table 3-5. System evaluation assumptions

Parameters	Values
Cell Layout	Hexagonal grid, 3 sectors per site, 19 macro sites (ISD = 500 m)
System bandwidth (Carrier frequency)	10 MHz (2.0 GHz)
Total BS TX power (Ptotal per carrier)	46 dBm
Distance-dependent path loss	ITU UMa
Penetration loss	For outdoor UEs: 0 dB For indoor UEs: 20 dB+0.5din (din: independent uniform random value between [0, min(25,d)] for each link)
Shadowing	ITU Uma
Antenna pattern / height	3D [26] / 25 m
UE antenna height	1.5 m
Antenna gain + connector loss	17 dBi
Antenna gain of UE	0 dBi
Fast fading channel	ITU UMa
Antenna configuration	BS: 2 Txs (0.5 lambda), cross-polarized UE: 2 Rxs (0.5 lambda), cross-polarized
UE dropping	20% UEs are outdoor and 80% UEs are indoor.
Minimum distance from macrocell	35 m
Traffic model (Packet size)	FTP traffic model type 1 (0.1 MByte) [25]
UE noise figure	9 dB
UE speed	3 km/h
Cell selection criteria	Reference Signal Receive Power (RSRP)
Handover margin	3 dB
Control delay (Scheduling, AMC)	5 ms
HARQ combining / Round trip delay	Chase combining / 8 ms
Feedback periodicity of CQI, PMI / RI	5 ms / 100 ms
OLLA	ON
Channel estimation	2D-MMSE
EVM	Tx EVM: 8%, UE Rx EVM: 4%
Maximum transfer time (Dropping time)	1.6 s
Receiver assumption	For OMA: R-ML for Rank 2, MMSE-IRC for Rank 1 For NOMA: R-ML/ideal IC

wideband scheduling is lower than that of the R-ML with subband scheduling from Table 3-7. As the cell-average performance, for example, 8.42 Mbps can be achieved by the ideal IC, while 12.3 Mbps is achieved by the R-ML. This is because the frequency-selective scheduling gain from subband scheduling can be obtained in the R-ML case. From these results, we conclude that the R-ML with subband scheduling achieves higher system performance than the other cases. Additionally, we observed that the performance gain of the R-ML is reduced compared to the ideal IC. This is because the transmission precoder restriction due to the R-ML incurs a lower probability of superposed user multiplexing (NOMA user-paring) as shown in Fig. 3-9. Even though the performance gain is reduced by the R-ML, NOMA can also provide a significant performance gain compared to OMA. For example, in the R-ML with subband scheduling, the cell-average gain of 10.5% (5%tile gain of 14%) can be achieved for the packet arrival rate = 14.5 UE/s case.

Table 3-6. System evaluation results (ideal IC with wideband scheduling)

Tput (Mbps)	Packet Arrival Rate								
	10.5 UE/s			11.5 UE/s			12.0 UE/s		
	OMA	NOMA	Gain	OMA	NOMA	Gain	OMA	NOMA	Gain
Average	10.52	12.65	20.3%	7.44	9.73	30.7%	6.10	8.42	37.9%
0.95	36.36	40.00	10.0%	27.59	32.00	16.0%	23.53	29.63	25.9%
0.5	6.20	8.00	29.0%	3.96	5.71	44.3%	3.11	4.65	49.4%
0.05	1.00	1.31	31.1%	0.63	0.87	38.9%	0.52	0.72	39.7%
RU (%)	72.9%	68.1%	----	83.8%	78.7%	----	87.8%	83.2%	----

Table 3-7. System evaluation results (R-ML with subband scheduling)

Tput (Mbps)	Packet Arrival Rate								
	12.0 UE/s			13.5 UE/s			14.5 UE/s		
	OMA	NOMA	Gain	OMA	NOMA	Gain	OMA	NOMA	Gain
Average	11.84	12.28	3.8%	8.77	9.37	6.9%	6.99	7.73	10.5%
0.95	36.36	38.10	4.8%	29.63	30.77	3.8%	24.24	25.81	6.5%
0.5	7.69	8.08	5.0%	5.30	5.80	9.4%	4.00	4.55	13.6%
0.05	1.46	1.57	6.9%	1.00	1.10	10.5%	0.76	0.87	14.3%
RU (%)	71.8%	70.9%	----	82.6%	81.5%	----	88.2%	87.0%	----

Table 3-8. System evaluation results (R-ML with wideband scheduling)

Tput (Mbps)	Packet Arrival Rate								
	10.5 UE/s			11.5 UE/s			12.0 UE/s		
	OMA	NOMA	Gain	OMA	NOMA	Gain	OMA	NOMA	Gain
Average	10.52	11.85	12.6%	7.44	9.01	21.1%	6.10	7.70	26.2%
0.95	36.36	38.10	4.8%	27.59	30.77	11.5%	23.53	27.59	17.2%
0.5	6.20	7.41	19.4%	3.96	5.16	30.3%	3.11	4.21	35.3%
0.05	1.00	1.20	20.4%	0.63	0.80	28.2%	0.52	0.67	28.8%
RU (%)	72.9%	69.8%	----	83.8%	80.1%	----	87.8%	84.5%	----

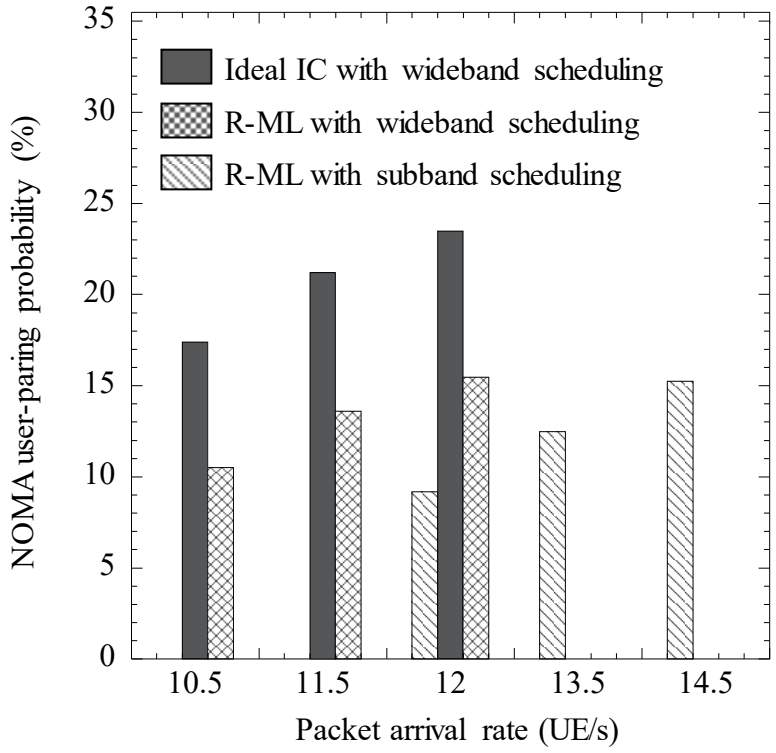

Figure 3-9. NOMA user-paring probability

3.5. Conclusion

In this section, we proposed and investigated a link performance modeling and the system level throughput performance of the R-ML in NOMA. As a link performance modeling for the R-ML in NOMA, we proposed a variant of the EESM scheme, and showed that the proposed scheme can accurately predict the BLER performance of the R-ML. Furthermore, the proposed link performance modeling demonstrated that the R-ML in NOMA with subband scheduling can provide a significant performance gain compared to OMA. In addition, we described that the wideband scheduling is a reasonable choice for the CWIC to reduce the signaling overhead, and showed the system level throughput performance of the ideal IC in NOMA with wideband scheduling as the upper bound of the CWIC. Numerical results showed that the ideal IC can also provide a significant performance gain for NOMA, but absolute throughput performance is degraded compared to the R-ML due to the lack of scheduling flexibility.

References

[1] K. Higuchi and Y. Kishiyama, “Non-orthogonal access with random beamforming and intra-beam SIC for cellular MIMO downlink,” *IEICE technical report*, RCS2012-89, vol. pp. 85-90, July 2012.

[2] D. Tse and P. Viswanath, “Fundamentals of Wireless Communication,” Cambridge University Press, 2005.

[3] A. Benjebbour, A. Li, Y. Saito, Y. Kishiyama, A. Harada, T. Nakamura, "System-Level Performance of Downlink NOMA for Future LTE Enhancements ," *2013 IEEE Globecom Workshops*, Dec. 2013.

[4] T. Yazaki, Y. Sanada, “Throughput Performance of Non-orthogonal Multiple Access with Joint Detection in Far User, ” *in Proc. ISPACS 2015*, Nov. 2015.

[5] Y. Saito, A. Benjebbour, Y. Kishiyama, T. Nakamura, “System-Level Performance of Downlink Non-orthogonal Multiple Access (NOMA) Under Various Environments, ” *in Proc. VTC-spring 2015*, May 2015.

[6] Z. Ding, Z. Yang, P. Fan, “On the Performance of Non-Orthogonal Multiple Access in 5G Systems with Randomly Deployed Users,” *IEEE Signal Processing Letters*, Dec. 2014.

[7] 3GPP, TR 36.859 (V13.0.0), "Study on Downlink Multiuser Superposition Transmission (MUST) for LTE," Jan. 2016.

[8] 3GPP, RP-160680, "New work item proposal: Downlink Multiuser Superposition Transmission for LTE," Mar. 2016.

[9] H. Kawai, K. Higuchi, N. Maeda and M. Sawahashi, “Performance of QRM－MLD employing two－dimensional multi－slot and carrier－averaging channel estimation using orthogonal pilot channel for OFCDM MIMO multiplexing in multipath fading channel,” *in Proc. Wireless2004*, Jul. 2004.

[10] C. Yan, A. Harada, A. Benjebbour, Y. Lan, A. Li, and H. Jiang, “Receiver design for downlink non-orthogonal multiple access (NOMA),” *in Proc. VTC-Spring 2015*, May 2015.

[11] O. Nakamura, J. Goto, Y. Hamaguchi, S. Ibi, and S. Sampei, “Performance Comparison of Superposition Coding Schemes for Downlink Non-Orthogonal Multiple Access,” *IEICE Technical Report*, RCS2015-43, May 2015.

[12] O. Nakamura, J. Goto, and Y. Hamaguchi, “Frequency Selection Diversity Effect for Downlink Non-Orthogonal Multiple Access with Maximum Likelihood Detection,” *IEICE Technical Report*, RCS2014-284, Jan. 2015.

[13] K. Brueninghaus, D. Astély, T. Sälzer, S. Visuri, A. Alexiou, S. Karger, and G.-A. Seraji, “Link performance models for system level simulations of broadband radio access systems,” *in Proc. IEEE PIMRC2005*, Sept. 2005.

[14] V. Pauli, I. Viering, C. Buchner, E. Saad, G. Liebl, A. Klein, "Efficient link-to-system level modeling for accurate simulations of MIMO-OFDM systems," *in proc. IEEE ICC2009*, Jun. 2009.

[15] 3GPP, TR 25.892 (V6.0.0), "Feasibility study for orthogonal frequency division multiplexing (OFDM) for UTRAN enhancement," June 2004.

[16] 3GPP, R1-031303, Ericsson, "System-level evaluation of OFDM - further considerations," Nov. 2003.

[17] K. Brüninghaus, D. Astely, Th. Sälzer, S. Visuri, A. Alexiu, St. Karger, G. A. Seraji, "Link Performance Models for System Level Simulations of Broadband Radio Access Systems", *in Proc. PIMRC*, Sept. 2005.

[18] S.-H. Moon, K.-J. Lee, J. Kim, and I. Lee, "Link performance estimation techniques for MIMO-OFDM systems with maximum likelihood receiver," *IEEE Trans*., vol. 11, pp. 1808 –1816, may 2012.

[19] H. Lee, J. Lim, W. Park and T. Kim, "Link Performance Abstraction for Interference-Aware Communications (IAC)," *in Proc. VTC-fall 2014*, Sept. 2014.

[20] Y. Fadlalah, R. Visoz, A. O. Berthet, "A Novel Calibration Framework for the Physical Layer Abstraction of (turbo) Codeword IC Receivers," *in Proc. VTC-spring 2015*, May 2015.

[21] 3GPP TS36.211 (V8.9.0), Evolved Universal Terrestrial Radio Access (E-UTRA); Physical channels and modulation, Dec.2009.

[22] P. Hoeher, S. Kaiser, and P. Robertson, "Two-dimensional pilot-symbol-aided channel estimation by Wiener filtering," *in Proc. ICASSP'97*, pp. 1845-1848, Apr. 1997.

[23] M. Moisio, and A. Oborina, "Comparison of effective SINR mapping with traditional AVI approach for modeling packet error rate in multi–state channel," Proceedings in the 6th international conference on Next Generation Teletraffic and Wired/Wireless Advanced Networking, June 2006.

[24] F. Kelly, "Charging and Rate Control for Elastic Traffic," *Eur. Trans. on Telecommun*, 1997.

[25] 3GPP TR36.814 (V9.0.0), "Further advancements for E-UTRA physical layer aspects," Mar. 2010.

[26] 3GPP, TR36.819 (V11.2.0), Coordinated multi-point operation for LTE physical layer aspects, Sept. 2013.

Chapter 4. Conclusion

This dissertation investigates system capacity enhancement of mobile communication system such as LTE/LTE-Advanced, which is specified in 3GPP, to deal with the expected mobile traffic explosion in future. Considering the development of the radio signal processing technologies, especially the interference suppression and cancellation technologies at the mobile terminals in recent years, an improvement of system capacity using such an advanced interference mitigation receiver is deeply investigated. The results obtained in Chapter 2 and 3 are summarized below.

Chapter 2 focus on the IRC receiver, which can suppress the inter-cell interference based on MMSE criteria. The IRC receiver needs to the knowledge, i.e. the covariance matrix, of the inter-cell interference to suppress it, and it is typically estimated by the reference signals transmitted from the serving cell. In LTE/LTE-Advanced, various transmission modes and the reference signal structures are supported. Especially in CRS based transmission mode, it is expected that the estimation accuracy of the covariance matrix of the interference signals is affected by CRS-to-CRS collision among the serving and interference cells. Therefore, the impact is deeply analyzed in the first half of this chapter. As a result, it is shown that the IRC receiver can surely provide enough link performance gain compared with the conventional MRC/MMSE receivers, although CRS-to-CRS collision reduces the performance gain of the IRC receiver. From the results, we can recognize that the IRC receiver can improve system capacity of the mobile communication system. Moreover, it is expected that the further capacity gain can be obtained by using the IRC receiver together with other technologies, e.g. ICIC and CoMP. For evaluating the improvement of the system capacity, the system level simulation needs to be developed for the IRC receiver. To do this, the link performance modeling for the IRC receiver also needs to be developed. Therefore, it is investigated in the latter half of this chapter. It is shown that the proposed link performance modeling of the IRC receiver can accurately model the link performance of the IRC receiver compared with the conventional one, specifically in the frequency selective channel. This means that the system capacity enhancement due to the IRC

receiver can be accurately evaluated by the system level simulation employing the proposed scheme.

Chapter 3 focus on enhancement of the multiple access scheme. In LTE/LTE-Advanced, OFDM based multiple access was adopted. This type of orthogonal multiple access is a reasonable choice for achieving good system-level throughput performance. When considering advanced multi-user detection, however, there is room for achieving higher performance using NOMA. As a multi-user detection in NOMA, the R-ML and CWIC receivers can be considered. Those receivers have advantage and disadvantage in system level design, e.g. flexibility of user scheduling and transmission precoding allocation. To analyze the such aspects, in this chapter, the link performance modeling of the R-ML receiver is proposed for evaluating the system level performance. Validation results by the link level simulation show that the proposed scheme can accurately model the link performance of the R-ML receiver in NOMA including the effect of the channel estimation error. The system level evaluation using the proposed scheme also show that the R-ML receiver can provide better system capacity than the CWIC receiver in NOMA.

The results in Chapter 2 and 3 indicate the system capacity of the mobile communication system can be surely improved by the IRC receiver and NOMA employing the R-ML receiver. However, it is very challenging to achieve desired improvement of system capacity by only those technologies because it is predicted that the amount of mobile traffic continuously and seriously increases, e.g. 1.47-fold per year from 2016 to 2021. Therefore, a combination of those and other technologies needs to be further investigated. This is a potential remaining study in this research field.

Acknowledgement

I would like to express my deepest gratitude to my supervisor, Professor Kazuhiko Fukawa for his continual encouragement, infinite support, and stimulating discussions.

I deeply appreciate to the juries of this dissertation, Professor Isao Yamada, Professor Minoru Nakayama, Professor Shigetaka Takagi and Professor Tomohiko Uematsu, for the valuable suggestions and discussions.

I am very grateful to Dr. Yusuke Ohwatari, Dr. Kazuaki Takeda, Mr. Satoshi Nagata, Dr. Akihito Morimoto, Dr. Yukihiko Okumura and Mr. Takehiro Nakamura at NTT DOCOMO, and Associate Professor Nobuhiko Miki at Kagawa University for their patient guidance and beneficial discussion throughout this study.

I would like to thank Mr. Xiaohang Chen, Dr. Anxin Li, Mr. Xu Zhang and Ms. Jiang Huiling at DOCOMO Beijing Communications Laboratories for their valuable discussion and assistance.

I sincerely appreciate Mr. Hiroshi Nakamura, Executive General Manager of R&D Innovation Division and Director at NTT DOCOMO, Mr. Wataru Takita, General Manager of Research Laboratories at NTT DOCOMO, and Mr. Akihiro Maebara, General Manager of Radio Access Network Development Department at NTT DOCOMO, for allowing the opportunity for this study.

I am also grateful to my colleagues at NTT DOCOMO and my family.

Appendix A: List of Notations

$BLER^{t}_{actual}$	Actual BLER performance of the conventional receiver with a given MCS and rank in trial t
$BLER^{t}_{predicted,\beta}$	Predicted BLER performance for given β by EESM in trial t
$\beta_{MCS,\ rank}$	Training parameter of EESM for given MCS and rank
$\beta_{MCS,\ rankcombi,pu}$	Training parameter of proposed EESM for given MCS, rank combination of multiplexed users and transmission power ration in NOMA
$\mathbf{d}_0(k,l)$	DMRS sequence of the serving cell at k-th subcarrier and l-th OFDM symbol
$\mathbf{d}_q(k,l)$	N_{Tx}-dimensional CRS sequence vector of the q-th cell at k-th subcarrier and l-th OFDM symbol
$d_{m,q}(k,l)$	CRS sequence at the m-th transmitter antenna branch of q-th cell at k-th subcarrier and l-th OFDM symbol
Φ	Auto-covariance matrix of channel vector
$\mathbf{G}_q(k,l)$	($N_{\mathrm{Rx}} \times N_{\mathrm{Stream}}$) composite channel matrix defined as $\boldsymbol{H}_q(k,l)\boldsymbol{W}_{\mathrm{Tx},q}(k,l)$ between q-th cell and the UE
$\mathbf{H}_q(k,l)$	($N_{\mathrm{Rx}} \times N_{\mathrm{Tx}}$) channel matrix between the q-th cell and UE at k-th subcarrier and l-th OFDM symbol
$\mathbf{H}_u(k,l)$	($N_{\mathrm{Rx}} \times N_{\mathrm{Tx}}$) channel matrix between serving cell and UE at k-th subcarrier and l-th OFDM symbol for user u in NOMA
$\mathbf{I}$	Identity matrix
k	Subcarrier index in frequency domain for OFDM based system
l	OFDM symbol index in time domain for OFDM based system
$\mathbf{M}_{\mathrm{CRS}}$	CRS RE group in serving cell
$\mathbf{M}_{\mathrm{DMRS}}$	DMRS RE group in serving cell
$\mathbf{n}(k,l)$	N_{Rx}-dimensional noise vector at k-th subcarrier and l-th OFDM symbol
N_{Cell}	Number of total cells
N_{Rx}	Number of the received antenna branches at UE
N_{sp}	Number of RSs for averaging of covariance matrix for IRC receiver
N_{Stream}	Number of the transmission data streams of serving cell
N_{subcar}	Number of allocated subcarriers for OFDM signal
N_{Trial}	Number of trials for the training process of EESM

N_{Tx}	Number of the transmission antenna branches at BS
P_{CRS}	Transmit power of the CRS
P_{Data}	Total transmit data signal power per symbol of serving cell
$P_{\mathrm{Data},\,q}$	Total transmit data signal power per symbol of q-th interfering cell
P_{g}	Average channel amplitude
$\boldsymbol{\theta}$	Cross-covariance matrix of channel vectors
q	Cell index (q=0 means serving cell)
$\mathbf{R}_{I+N}$	($N_{\mathrm{Rx}} \times N_{\mathrm{Rx}}$) Covariance matrix including only interference signal and noise component
$\mathbf{R}_{yy}(k,l)$	($N_{\mathrm{Rx}} \times N_{\mathrm{Rx}}$) covariance matrix including serving/interference signals and noise component at k-th subcarrier and l-th OFDM symbol
R	Code rate for channel coding
ρ_{Rx}	Correlation coefficient between the receiver antenna branches
$\mathbf{s}_q(k,l)$	N_{Stream}-dimensional information signal vector of the q-th cell at k-th subcarrier and l-th OFDM symbol
$SINR_{\mathrm{out},n}(k,l)$	Output SINR of the n-th transmission stream for k-th subcarrier and the l-th OFDM symbol
$SINR_{\mathrm{eff},n}$	Effective SINR of the n-th transmission stream
$SINR_{out,k,u,n}^{ideal}$	Output SINR of the n-th transmission stream at the k-th subcarrier and user u for ideal user interference canceller in NOMA
$SINR_{out,k,u,n}$	Output SINR of the n-th transmission stream at the k-th subcarrier and user u for conventional MMSE receiver in NOMA
σ_N^2	Averaged noise power
σ_I^2	Averaged interfere
u	User index for NOMA
$\mathbf{w}_{\mathrm{CE}}$	Channel estimation filter
$\mathbf{W}_{\mathrm{IRC}}(k,l)$	($N_{\mathrm{Rx}} \times N_{\mathrm{Stream}}$) IRC receiver weight matrix (or vector if $N_{\mathrm{Stream}} = 1$) at k-th subcarrier and l-th OFDM symbol
$\mathbf{W}_{\mathrm{Tx},q}(k,l)$	($N_{\mathrm{Tx}} \times N_{\mathrm{Stream}}$) precoding weight matrix of the q-th cell at k-th subcarrier and l-th OFDM symbol
$\mathbf{W}_{\mathrm{Rx},\,q}(k,l)$	($N_{\mathrm{Stream}} \times N_{\mathrm{Rx}}$) receiver weight matrix (or vector if $N_{\mathrm{Stream}} = 1$) of q-th cell at k-th subcarrier and l-th OFDM symbol
$\mathbf{w}_{\mathrm{Rx},n}(k,l)$	N_{Rx}-dimensional receiver weight vector of n-th transmission data stream at k-th subcarrier and l-th OFDM symbol of serving cell
$\boldsymbol{w}_{Rx,u,n}^{ideal}$	N_{Rx}-dimensional receiver weight vector of n-th transmission data stream at k-th subcarrier for ideal user interference canceller in NOMA

$\boldsymbol{w}_{Rx,u,n}$	N_{Rx}-dimensional receiver weight vector of n-th transmission data stream at k-th subcarrier for conventional MMSE receiver in NOMA
$W_{N\mathrm{Rx}}$	Complex Wishart distribution
$\mathbf{y}(k,l)$	N_{Rx}-dimensional received signal vector at k-th subcarrier and l-th OFDM symbol for CRS-to-CRS collision case in DMRS-based transmission mode
$\mathbf{y}_{\mathrm{u}}(k,l)$	N_{Rx}-dimensional received signal vector of the k-th subcarrier and the l-th OFDM symbol for user u in NOMA
$\mathbf{y}_{\mathrm{CtoC}}(k,l)$	N_{Rx}-dimensional received signal vector at k-th subcarrier and l-th OFDM symbol for CRS-to-CRS collision case
$\mathbf{y}_{\mathrm{CtoD}}(k,l)$	N_{Rx}-dimensional received signal vector at k-th subcarrier and l-th OFDM symbol for desired-CRS-with-data-signal-interference case
$\mathbf{y}_{\mathrm{DtoC}}(k,l)$	N_{Rx}-dimensional received signal vector at k-th subcarrier and l-th OFDM symbol for CRS-to-CRS collision case
$\mathbf{y}_{\mathrm{DtoD}}(k,l)$	N_{Rx}-dimensional received signal vector at k-th subcarrier and l-th OFDM symbol for desired-data-signal-with-data-signal-interference case
$\mathbf{Z}_{\mathrm{c}}(k,l)$	($N_{\mathrm{Rx}} \times N_{\mathrm{Stream}}$) estimation error matrix to be $\mathbf{Z}_{\mathrm{c}}$ due to the DMRS at k-th subcarrier and l-th OFDM symbol

Appendix B: Acronyms

3GPP	The Third Generation Partnership Project
AMC	Adaptive Modulation and Coding scheme
ARQ	Automatic Repeat reQuest
AWGN	Additive White Gaussian Noise
BER	Bit Error Rate
BLER	BLock Error Rate
BPSK	Binary Phase Shift Keying
BS	Base Station
CDD	Cyclic Delay Diversity
CDF	Cumulative Distribution Function
CDM	Code Division Multiplexing
CoMP	Coordinated Multi-Point transmission
CP	Cyclic Prefix
CQI	Channel Quality Indicator
CRE	Cell Range Expansion
CRS	Cell-specific RS
CSI	Channel State Indicator
CSI-RS	Channel State Information-RS
CWIC	Codeword Level Interference Canceller
DMRS	DeModulation RS
EESM	Exponential Effective SINR Mapping
EVA	Extended Vehicular A model
EVM	Error Vector Magnitude
FTP	File Transfer Protocol
HARQ	Hybrid Automatic Repeat request
HetNet	Heterogeneous Network
IC	Interference Canceller
ICIC	Inter-Cell Interference Coordination
IoT	Internet of Things
IRC	Interference Rejection Combining
ISD	Inter Site Distance
ITU	International Telecommunication Union

LTE	Long-Term Evolution
M2M	Machine-to-Machine
MCS	Modulation and Coding Scheme
MIESM	Mutual Information based Exponential SINR Mapping
MIMO	Multiple-Input Multiple-Output
ML	Maximum Likelihood
MLD	Maximum Likelihood Detector
MMSE	Minimum Mean Square Error
MPI	MultiPath Interference
MRC	Maximal Ratio Combining
MSE	Mean Square Error
NAICS	Network Assisted Interference Cancellation and Suppression
NOMA	Non-Orthogonal Multiple Access
OFDM	Orthogonal Frequency Division Multiplexing
OLLA	Outer Loop Link Adaptation
OMA	Orthogonal Multiple Access
PDCCH	Physical layer Downlink Control CHannel
PMI	Precoding Matrix Indicator
QAM	Quadrature Amplitude Modulation
QPSK	Quadrature Phase Shift Keying
QRM-MLD	complexity reduced MLD with QR decomposition and M-algorithm
RB	Resource Block
RE	Resource Element
RF	Proportional Fair
RI	Rank Indicator
R-ML	Reduced complexity-Maximum Likelihood detector
RMS	Root Mean Square
RSRP	Reference Signal Receive Power
SFBC	Space-Frequency Block Code
SIC	Successive Interference Cancellation
SINR	Signal-to-Interference-plus-Noise power Ratio
SIR	Signal-to-Interference power Ratio
SNR	Signal-to-Noise power Ratio
TM	Transmission Mode
UE	User Equipment
UMa	Urban Macro

Appendix C: List of Publications

Journals

1. Yousuke Sano, Yusuke Ohwatari, Nobuhiko Miki, Yuta Sagae, Yukihiko Okumura, Yasutaka Ogawa, Takeo Ohgane, Toshihiko Nishimura, "Impact on Inter-Cell Interference of Reference Signal for Interference Rejection Combining Receiver in LTE-Advanced Downlink," *IEICE Trans.* 95-B(12): pp.3728-3738, 2012.
2. Yousuke Sano, Yusuke Ohwatari, Nobuhiko Miki, Akihito Morimoto, Yukihiko Okumura, "Link Performance Modeling of Interference Rejection Combining Receiver in System Level Evaluation for LTE-Advanced Downlink," *IEICE Trans.* 95-B(12): pp.3739-3751, 2012.
3. Yousuke Sano, Kazuaki Takeda, Satoshi Nagata, Takehiro Nakamura, Xiaohang Chen, Anxin Li, Xu Zhang, Jiang Huiling, Kazuhiko Fukawa, ”Investigation on Non-Orthogonal Multiple Access with Reduced Complexity Maximum Likelihood Receiver and Dynamic Resource Allocation,” *IEICE Trans.* 100-B(8): pp.1301-1311, 2017.

International Conferences

1. Yousuke Sano, Yusuke Ohwatari, Nobuhiko Miki, Akihito Morimoto, Yukihiko Okumura, "Investigation on link performance modeling of advanced receiver employing interference rejection combining in system level evaluation for LTE-Advanced downlink," *in Proc. ISWCS 2012*, Aug. 2012
2. Yousuke Sano, Yusuke Ohwatari, Yuta Sagae, Akihito Morimoto, Yukihiko Okumura, "Investigation on Feedback Channel State Information for Interference Rejection Combining Receiver in LTE-Advanced Downlink," *in Proc. VTC Spring 2014*, May 2014